Geometry & Topology

Volume 27 (2023)

Unexpected Stein fillings, rational surface singularities and plane curve arrangements

Olga Plamenevskaya
Laura Starkston

msp

msp

Geometry & Topology **27**:3 (2023) 1083–1202
DOI: 10.2140/gt.2023.27.1083
Published: 8 June 2023

Unexpected Stein fillings, rational surface singularities and plane curve arrangements

OLGA PLAMENEVSKAYA
LAURA STARKSTON

We compare Stein fillings and Milnor fibers for rational surface singularities with reduced fundamental cycle. Deformation theory for this class of singularities was studied by de Jong and van Straten (1998); they associated a germ of a singular plane curve to each singularity and described Milnor fibers via deformations of this singular curve.

We consider links of surface singularities, equipped with their canonical contact structures, and develop a symplectic analog of de Jong and van Straten's construction. Using planar open books and Lefschetz fibrations, we describe all Stein fillings of the links via certain arrangements of symplectic disks, related by a homotopy to the plane curve germ of the singularity.

As a consequence, we show that many rational singularities in this class admit Stein fillings that are not strongly diffeomorphic to any Milnor fibers. This contrasts with previously known cases, such as simple and quotient surface singularities, where Milnor fibers are known to give rise to all Stein fillings. On the other hand, we show that if for a singularity with reduced fundamental cycle, the self-intersection of each exceptional curve is at most -5 in the minimal resolution, then the link has a unique Stein filling (given by a Milnor fiber).

14J17, 32S30, 32S50, 57K33, 57K43; 14H50, 32S25

1 Introduction

The goal of this paper is to compare and contrast deformation theory and symplectic topology of certain rational surface singularities. Using topological tools, we examine symplectic fillings for links of rational surface singularities with reduced fundamental cycle and compare these fillings to Milnor fibers of the singularities. Each Milnor fiber carries a Stein structure and thus gives a Stein filling of the link; however, we show that there is a plethora of Stein fillings that do not arise from Milnor fibers. Milnor fibers and deformation theory are studied in the work of de Jong and van Straten [27] for sandwiched surface singularities (this class includes rational singularities with reduced fundamental cycle). The main feature of their construction is a reduction from *surfaces* to *curves*: deformations of a surface singularity in the given class can be understood via deformations of the germ of a reducible plane curve associated to the singularity. To describe Stein fillings, we develop a symplectic analog of de Jong and van Straten's constructions, representing the fillings via arrangements of smooth (or symplectic) disks in $\mathbb{C}^2$. Our approach is purely topological and thus different from de Jong and van Straten's; their algebrogeometric techniques do not apply in our more general symplectic setting. We work with Lefschetz fibrations and open books, referring to algebraic geometry only for motivation and for the description of smoothings from [27].

Let $X \subset \mathbb{C}^N$ be a singular complex surface with an isolated singularity at the origin. For small $r > 0$, the intersection $Y = X \cap S^{2N-1}_r$ with the sphere $S^{2N-1}_r = \{|z_1|^2 + |z_2|^2 + \cdots + |z_N|^2 = r\}$ is a smooth 3–manifold called the *link of the singularity* $(X, 0)$. The induced contact structure ξ on Y is the distribution of complex tangencies to Y, and is referred to as the *canonical* or *Milnor fillable* contact structure on the link. The contact manifold (Y, ξ), which we will call the *contact link*, is independent of the choice of r, up to contactomorphism.

An important problem concerning the topology of a surface singularity is to compare the Milnor fibers of smoothings of $(X, 0)$ to symplectic or Stein fillings of the link (Y, ξ). A *smoothing* is given by a deformation of X to a surface (the *Milnor fiber*) that is no longer singular. (We discuss smoothings in more detail in Section 2.) Milnor fibers themselves are Stein fillings of (Y, ξ), called *Milnor fillings*. An additional Stein filling can be produced by deforming the symplectic structure on the minimal resolution of $(X, 0)$; see Bogomolov and de Oliveira [10]. For rational singularities, this filling agrees with the Milnor fiber of the *Artin smoothing* component and need not be considered separately; see Section 4. An interesting question is whether the collection

of these expected fillings, taken for all singularities with the same link (Y,ξ), gives all possible Stein fillings of the link. In this article, we will use the term *unexpected Stein filling* to refer to any Stein filling which does not arise as a Milnor fiber or the minimal resolution.

There are very few examples of unexpected Stein fillings in the previously existing literature, none of which are simply connected. In this article, we show that, in fact, unexpected Stein fillings are abundant, and in many cases simply connected, even for the simple class of *rational singularities with reduced fundamental cycle*. These singularities, also known as *minimal singularities* (see Kollár [29]), can be characterized by the conditions that the dual resolution graph is a tree, where each vertex v corresponds to a curve of genus 0, and its self-intersection $v\cdot v$ and valency $a(v)$ satisfy the inequality $-v\cdot v \geq a(v)$. (See Section 2 for more details.) In low-dimensional topology, such graphs are often referred to as trees with no bad vertices. The corresponding plumbed 3–manifolds are L–spaces, ie they have the simplest possible Heegaard Floer homology; see Ozsváth and Szabó [51]. In a sense, links of rational singularities with reduced fundamental cycle are just slightly more complicated than lens spaces. As another measure of low complexity, these contact structures admit planar open book decompositions. In the planar case, the set of Stein fillings satisfies a number of finiteness properties (see for instance Kaloti [28], Lisi and Wendl [35], Plamenevskaya [54] and Stipsicz [60]), which makes it rather surprising that these singularities diverge from the expected.

We construct many specific examples of unexpected Stein fillings for rational singularities with reduced fundamental cycle. Then we show that our examples can be broadly generalized to apply to a large class of singularities with reduced fundamental cycle: we only require that the resolution graph of the singularity contain a certain subgraph to ensure that the link has many unexpected Stein fillings.

Theorem 1.1 *For any $N>0$, there is a rational singularity with reduced fundamental cycle whose contact link (Y_N,ξ_N) admits at least N pairwise nonhomeomorphic simply connected Stein fillings, none of which is diffeomorphic to a Milnor filling (**rel** certain boundary data). Examples of such (Y_N,ξ_N) include Seifert fibered spaces over S^2 corresponding to certain star-shaped resolution graphs.*

The statement also holds for any rational singularity with reduced fundamental cycle whose resolution graph has a star-shaped subgraph as above.

More precise statements are given in Section 7. Our first example which admits simply connected unexpected Stein fillings corresponds to the singularity with resolution

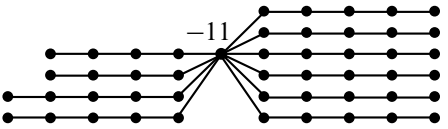

Figure 1: A resolution graph for a singularity whose link admits simply connected unexpected fillings. (Unlabeled vertices have self-intersection -2.) Any graph containing this as a subgraph corresponds to a singularity which also admits simply connected unexpected fillings.

graph in Figure 1. More generally, for every $N > 4$ we can find N distinct unexpected Stein fillings for singularities whose dual resolution graph is star-shaped with at least $2N + 5$ sufficiently long legs, the self-intersection of the central vertex is a large negative number, and the self-intersection of any other vertex is -2.

By contrast, previous results have indicated that for simple classes of singularities, all Stein fillings come from Milnor fibers or the minimal resolution (there are no unexpected fillings). This is true for (S^3, ξ_{std}) by Eliashberg [13], for links of simple and simple elliptic singularities by Ohta and Ono [49; 50], for lens spaces (links of cyclic quotient singularities) by Lisca [34] and Némethi and Popescu-Pampu [45], and in general for quotient singularities by Bhupal and Ono [8] and Park, Park, Shin and Urzúa [52]. Theorem 1.1 breaks this pattern and provides many unexpected fillings. However, we are also able to show that certain classes of rational singularities with reduced fundamental cycle do not admit any unexpected fillings:

Theorem 1.2 *Let $(X, 0)$ be a rational singularity with reduced fundamental cycle with link (Y, ξ), and suppose that each exceptional curve in its minimal resolution has self-intersection at most -5. Then the resolution of $(X, 0)$ is the unique weak symplectic filling of (Y, ξ), up to blow-up, symplectomorphism and symplectic deformation.*

This theorem proves a symplectic analogue of [27, Theorem 6.21], which establishes a special case of a conjecture of Kollár, showing that for singularities as in Theorem 1.2, the base space of a semiuniversal deformation has one component. Thus, they show there is a unique smoothing, whereas we generalize this to show there is a unique minimal symplectic filling. To prove Theorem 1.2, we build on the combinatorial argument of [27] and use mapping class group arguments to establish the symplectic case.

The bound of -5 on the self-intersection of the exceptional curves in Theorem 1.2 cannot generally be improved. Indeed, any singularity whose minimal resolution

contains a sphere of self-intersection -4 has at least two distinct Stein fillings, because a neighborhood of the (-4) sphere can be rationally blown down to produce another filling with smaller Euler characteristic; see Symington [61]. This corresponds to the fact that the singularity has at least two smoothing components if a (-4) sphere is present; see Kollár [30]. While our Theorem 1.1 shows there are unexpected fillings in many examples, we do not cover all examples which fail the hypotheses of Theorem 1.2; there are many cases where we cannot determine whether or not the link has unexpected fillings.

Theorem 1.2 extends the list of singularities with no unexpected Stein fillings. However, when complexity of the singularity increases, one should expect the unexpected: as predicted in Némethi [43], more complicated singularities are likely to have Stein fillings that do not arise from Milnor fibers. To our knowledge, the only previous examples of unexpected Stein fillings in the literature are detected by their first Betti number. By Greuel and Steenbrink [22], Milnor fibers for normal surface singularities always have $b_1 = 0$. An infinite family of Stein fillings with $b_1 \neq 0$ was given in Akhmedov and Ozbagci [3; 4] for links of certain nonrational singularities; these links are Seifert fibered spaces over higher genus surfaces. It follows from [3; 4] that most of these fillings are different from both the Milnor fibers and the resolution of the singularity. The constructions in these papers use surgeries and produce infinite families of exotic fillings (which are all homeomorphic but pairwise nondiffeomorphic). Note that for rational singularities, the first Betti number cannot detect unexpected fillings: the link is a rational homology sphere, and a homology exact sequence argument shows that $b_1 = 0$ for any Stein filling; see Remark 6.5.

Note that, in general, known results allow us to find many nonrational singularities whose links have infinitely many Stein fillings. As an example, consider a normal surface singularity whose resolution has a unique exceptional curve of genus $g \geq 2$ with self-intersection $-d$, for $d > 0$. The resolution is the total space of the complex line bundle of degree d over the corresponding Riemann surface, and the singularity can be thought of as cone point. If $g = \frac{1}{2}(d-1)(d-2)$, one of the analytic singularities in this topological type is the hypersurface $(X_d, 0)$ in $\mathbb{C}^3$, given by $x^d + y^d + z^d = 0$. For each $d \geq 5$, the results of Baykur, Monden and Van Horn-Morris [7] produce arbitrarily long positive factorizations of the corresponding open book monodromy, which in turn yields infinitely many Stein fillings for the link (Y_d, ξ_d); in particular, there are Stein fillings with arbitrarily large b_2. One might hope that most of these Stein fillings are unexpected: indeed, a hypersurface singularity has a unique Milnor fiber, and its topology is well understood; see Milnor [39] and Tyurina [64]. However,

the question is more subtle: because $(X_d, 0)$ is not (*pseudo*)*taut* (see Laufer [32]), there are infinitely many singularities with the same link (Y_d, ξ_d). Milnor fibers of these singularities may yield additional Stein fillings. Describing all such Milnor fibers seems to be out of reach; conceivably, they may produce all the Stein fillings given by the arbitrarily long factorizations of [7]. We will discuss related questions in more detail in Section 4, although we do not have any answers for this case.

Our present work gives the first examples of unexpected Stein fillings for rational singularities, and for the case where the link Y is a rational homology sphere. In the case of rational singularities, the fillings must be differentiated from Milnor fibers by more subtle means than b_1, as all Stein fillings have $b_1 = 0$ in this case. For singularities with reduced fundamental cycle, the contact link admits a planar open book decomposition; see Némethi and Tosun [46] and Schönenberger [58]. By Kaloti [28], Plamenevskaya [54] and Stipsicz [60], it follows that the number of Dehn twists in any positive monodromy factorization, and thus b_2 of Stein fillings, is bounded above. This means that we cannot generate unexpected fillings by arbitrarily long positive factorizations. On the other hand, even though there is typically an infinite collection of singularities with the given link, the reduced fundamental cycle hypothesis, together with the de Jong–van Straten theory, gives us certain control over the topology of all possible Milnor fibers.

In general, comparing Stein fillings to Milnor fillings is a two-fold challenge: classification is typically out of reach, both on the deformation theory side (smoothings and Milnor fibers) and on the symplectic side (Stein fillings). In the particular case of rational singularities with reduced fundamental cycle, two important tools facilitate the study of fillings. On the algebraic geometry side, de Jong and van Straten reduce the study of deformations of the surface to certain deformations of a decorated germ of a reducible singular complex curve $\mathcal{C} \subset \mathbb{C}^2$. (The germ $\mathcal{C}$ is associated to the surface as explained in Section 2. For now, we omit the decoration from notation.) The construction of [27] works for a more general class of *sandwiched* rational singularities; in the case of reduced fundamental cycle, the associated plane curve germ has smooth irreducible components. Thus in this case, $\mathcal{C}$ is simply the union of smooth complex disks $C_1, C_2, \dots, C_m$, all passing through 0. The decoration of the germ is given by marked points, initially concentrated at the origin. To encode deformations of the surface singularity, one considers 1–parameter δ–constant deformations of $\mathcal{C}$, where the marked points are redistributed so that all singularities of the deformed curve $\mathcal{C}^s$ are marked (additional "free" marked points are also allowed). Smoothings of the corresponding singularities are given by *picture deformations*, where the only singularities of the

deformed curve are transverse multiple points. While picture deformations are still hard to classify directly and thus rarely give explicit classification of smoothings, they do provide a lot of useful information. In certain examples, they allow us to understand the topology of Milnor fibers and compute their basic invariants.

The following theorem summarizes the results of de Jong–van Straten that we use. Detailed definitions and precise statements will be given in Section 2.

Theorem 1.3 [27, Theorem 4.4, Lemma 4.7] *Let $(X,0)$ be a rational singularity with reduced fundamental cycle, and $\mathcal{C}\subset\mathbb{C}^2$ its decorated germ of a reducible complex curve such that all the branches $C_1,\dots,C_m$ of $\mathcal{C}$ are smooth complex disks. Then smoothings of $(X,0)$ are in one-to-one correspondence with **picture deformations** of $\mathcal{C}$. A picture deformation gives an arrangement $\mathcal{C}^s$ of the deformed branches $C_1^s,\dots,C_m^s$, $s\neq 0$, with marked points that include all the intersections of the branches. The Milnor fiber $W_{\mathcal{C}^s}$ of the corresponding smoothing can be constructed by blowing up at all marked points and taking the complement of the proper transforms of $C_1^s,\dots,C_m^s$.*

The Milnor fibers described in Theorem 1.3 are noncompact, but a slight modification yields compact Milnor fillings of the contact link (Y,ξ) of $(X,0)$. We consider the germ $\mathcal{C}$ in a small closed ball $B\subset\mathbb{C}^2$ centered at 0, such that all the branches of $\mathcal{C}$, and thus all the deformed branches for small s, intersect ∂B transversely, and B contains all marked points. To obtain a smooth compact 4–manifold whose boundary is the link Y, we blow up B at the marked points, take the complement of disjoint tubular neighborhoods of the proper transforms of $C_1^s,\dots,C_m^s$, and smooth the corners.

In turn, on the symplectic side, contact links of singularities with reduced fundamental cycle are more accessible because they are supported by planar open books; see Némethi and Tosun [46] and Schönenberger [58]. By a theorem of Wendl [65], all Stein fillings of a planar contact manifold are given by Lefschetz fibrations whose fiber is the page of the open book. In other words, all these Lefschetz fibrations arise from factorizations of the monodromy of the *given* open book into a product of positive Dehn twists. In most cases, such positive factorizations cannot be explicitly classified, but they give a combinatorial approach to Stein fillings.

To relate the two sides of the story, we generalize the notion of picture deformation and consider *smooth graphical homotopies* of the decorated germ $\mathcal{C}$ with smooth branches. A smooth graphical homotopy of $\mathcal{C}$ is a real 1–parameter family of embedded disks $C_1^t,\dots,C_m^t$ such that for $t=0$ the disks $C_1^0,\dots,C_m^0$ are the branches of $\mathcal{C}$, and

for $t = 1$, the intersections between C_i^1 and C_j^1 are transverse and positive for all i, j. There is a collection of marked points on $C_1^1, \dots, C_m^1$, coming from a redistribution of the decoration on $\mathcal{C}$, such that all intersection points are marked. (See Definition 3.1.)

We prove that just as picture deformations yield smoothings in [27], every smooth graphical homotopy gives rise to a Stein filling naturally supported by a Lefschetz fibration.

Theorem 1.4 *Let (Y, ξ) be the contact link of a singularity $(X, 0)$ with reduced fundamental cycle, and let $\mathcal{C}$ be a decorated plane curve germ representing $(X, 0)$, with m smooth components $C_1^0, \dots, C_m^0$. For any smooth graphical homotopy, let W be the smooth 4–manifold obtained by blowing up at all marked points and taking the complement of the proper transforms of $C_1^1, \dots, C_m^1$. (In the case of a picture deformation $\mathcal{C}^s$, W is the Milnor fiber $W_{\mathcal{C}^s}$ from Theorem 1.3).*

Then W carries a planar Lefschetz fibration that supports a Stein filling of (Y, ξ). When $W = W_{\mathcal{C}^s}$, the Lefschetz fibration is compatible with the Stein structure on the Milnor fiber.

The fiber of the Lefschetz fibration on W is a disk with m holes, and the vanishing cycles can be computed directly from the decorated curve configuration $C_1^1, \dots, C_m^1$. On (Y, ξ), the Lefschetz fibration induces a planar open book decomposition, which is independent of the smooth graphical homotopy of the given decorated germ $\mathcal{C}$.

Each rational singularity with reduced fundamental cycle has a distinguished *Artin* smoothing component, which corresponds to a picture deformation called the *Scott deformation*; see Section 4. Applying Theorem 1.4 to the Scott deformation yields a planar Lefschetz fibration filling (Y, ξ) where the vanishing cycles are disjoint; see Proposition 4.1. This gives a natural model for the planar open book decomposition on (Y, ξ). This open book is closely related to the braid monodromy of the singularity of $\mathcal{C}$. Note that we need to consider all singularities topologically equivalent to $(X, 0)$ to describe all Milnor fillings for (Y, ξ), since all such singularities have the same contact link. However, topologically equivalent singularities can be represented by topologically equivalent decorated germs and produce the same open book decompositions.

The process of computing the monodromy factorization resembles a known strategy for monodromy calculation for a plane algebraic curve; see Moishezon and Teicher [40; 41]. The necessary information can be encoded by a *braided wiring diagram* given by the intersection of $\mathcal{C}^s$ with a suitably chosen copy of $\mathbb{C} \times \mathbb{R} \subset \mathbb{C}^2$.

A reversal of the above constructions allows us to represent Stein fillings of (Y,ξ) via arrangements of symplectic curves, as follows. Let W be an arbitrary Stein filling of the link (Y,ξ). We fix an open book for (Y,ξ) defined by the germ $\mathcal{C}$ as above. By Wendl's theorem, W can be represented by a Lefschetz fibration with the planar fiber given by the page. The Lefschetz fibration corresponds to a factorization of the open book monodromy into a product of positive Dehn twists. We reverse-engineer a braided wiring diagram producing this factorization, and then use the diagram to construct an arrangement Γ of symplectic disks. (In fact, an arrangement of smooth graphical disks is sufficient for our constructions, but the symplectic condition can be satisfied at no extra cost.) We require that the disks intersect transversally (multiple intersections are allowed), and equip Γ with a collection of marked points that include all intersections and possibly additional "free" points. We also show that the resulting arrangement of disks and points is related to the decorated germ $\mathcal{C}$ by a smooth homotopy, which is graphical in suitable coordinates. (The homotopy moves the disks and the marked points.) This yields a symplectic analog of Theorem 1.3.

Theorem 1.5 *Let (Y,ξ) be the contact link of a singularity $(X,0)$ with reduced fundamental cycle that corresponds to a decorated plane curve germ $\mathcal{C}$. Then any Stein filling of (Y,ξ) arises from an arrangement Γ of symplectic graphical disks with marked points, as in Theorem 1.4. The arrangement Γ is related to the decorated germ $\mathcal{C}$ by a smooth graphical homotopy.*

Theorems 1.3 and 1.5 mean that both Milnor fibers and arbitrary Stein fillings of a given link of rational singularity with reduced fundamental cycle can be constructed in a similar way, starting with the decorated plane curve germ $\mathcal{C}$ representing the singularity. Milnor fibers arise from algebraic picture deformations of the branches of $\mathcal{C}$, while Stein fillings come from smooth graphical homotopies of the branches.

Once the comparison of Milnor fibers and Stein fillings is reduced to comparison of arrangements of complex curves or smooth disks with certain properties, we can construct examples of arrangements that generate Stein fillings not diffeomorphic to Milnor fibers. We need arrangements that are related to a particular plane curve germ by a smooth graphical homotopy but not by an algebraic picture deformation. We build *unexpected line arrangements* satisfying this property in Section 7, using classical projective geometry and a study of analytic deformations. We use these to construct unexpected Stein fillings; then we verify that they are not diffeomorphic (relative to the boundary open book data) to Milnor fillings by an argument based on Némethi

and Popescu-Pampu [44]. This leads to the proof of Theorem 1.1 and other similar examples.

At first glance, the difference between algebraic and smooth plane curve arrangements seems rather obvious. However, because we are in an open situation, working with germs of curves and smooth disks with boundary as opposed to closed algebraic surfaces, the question is quite subtle. In particular, we cannot simply use known examples of topological or symplectic line arrangements in $\mathbb{C}\mathrm{P}^2$ not realizable by complex lines. Indeed, in many cases the smooth surfaces can be closely approximated by high-degree polynomials, so that a Lefschetz fibration on the corresponding Stein filling can be realized by a Milnor fiber. We discuss the relevant features of the picture deformations and smooth (or symplectic) graphical homotopies in detail in Section 8, and explain what makes our examples work.

It is worth stating that while Stein fillings and Milnor fillings are the same for certain small families of singularities, the two notions are in fact fundamentally different. A Milnor filling is given by a smoothing of a singular complex surface, so there is a family of Stein homotopic fillings of (Y,ξ) that degenerate to the singular surface. A Stein filling of the link has no *a priori* relation to the singular surface and is not part of any such family. This distinction becomes apparent in our present work, by the following heuristic reasoning. A picture deformation $\mathcal{C}^s$ of the decorated germ $\mathcal{C}$ gives, for any $s \neq 0$, a Milnor filling $W_{\mathcal{C}^s}$, so that all these fillings are diffeomorphic and even Stein homotopic. The Milnor fillings look the same for all $s \neq 0$ because the arrangements of deformed branches $\{C_1^s, \dots, C_m^s\}$ have the same topology. By contrast, if the germ $\mathcal{C}$ is homotoped via a family of smooth disk arrangements Γ^t, the topology of the arrangement $\{\Gamma_1^t, \dots, \Gamma_m^t\}$ may change during the homotopy. Under certain conditions we can construct a family of Lefschetz fibrations W_t that includes the given Stein filling and changes its diffeomorphism type at finitely many discrete times as it connects to the minimal resolution. In other cases, at some time t the homotopy gives an arrangement Γ^t which produces an *achiral* Lefschetz fibration, so the 4–manifolds in the corresponding family do not necessarily carry a Stein structure. We return to this discussion in Section 8.

One can also ask whether unexpected fillings exist for rational singularities with reduced fundamental cycle that are not covered by Theorem 1.1 or Theorem 1.2. For certain additional simple examples, we can use Theorem 1.5 and pseudoholomorphic curve arguments to verify that there are no unexpected fillings, even though the smoothing

may not be unique. This approach only works when the germ of the singularity is a pencil of lines satisfying certain restrictive constraints. Namely, we can consider

(1) arrangements of 6 or fewer symplectic lines, or

(2) arrangements of symplectic lines where one of the lines has at most two marked points where it meets all the other lines in the arrangement.

Since the boundary behavior of symplectic lines is controlled, we can cap off symplectic lines in a ball to symplectic projective lines in $\mathbb{C}\mathrm{P}^2$, together with the line at infinity. The corresponding arrangements in $\mathbb{C}\mathrm{P}^2$ are shown to have a unique symplectic isotopy class and are symplectically isotopic to an actual complex algebraic line arrangement in $\mathbb{C}\mathrm{P}^2$; see Starkston [59, Lemma 3.4.5]. It follows that every symplectic arrangement as above can be obtained as picture deformation of a pencil of complex lines, and therefore, the corresponding Stein fillings are given by Milnor fibers. The links of the corresponding singularities are Seifert fibered spaces, for which Stein fillings were completely classified and presented as planar Lefschetz fibrations in [59, Chapter 4]. The line arrangements appearing in that classification precisely coincide with the symplectic disk arrangements from the perspective of this article. (Here, gluing in the deleted neighborhood of the disk provides an embedding of the Stein filling into a blow-up of $\mathbb{C}^2$. In [59], gluing on the cap, which augments the configuration of lines by the additional line at infinity, provides an embedding of the Stein filling in a blow-up of $\mathbb{C}\mathrm{P}^2$.) In general, Theorem 1.5 seems to have limited applications to classification of fillings, due to complexity of arrangements of curves.

It is interesting to note that while de Jong and van Straten describe deformations of sandwiched singularities, our constructions only work for the subclass of rational singularities with reduced fundamental cycle. Indeed, a planar open book decomposition of the contact link plays a key role in our work because we need Wendl's theorem to describe Stein fillings. By Ghiggini, Golla and Plamenevskaya [19] the Milnor fillable contact structure on the link of a normal surface singularity is planar *only if* the singularity is rational and has reduced fundamental cycle. This means that our methods in the present paper cannot be used for classification for any other surface singularities. However, for future work, we are investigating extensions of these methods to produce examples of unexpected fillings for more general surface singularities. Finally, recall that all weak symplectic fillings of a planar contact 3–manifold are in fact given by planar Lefschetz fibrations, up to blow-ups and symplectic deformation; see Niederkrüger and Wendl [48]. It follows that Theorem 1.5 and related results apply to describe all

minimal weak symplectic fillings. However, we focus on Stein fillings and will give all statements, with the exception of Theorem 1.2, only for the Stein case.

Organization of the paper

In Section 2 we review the definitions of rational singularities with reduced fundamental cycle as well as their deformation theory from [27], and prove some of their properties from the topological perspective. In Section 3 we prove the first direction of the symplectic correspondence, namely Theorem 1.4. In Section 4 we explain the smoothing in the Artin component from the perspective of symplectic topology, discuss the corresponding open books, and also raise some questions related to open book factorizations and nonrational singularities. In Section 5 we prove the other half of the correspondence, establishing Theorem 1.5 using braided wiring diagrams and Wendl's theorem [65]. In Section 6 we prove Theorem 1.2 and explain how to calculate algebraic topological invariants of the fillings, which we will use to distinguish our examples of unexpected Stein fillings from Milnor fillings. In Section 7 we prove that there are many examples of unexpected Stein fillings for links of rational surface singularities with reduced fundamental cycle, establishing Theorem 1.1. Finally, in Section 8 we explain what key differences between picture deformations and smooth graphical homotopies contributed to the distinction between expected and unexpected Stein fillings.

Acknowledgements We are grateful to Stepan Orevkov for suggesting Example 7.14 to us. This example played a crucial role in our understanding of arrangements that produce unexpected fillings. We thank Roger Casals, Eugene Gorsky and Marco Golla for their interest in this project and numerous motivating and illuminating discussions in the early stages of this work. In particular, Eugene helped us understand some of the results of [27]. We are grateful to Eugene and Marco for their comments on the preliminary version of this article, and to Jonathan Wahl, Jeremy Van Horn-Morris and Patrick Popescu-Pampu for interesting correspondence. Many thanks to İnanc Baykur for illuminating correspondence and discussion on the higher genus case. Starkston would also like to thank Sari Ogami, who learned and explained to her a great deal about the monodromy of braided wiring diagrams. Plamenevskaya is also grateful to John Etnyre, Jonny Evans, Mark McLean and Oleg Viro for a few helpful discussions. We thank the referees for their thoughtful comments and suggestions. Plamenevskaya was supported by NSF grants DMS-1510091 and DMS-1906260 and a Simons Fellowship. Starkston was supported by NSF grant DMS-1904074.

2 Rational singularities with reduced fundamental cycle, their decorated curve germs, and relation to deformations

In this section, we collect some facts about rational singularities with reduced fundamental cycle and state de Jong and van Straten's results on their smoothings [27]. De Jong and van Straten's results are in fact more general: they fully describe deformation theory for a wider class of *sandwiched* singularities. We state only the results we need. Some of our statements are slightly different from [27]: we describe their constructions from the topological perspective and set the stage for our work. Although we aim for a mostly self-contained discussion, the reader may find it useful to consult [42] for a general survey on topology of surface singularities. The survey [56] focuses on the interplay between singularity theory and contact topology and provides very helpful background. Additionally, a brief survey of the key results of [27] from the topological perspective can be found in [44].

2.1 Resolutions and smoothings.

We begin with some general facts about surface singularities. Let $(X,0)$ be a normal surface singularity. Its resolution $\pi\colon \widetilde{X} \to X$ is a proper birational morphism such that $\widetilde{X}$ is smooth. The *exceptional divisor* $\pi^{-1}(0)$ is the inverse image of the singular point. For a given singularity $(X,0)$, the resolution is not unique, as one can always make additional blow-ups; however, for a surface singularity, there is a unique *minimal* resolution [31]. The minimal resolution is characterized by the fact that $\widetilde{X}$ contains no embedded smooth complex curves of genus 0 and self-intersection -1 (thus it does not admit a blow-down).

After performing additional blow-ups if necessary, we can assume that the exceptional divisor $\pi^{-1}(0)$ has normal crossings. This means that $\pi^{-1}(0) = \bigcup_{v\in G} E_v$, where the irreducible components E_v are smooth complex curves that intersect transversally at double points only. A resolution with this property is called a *good* resolution. For a surface singularity, a minimal good resolution is also unique [31].

The topology of a good resolution is encoded by the (dual) resolution graph G. The vertices $v \in G$ correspond to the exceptional curves E_v and are weighted by the genus and self-intersection $E_v \cdot E_v$ of the corresponding curve. We will often refer to $E_v \cdot E_v$ as the self-intersection of the vertex v, and use the notation $v \cdot v$ for brevity. The edges of G record intersections of different irreducible components. Note that the link of the

singularity is the boundary of the plumbing of disk bundles over surfaces according to G. In this paper, we focus on *rational* singularities; in this case G is always a tree, and each exceptional curve E_v has genus 0. (Genus 0 curves are also called *rational curves*.) Therefore we will typically omit the genus from the markings on the vertices and only record the self-intersection numbers.

It is well known that the dual resolution graph of every normal surface singularity is negative definite, and conversely, every negative definite connected graph corresponds to some normal surface singularity; see eg [42]. The link of the singularity determines the dual graph of the minimal good resolution, and vice versa. By a result of W Neumann [47], the links of two normal surface singularities have the same oriented diffeomorphism type if and only if their dual resolution graphs are related by a finite sequence of blow-ups/blow-downs along rational (-1) curves. Moreover, the links of two normal surface singularities are orientation-preserving diffeomorphic if and only if their minimal good resolutions have the same dual graphs. Minimal good resolutions are easy to recognize: if a good resolution is not minimal, its graph will have a vertex representing a genus 0 curve with self-intersection -1. (This follows from [47]; see also [19, Lemma 5.2] for a direct proof that any possible blow-downs can be seen directly from the graph.)

The local topological type of the singularity $(X,0)$ can be understood from its link Y, as a cone on the corresponding 3–manifold. We will say that two singularities are *topologically equivalent* if they have the same link. It is important to note that the analytic type of the singularity is not uniquely determined by the link; typically, many analytically different singularities have diffeomorphic links. It is known that the canonical contact structures are all isomorphic for different singularities of the same topological type [11]; thus, the dual resolution graph encodes the canonical contact structure. Indeed, this contact structure can be recovered as the convex boundary of the plumbing, according to the graph, of the standard neighborhoods of the corresponding symplectic surfaces.

We now turn our attention to deformations and Milnor fibers. A deformation of a surface singularity $(X,0)$ is any flat map $\lambda\colon(\mathcal{X},0)\to(\mathcal{T},0)$ such that $\lambda^{-1}(0)=(X,0)$. A versal (or semiuniversal) deformation $f\colon(\mathcal{X},0)\to(B,0)$ parametrizes all possible deformations of $(X,0)$. The base space $(B,0)$ generally has multiple irreducible components, which may have different dimensions. It is generally difficult to understand the space B, its irreducible components, and the dimensions of these components.

A deformation $\lambda:(\mathcal{X},0)\to(D,0)$ over the disk in $\mathbb{C}$ is called a (1–parameter) *smoothing* of $(X,0)$ if $X_s:=\lambda^{-1}(s)$ is smooth for all $s\neq 0$. For any smoothing all such X_s are diffeomorphic, and we call X_s the *Milnor fiber* of the smoothing. For example, for a hypersurface $X=\{f(x,y,z)=0\}\subset\mathbb{C}^3$ with $f(0)=0$ and $df(0)=0$, a smoothing of the singularity at 0 can be given by $f:\mathbb{C}^3\to\mathbb{C}$, with Milnor fiber $X_\epsilon=\{f(x,y,z)=\epsilon\}$ for a small $\epsilon\neq 0$. Each Milnor fiber is endowed with a Stein structure, and for different $t_0,t_1\in D\setminus 0$, X_{s_0} and X_{s_1} are Stein homotopic (the Stein homotopy is obtained by choosing a path from s_0 to s_1 in D which avoids 0).

We need to work with a compact version of the Milnor fiber. For a sufficiently small radius $r>0$, the surface $X\subset\mathbb{C}^N$ is transverse to the sphere S_r^{N-1}. We fix a ball $B_r^N\subset\mathbb{C}^N$ centered at 0, sometimes called *a Milnor ball*, and consider $X\cap B_r^N$ as the *Milnor representative* of X. The boundary $\partial(X\cap B_r^N)$ is the link Y of $(X,0)$, and the complex structure on X induces the canonical contact structure ξ on Y. For sufficiently small $s\neq 0$, we can similarly find a compact version of X_s whose boundary is contactomorphic to the link (Y,ξ), which provides a Stein filling of (Y,ξ).

For a semiuniversal deformation $f:(\mathcal{X},0)\to(B,0)$ of the surface singularity $(X,0)$, an irreducible component B_i of B is called a *smoothing component* of $(X,0)$ if the general fiber over B_i is smooth. We note that B_i may have lower (complex) dimensional strata where the fibers over these strata are not smooth. For example, these nongeneral strata could arise from singularities in the component B_i or intersections of B_i with other irreducible components of B. Nevertheless, these nongeneral strata have positive complex codimension, so the subset of B_i over which the fiber is smooth will be connected. Any 1–parameter smoothing of $(X,0)$ lies in a unique smoothing component B_i.

In general, not every surface singularity admits a smoothing. However, for rational singularities every irreducible component of B is a smoothing component; see [5] and also [56, Theorem 4.24]. Moreover, there is one distinguished component, called the *Artin component*. This component is associated to the minimal resolution $\widetilde{X}$ of $(X,0)$; see [5] and also [56, Theorem 4.25]. (For rational singularities, deformations of $\widetilde{X}$ come from deformations of $(X,0)$, and these deformations of $(X,0)$ form the Artin component.) We discuss Milnor fibers in this component in greater detail in Section 4.

In this paper, we study Stein fillings for the contact link (Y,ξ) of a surface singularity, and compare them to Milnor fillings. As explained above, in general the link determines only the topological, but not the analytic, type of the singularity. Normal surface singularities whose topological type admits a unique analytic type are called *taut*; if there are only finitely many analytic types, the singularity is *pseudotaut*. Taut and

pseudotaut singularities were classified by Laufer [32]: there are several very restrictive lists for the dual resolution graphs, in particular, the graphs cannot have any vertices of valency greater than 3. Thus, most singularities are not (pseudo)taut, even if we restrict to a very special kind that we consider in this paper, rational singularities with reduced fundamental cycle. If we are to compare Stein fillings and Milnor fillings of the link, we need to consider Milnor fibers for *all* possible singularities of the given topological type. In principle, it is quite possible that topologically equivalent singularities have nondiffeomorphic Milnor fibers: for example, the hypersurface singularities $x^2+y^7+z^{14}=0$ and $x^3+y^4+z^{12}=0$ have the same topological type, but their (unique) Milnor fibers have different b_2; see [33] and also the discussion in [56, Section 6.2]. Fortunately, in the case of reduced fundamental cycle we will have some control over the topology of Milnor fibers for different analytic types, thanks to the de Jong–van Straten construction.

2.2 Sandwiched singularities, extended graphs, and decorated germs

Definition 2.1 $(X,0)$ is a *rational singularity with reduced fundamental cycle* if it admits a normal crossing resolution such that all exceptional curves have genus 0, the dual resolution graph G is a tree, and for each vertex $v\in G$, the valency $a(v)$ of v and the self-intersection $v\cdot v$ satisfy the inequality

$$a(v)\le -v\cdot v. \tag{2-1}$$

It follows from (2-1) that the graph as above can only have vertices with self-intersection -1 as the leaves of the tree. Blowing down all such vertices, we obtain a graph that still satisfies (2-1) and represents the minimal resolution of $(X,0)$.

To explain the terminology of Definition 2.1, we recall the definition of a fundamental cycle. For a given resolution, consider the set of divisors

$$\left\{ Z=\sum_{v\in G} m_v E_v \;\middle|\; Z>0, \text{ and } Z\cdot E_v\le 0 \text{ for all } E_v \right\}.$$

This set has a partial order, defined by $\sum m_v E_v \ge \sum n_v E_v$ if $m_v\ge n_v$ for all v. There is a minimal element with respect to this partial order, denoted by $Z_{\min}$ and called Artin's fundamental cycle. The resolution dual graph is connected, different components E_v intersect positively, and $Z>0$, so any element in the set has $m_v>0$. Therefore, $Z_{\min}\ge \sum_{v\in G} E_v$. It is easy to see that $\big(\sum_{v\in G} E_v\big)\cdot E_v\le 0$ for all E_v if and only if condition (2-1) is satisfied. In this case $Z_{\min}=\sum_{v\in G} E_v$, and since each exceptional curve enters with multiplicity 1, we say that the fundamental cycle $Z_{\min}$ is reduced.

In [27], de Jong and van Straten work with *sandwiched* singularities. By definition, a sandwiched singularity $(X,0)$ is analytically isomorphic to the germ of an algebraic singular surface which admits a birational morphism to $(\mathbb{C}^2,0)$. For a resolution $\pi\colon \widetilde{X}\to X$, we get a diagram $(\widetilde{X},\pi^{-1}(0)) \dashrightarrow (X,0) \dashrightarrow (\mathbb{C}^2,0)$. In particular, X is sandwiched between two smooth spaces via birational maps. Sandwiched singularities are rational and can be characterized by their resolution graphs as follows, by translating the sandwiched condition. The graph G is *sandwiched* if we can add to it a number of edges and their end vertices with self-intersections (-1), so that the resulting graph G' gives a plumbing whose boundary represents S^3. In other words, G' gives a configuration of rational curves that can be blown down to a smooth point. The choice of the graph G' is not unique. It is not hard to see that every rational singularity with reduced fundamental cycle is sandwiched. In Proposition 2.2 below, we discuss in detail the construction of the possible graphs G' for this case.

Any sandwiched singularity can be associated to a (germ of a) complex plane curve singularity, constructed as follows. The choice of the graph G' corresponds to an embedding of the tubular neighborhood of the exceptional set of the resolution $\widetilde{X}$ into some blow-up of $\mathbb{C}^2$. This blown-up surface also has a distinguished collection of (-1) curves, so that the configuration of these (-1) together with the exceptional set can be completely blown down. For each distinguished (-1) curve, choose a transverse complex disk (called a *curvetta*) through a generic point. Now, contract the curve configuration corresponding to G'. The union of the curvettas becomes a germ of a reducible curve $\mathcal{C}$ in $\mathbb{C}^2$, with components passing through 0. Let C_i, $i=1,2,\dots,m$, be the irreducible components of $\mathcal{C}$; following [27], we also refer to C_i as *curvettas*. We emphasize that only the germ of $\mathcal{C}$ at the origin is defined; when we use the notation $\mathcal{C}\subset\mathbb{C}^2$, we only consider a small neighborhood of $0\in\mathbb{C}^2$. In particular, we are only interested in the singularity of the reducible curve $\mathcal{C}$ at 0. In this paper, we will focus on the case where the components C_i are smooth at 0, so that locally C_i is a smooth disk. This suffices to study rational singularities with reduced fundamental cycle, as we will soon see. This disk may be locally parametrized by a high-degree algebraic curve in $\mathbb{C}^2$, but the global topology of this curve is unimportant to us, because we only use the part of the curve in a neighborhood of the origin.

Each curvetta C_i comes with a weight $w_i = w(C_i)$, given by the number of exceptional spheres that intersect the corresponding curve in the blow-down process from G' to the empty graph. In other words, w_i is the number of blow-down steps that affect the corresponding curvetta before it becomes C_i. The weighted curve $(\mathcal{C},w)$ is called a

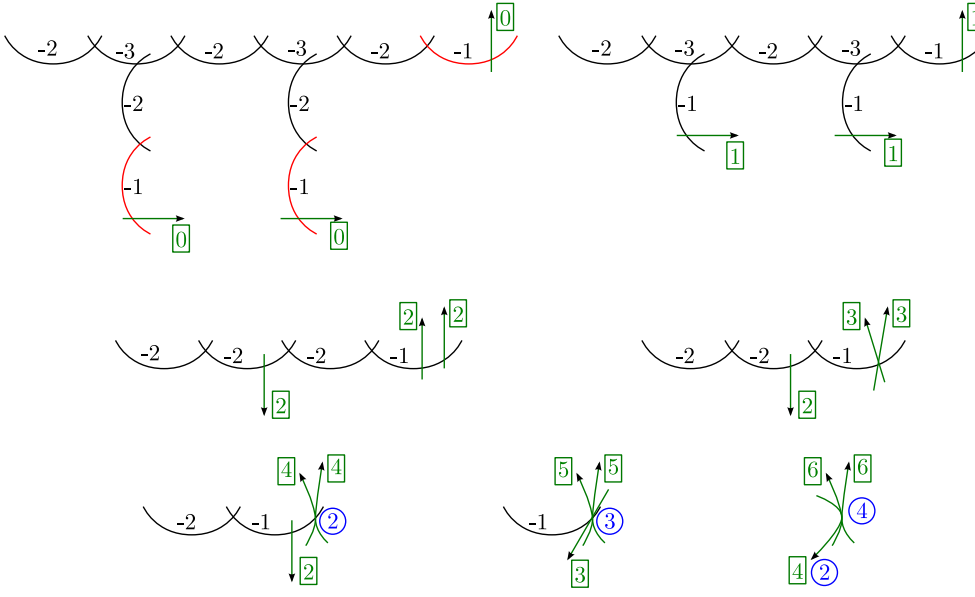

Figure 2: An example of a sandwiched singularity and a choice of corresponding curvettas (green arrows). The first diagram shows the resolution curves together with extra (red) (-1) exceptional curves attached. Then there is a sequence of blow-downs. We keep track of the weights $w(C_i)$ in rectangular boxes next to each green curvetta arrow. The multiplicities of tangencies between bunches are recorded in blue circled numbers.

decorated germ corresponding to $(X, 0)$. An example of this process, and the resulting decorated germ for the given singularity, is shown in Figure 2.

It is convenient to start the process with the minimal normal crossings resolution of $(X, 0)$. For rational singularities with reduced fundamental cycle, it is easy to see that the graph of the minimal normal crossings resolution has no (-1) vertices. (From (2-1), only vertices of valency 1 can have self-intersection -1 in any resolution graph, and these can be blown down to get the minimal graph.) If G has no (-1) vertices, then *all* the (-1) vertices of G' are those that come from the extension: each (-1) vertex is a leaf of G', connected by an edge to a unique vertex of G. The transverse curvetta slices are added to all these (-1) vertices.

In what follows, we will only consider decorated germs that arise from the above construction. (These are called *standard* decorated germs in [44]. Some statements in [27] allow for more general decorated germs.)

The singularity $(X,0)$ can be reconstructed from $(\mathcal{C},w)$. We iteratively blow up points infinitely near 0 on proper transforms of curvettas $C_1,\dots,C_k$ until we obtain a minimal embedded resolution of $\mathcal{C}$. Then we perform additional blow-ups at the intersection of C_i with the corresponding exceptional curve, so that the sum of multiplicities of proper transforms of C_i at the blow-up points is exactly w_i. The union of the exceptional curves that *do not* meet the proper transforms of the curvettas is then contracted to form $(X,0)$.

We emphasize that $\mathcal{C}$ depends on the choice of the graph G', ie on the particular extension of the resolution graph of $(X,0)$ by (-1) curves. Any of these choices can be used to classify Milnor fillings as in [27]. In general, the branches of $\mathcal{C}$ are singular curves. However, if $(X,0)$ is a rational singularity with reduced fundamental cycle, an appropriate choice of G' ensures that $\mathcal{C}$ has smooth branches. We will always work in this setting and only consider decorated germs with smooth components. In the following proposition, we establish a necessary and sufficient condition for smoothness purely in terms of the graph G'. Although similar questions were studied in [27; 26], we formulate the condition here in a way that seems simplest from the topological point of view. In the next section, we will reinterpret the statement for open book decompositions.

Proposition 2.2 *Let the graph G' be a negative definite plumbing tree, and P' the corresponding plumbing of disk bundles over rational curves. Suppose that the boundary of the plumbing P' is S^3; equivalently, G' encodes a configuration of rational curves that can be blown down to a smooth point. For each (-1) vertex, let $\widetilde{C}_j$ be a complex disk intersecting the corresponding (-1) sphere in P' transversally once. Let $C_1,\dots,C_m$ be the images of $\widetilde{C}_1,\dots,\widetilde{C}_m$ under blowing down the configuration G'. Then the following are equivalent*:

(1) *Each C_j is smooth.*

(2) *There exists exactly one $v_0'\in G'$ such that*

$$\begin{aligned} v_0'\cdot v_0' + a(v_0') &= -1,\\ v'\cdot v' + a(v') &= 0 \quad \text{for all } v'\neq v_0'. \end{aligned}$$

(We will often refer to v_0' as the *root*.)

As before, $v'\cdot v'$ denotes the self-intersection of a vertex $v'\in G'$, and $a(v')$ its valence.

Proof Consider $\mathcal{C} = C_1 \cup \cdots \cup C_m$ with smooth branches C_j. We obtain G' as described above, by blowing up repeatedly at intersections of the C_j with each other and with the exceptional divisors. We stop when the resulting configuration of curves has the following property: if an exceptional divisor intersects a proper transform $\widetilde{C}_j$ then it is disjoint from all other proper transforms $\widetilde{C}_{j'}$, $j' \neq j$ (in particular, different $\widetilde{C}_j$ are disjoint from each other), and the total number of blow-ups performed on (proper transforms of) C_j is exactly w_j, the weight on C_j.

We will show that G' has the structure of a rooted tree by repeatedly applying the following procedure. For the root v_0', we will have $v_0' \cdot v_0' + a(v_0') = -1$, and for all other vertices $v' \neq v_0'$, $v' \cdot v' + a(v') = 0$. We show that this condition is satisfied at every stage of the process.

Blow up at the common intersection point of all C_j. The resulting exceptional divisor (and its future proper transforms) gives the root of the tree. If proper transforms of all C_j still have a common point, we repeatedly blow up at the same point until some of the proper transforms $\widetilde{C}_j$ become disjoint from each other. (With a slight abuse of notation, $\widetilde{C}_j$ will denote the proper transform of C_j at any stage of the process.) Additional blow-ups create a chain of exceptional (-2) spheres with the root at one end and the most recent exceptional (-1) sphere at the other end. Up to relabeling, we can assume there are distinct intersection points $\widetilde{C}_1 \cap \cdots \cap \widetilde{C}_{a_1} = p_1^1$, $\widetilde{C}_{a_1+1} \cap \cdots \cap \widetilde{C}_{a_2} = p_2^1, \ldots, \widetilde{C}_{a_{r_1}^1} \cap \cdots \cap \widetilde{C}_m = p_{r_1}^1$ lying on the most recently introduced exceptional divisor B_1.

Assuming $m > 1$, since all the $\widetilde{C}_j$ intersect B_1, we must blow up exactly once at each p_i^1 to make them all disjoint from B_1. Here we use smoothness of the curvettas C_j (and thus of their proper transforms) to ensure that they become disjoint from B_1 after a single blow-up: every point on C_j has multiplicity 1, thus $\widetilde{C}_j$ intersects each exceptional divisor with multiplicity at most 1. Note that once $\widetilde{C}_1, \ldots, \widetilde{C}_m$ are all disjoint from B_1, we will not blow up at any point on B_1 again, therefore at this stage we can already compute the self-intersection and valency of the corresponding vertex in G'. The self-intersection of the proper transform of B_1 in G' (which we will also denote by B_1) is $-r_1 - 1$. If B_1 is not the root, it has valency $r_1 + 1$, and if it is the root it has valency r_1. Thus, condition (2) is satisfied for the vertex of G' given by B_1. All the other vertices in the graph at this stage are either (-2) spheres in a chain of valency 2 (if not the root) or valency 1 (if the root), or newly introduced (-1) vertices of valency 1, so condition (2) is satisfied at this stage.

In order to obtain G' we repeat this process iteratively, replacing the first exceptional sphere with the exceptional sphere obtained by blowing up at some p_i^s. (The points $p_1^1, \dots, p_{r_1}^1$ were introduced above; after blowing up at each of these new points, the new exceptional curves intersect the proper transforms of the curvettas at points $p_1^2, \dots, p_{r_2}^2$; similarly, points $p_i^s, \dots, p_{r_s}^s$ are the intersections that appear at step s.) Each time, condition (2) is preserved, since each curve $\widetilde{C}_j$ intersects each exceptional divisor with multiplicity at most 1. Repeating sufficiently many times, eventually all of the $\widetilde{C}_j$ will intersect only disjoint exceptional spheres. After potentially blowing up more times at the intersection of $\widetilde{C}_j$ with its intersecting exceptional sphere until the number of blow-ups is w_j, we obtain G'. (The additional blow-ups create a chain of (-2) vertices connecting to the last (-1) vertex.) Since condition (2) is preserved at each step of this procedure, G' satisfies condition (2).

Conversely, if G' satisfies condition (2), the only (-1) vertices are leaves of the rooted tree (valency 1). Blowing down a leaf preserves condition (2) because it decreases the valency of the adjacent vertex by 1 and increases the self-intersection by 1. The $\widetilde{C}_j$ are disks which transversally intersect the (-1) leaves of G' with multiplicity 1. Therefore each $\widetilde{C}_j$ intersects each exceptional divisor with multiplicity at most 1. This property is preserved under blowing down a (-1) leaf, because a multiplicity 1 intersection of $\widetilde{C}_j$ on a (-1) leaf becomes a multiplicity 1 intersection on the adjacent exceptional divisor after blowing down. Blowing down an exceptional divisor which intersects $\widetilde{C}_j$ with multiplicity 1 preserves smoothness of $\widetilde{C}_j$. Therefore after blowing down all leaves of G' and finally the root, the resulting proper transforms C_j are still smooth. □

Remark 2.3 Another way to see that G' must satisfy condition (2) is to consider what happens if G' has a vertex with $a(v') > -v' \cdot v'$. After blowing down, eventually the vertex v' will correspond to a (-1) sphere with valency ≥ 2, with at least one $\widetilde{C}_j$ intersecting it with multiplicity at least 1. (The existence of the intersecting $\widetilde{C}_j$ comes from the fact that intersections are transferred under blow-down to the adjacent vertices. Initially, every (-1) sphere in G' has an intersecting curvetta. Each time that a (-1) sphere is blown down, the curvetta intersection is transferred to the adjacent vertices, whose self-intersections are correspondingly increased. For v' to reach self-intersection -1, one must have blown down (-1) vertices adjacent to it. Throughout the process of blowing down, we maintain the condition that (-1) vertices always have at least one intersecting curvetta.) After blowing down the (-1) sphere of valency ≥ 2, we obtain a point where at least two exceptional divisors intersect at the same point

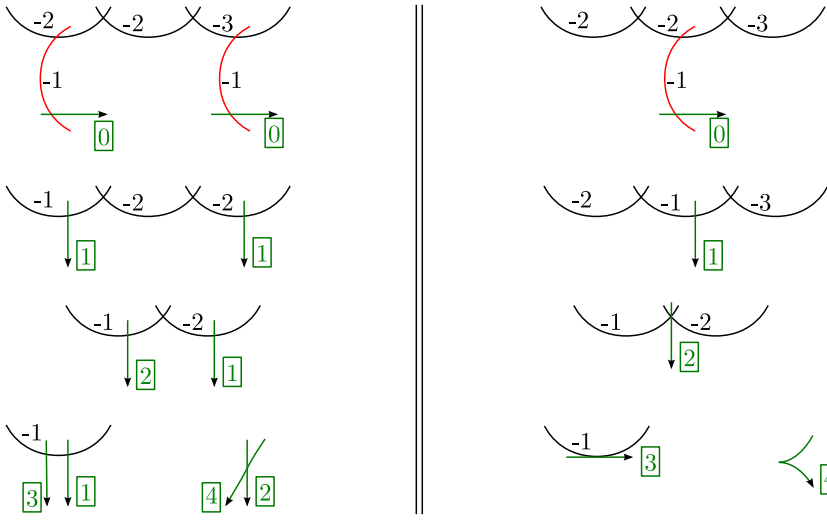

Figure 3: Two possible choices to add -1 curves to the same resolution graph, resulting in different curvettas, one with smooth components and another with a singular (cuspidal) component.

with a $\widetilde{C}_j$. Eventually one of these exceptional divisors will be blown down, forcing $\widetilde{C}_j$ to intersect the other exceptional divisor with multiplicity ≥ 2. Once this other exceptional divisor is blown down, the proper transform of $\widetilde{C}_j$ becomes singular.

Note that it is possible to have different choices of extension for G, such that one choice yields smooth curvettas and another yields singular curvettas; see Figure 3 for an example. In other words, some sandwiched resolution graphs G have extensions both to a graph which does satisfy condition (2) of Proposition 2.2 and to a graph which does not. For our classifications, we will always work with a choice of extension of G which does satisfy condition (2) and the corresponding smooth curvettas.

We can also deduce some basic numerical properties from Proposition 2.2. It turns out that for a rational singularity $(X, 0)$ with reduced fundamental cycle, the multiplicity of the singular point determines the number of choices for the defining plane curve germ $\mathcal{C}$ with smooth branches, as well as the number of curvetta branches in each such germ. Assuming that $(X, 0) \subset (\mathbb{C}^N, 0)$ for some large N, recall that the multiplicity mult X can be defined geometrically as the number of intersections $\#X \cap L$ of X with a generic complex $(N-2)$–dimensional affine subspace $L \subset \mathbb{C}$, passing close to the origin. For rational singularities, multiplicity is a topological invariant, which can be

computed from the resolution graph by the formula $\operatorname{mult} X = -Z_{\min}^2$; see eg [42]. The two statements below are also discussed in [27] from the algebrogeometric perspective, but they follow easily from the combinatorics of the resolution graph.

Proposition 2.4 *Let $(X,0)$ be a rational singularity with reduced fundamental cycle, and $\mathcal{C}$ a plane curve germ corresponding to $(X,0)$. If $\mathcal{C}$ has smooth branches, the number of branches is given by* $\operatorname{mult} X - 1$.

Proof The minimal normal crossings resolution graph G for $(X,0)$ has no (-1) vertices. Then G is obtained from (any choice of) the graph G' by deleting all vertices $v' \in G'$ with $v' \cdot v' = -1$. The curvetta branches are obtained by putting transverse slices on each (-1) sphere $v' \in G'$, thus the number m of curvetta branches is given by the number of the (-1) vertices in G'. By condition (2) of Proposition 2.2,

$$\sum_{v' \in G'} (v' \cdot v' + a(v')) = -1.$$

Again by condition (2), each (-1) vertex has valency 1 in G', so each addition of a (-1) vertex to G increases the sum $\sum_{v \in G}(v \cdot v + a(v))$ by 1, thus we have

$$\sum_{v \in G}(v \cdot v + a(v)) = \sum_{v' \in G'} (v' \cdot v' + a(v')) - m = -1 - m.$$

Finally, we relate this quantity to the fundamental cycle $Z_{\min}$, which is the sum of homology classes of the exceptional divisors, $Z_{\min} = \sum_{v \in G} E_v$:

$$\sum_{v \in G}(v \cdot v + a(v)) = \sum_{v} E_v^2 + \sum_{v \neq u} E_v \cdot E_u = Z_{\min}^2.$$

So $m = -1 - Z_{\min}^2 = \operatorname{mult} X - 1$. □

Decorated germs representing a given $(X,0)$ are obtained from extensions G' of the resolution graph G as above. These can be thought of as combinatorial choices for the decorated germ; in the next lemma, we compute the number of such extensions. Then, we show that the combinatorial choice, namely the choice of vertices of G on which the additional (-1) vertices are placed to form G', determines the *topological type* of the resulting decorated germ. By definition, the topological type of a germ of a singular curve $\mathcal{C} \subset \mathbb{C}^2$ is given by its link, which is the intersection of $\mathcal{C}$ with a sufficiently small 3–sphere $S^3 \subset \mathbb{C}^2$ centered at the origin. For a decorated germ, we additionally record the weights of the curvetta components. Later on, we will see that the different choices of G' correspond to natural different choices of data on the open book decomposition we construct in Section 4.

Lemma 2.5 *Up to topological equivalence, there are at most* mult X *choices of plane curve germs with smooth branches representing* $(X,0)$.

Proof We first show that there are at most mult $X = -Z_{\min}^2$ possible *combinatorial choices* for germs with smooth components representing $(X,0)$. These correspond to choices of extensions of G to G' by adding (-1) vertices. If we have a minimal graph G with an extension G' satisfying condition (2) of Proposition 2.2, then we can add another (-1) sphere leaf adjacent to the root to get a new graph G'' so that the valency of each vertex of G'' equals its negative self-intersection. All the other possible extensions of G to a graph satisfying condition (2) can be obtained by deleting one of the (-1) vertices of G''. (Indeed, adding a (-1) vertex to any other position in G would violate condition (2).) Since G' has (mult $X-1$) vertices of self-intersection -1, we know that G'' has exactly mult X vertices with this property, one of which must be deleted. Note that because of potential symmetries in the graph G'', some of the choices of G' will result in isomorphic germs C, but mult X gives an upper bound on the number of combinatorially different curvetta configurations.

Once the choice of the extension G' of the graph G is made, the topological type of the decorated germ $\mathcal{C}$ can be read off directly from G'. In particular, we can compute the relevant numerical invariants, such as linking numbers between the components of $\mathcal{C} \subset \mathbb{C}^2$. As before, we assume that G' satisfies condition (2) of Proposition 2.2, so that $\mathcal{C}$ has smooth branches.

Following [27, Definition 4.14], we define the *length* and *overlap* functions on the vertices of the graph G. For $v_0, v_i \in G$, let the length $l(v_0, v_i)$ be the number of vertices in the path from v_i to v_0 in the tree G (including endpoints). For $v_0, v_i, v_j \in G$, let the overlap $\rho(v_i, v_j; v_0)$ be the number of common vertices in the paths from v_i to v_0 and v_j to v_0.

Let $v_0 \in G \subset G'$ be the root. Now, if the curvetta C_i comes from the transverse slice on a (-1) sphere corresponding to a leaf of G', and this leaf is attached to the vertex $v_i \in G$, then the blow-down process gives $w(C_i) = 1 + l(v_0, v_i)$. If C_i and C_j are the curvettas at the (-1) vertices attached to v_i and v_j, the order of tangency $\operatorname{tang}(C_i, C_j)$ between the corresponding branches of $\mathcal{C}$ is given by $\operatorname{tang}(C_i, C_j) = \rho(v_i, v_j; v_0)$.

The topological type of $\mathcal{C} \subset \mathbb{C}^2$ is described via its link, given by the intersection $\mathcal{C} \cap S^3$, where S^3 is a small sphere centered at the origin. As each of the curvettas $C_1, \dots, C_m$ is a smooth disk, the intersection of C_i with S^3 is an unknot; $\mathcal{C} \cap S^3$ is a link with m components $C_1 \cap S^3, \dots, C_m \cap S^3$, each of them unknotted. The components of

$C_i \cap S^3$ are oriented as boundaries of $C_i \cap B^4$. Then, the linking number between two link components equals the order of tangency between the corresponding curvettas,

$$\mathrm{lk}(C_i \cap S^3, C_j \cap S^3) = \mathrm{tang}(C_i, C_j).$$

The topological equivalence of germs follows from the above calculations, by construction of the links of the germs that we consider; it can also be seen more directly. Any decorated germ for $(X, 0)$ comes, after a blow-down, from a particular placement of the transverse curvetta slices on the (-1) curves corresponding to vertices that we added to G to from the graph G'. This gives a configuration of curvetta slices together with the curve configuration corresponding to the graph G', embedded in a blow-up of $\mathbb{C}^2$. Clearly, for two different choices of the generic curvetta slices for the same graph G', the two configurations of curvettas+curves can be identified by an ambient homeomorphism (in the blown-up $\mathbb{C}^2$). After the blow-down, the induced ambient homeomorphism will identify the links of the resulting germs, showing that the germs are topologically equivalent. We already know that the weights will be same, so the decorated germs have the same topological type. □

The following observation will also be useful later. Let $t(C_i) = \max_j \mathrm{tang}(C_i, C_j)$ be the maximal order or tangency between C_i and another branch of $\mathcal{C}$. Then it follows that

$$t(C_i) < w(C_i) \tag{2-2}$$

for all curvettas C_i.

Remark 2.6 De Jong and van Straten [27] study deformation theory of the surface singularity $(X, 0)$; in particular, they are interested in the analytic type of the singularity and its deformations. To encode the analytic type of $(X, 0)$, one needs the analytic type of the corresponding decorated germ $\mathcal{C}$. By contrast, our focus is on the contact link (Y, ξ) of $(X, 0)$ and its Stein fillings. A priori there may be another surface singularity $(X', 0)$ whose link is Y, and by [11], the singularities $(X, 0)$ and $(X', 0)$ have contactomorphic links. By Neumann's results [47], all singularities with the same link have the same dual graph of minimal resolution, so both $(X, 0)$ and $(X', 0)$ correspond to the same minimal graph G. (Note that by [32], if G has any vertices of valency greater than 3, the analytic type of the singularity is not uniquely determined, so indeed $(X, 0)$ and $(X', 0)$ may be analytically different in the above scenario.) We can compare the decorated germs that describe singularities $(X, 0)$ and $(X', 0)$: any choice of the decorated germ for $(X, 0)$ arises from an extension G' of the graph G and

the corresponding placement of the curvettas. Although analytically the exceptional divisors of resolutions of $(X,0)$ and $(X',0)$ may be different, topologically they look the same, and we can choose the same extension G' and the corresponding placement of curvettas for $(X',0)$. By the argument above, the resulting germ for $(X',0)$ will be topologically equivalent to the germ for $(X,0)$, even if the two germs may be analytically different. This fact will play an important role in the proof of Theorem 7.8. In particular, the two germs will have the same number of branches, the same weights and the same pairwise orders of tangency for the branches.

Of course, if we only know the combinatorics of the graph G, we lose analytic information on the plane curve germ $\mathcal{C}$ (such as, for example, the angles between its transverse branches), but we will never need the analytic information. The contact 3–manifold (Y,ξ) is fully determined by the weights and pairwise orders of tangency of the branches of the decorated germ $\mathcal{C}$.

2.3 De Jong–van Straten theory: Milnor fibers from germ deformations

The main result of [27] says that deformations of the sandwiched singularity can be encoded via deformations of the germ $(C,0)$ satisfying certain hypotheses. We will state a special case of their theorem that will be relevant to us, but first we introduce some notation.

We have defined the weights as positive integers w_i associated to the irreducible components (curvettas) C_i of $\mathcal{C}$. It will be convenient to interpret the weight w_i as a collection of w_i marked points concentrated at $0 \in C_i$. More formally, we consider a subscheme $w(i)$ of length w_i at 0 in C_i. The normalization $\widetilde{\mathcal{C}}$ of the reducible curve $\mathcal{C}$ with smooth components is given by the disjoint union of the components C_i; thus we can think of the decoration $w = (w_1, w_2, \dots, w_m)$ as a subscheme of $\widetilde{\mathcal{C}}$, with components $w(i) \subset C_i$ as above. (We use the notation $\widetilde{\mathcal{C}}$ for normalization here and in the discussion below. Similar notation $\widetilde{C}_j$ had a different meaning in Proposition 2.2, though in a sense, both uses refer to resolutions of the curve $C_j \subset \mathcal{C}$. This should not lead to confusion as normalization is only mentioned in the next few paragraphs.)

De Jong and van Straten prove that for sandwiched singularities, 1–parameter smoothings correspond to *picture deformations*, which are 1–parameter deformations of the germ $\mathcal{C}$ together with the subscheme w. In fact, de Jong and van Straten describe all deformations of $(X,0)$, but in this paper we are only interested in smoothings. Since we do not use their results in full generality, we omit some technical points and give simpler versions of the definitions and statements from [27].

Informally, picture deformations look as follows. The deformation $\mathcal{C}^s$ is given by individual deformations C_i^s of the curvetta components, so that the deformed germ $\mathcal{C}^s$ is reduced and has irreducible smooth components C_i^s corresponding to the original curvettas. (In the case of plane curves, any deformation is given by *unfolding*, ie by deforming the defining equation of the curve.) The deformation is required to eliminate tangencies between the curvettas, so that for $s \neq 0$ all deformed curvettas C_i^s intersect transversally. Thus, the only singularities of the deformed germ $\mathcal{C}^s = \bigcup_i C_i^s$ for $s \neq 0$ are transverse multiple points. For $s = 0$, the decoration w consists of w_i marked points on the curvetta C_i for each $i = 1, \dots, m$, concentrated at 0. During the deformation, these marked points move along the curvettas, so that for $s \neq 0$, the deformed curvetta C_i^s contains exactly w_i *distinct* marked points, and all intersection points $C_i^s \cap C_j^s$ for $j \neq i$ are marked.

More formally, deforming the curvettas C_i individually means that we consider δ–constant deformations of the reducible germ $\mathcal{C} = \bigcup_i C_i$. Intersection points between deformed curvettas define the total multiplicity scheme m^s on the normalization $\widetilde{\mathcal{C}}^s$ for $s \neq 0$; if all intersections are transverse, the corresponding divisor is reduced, ie each point enters with multiplicity one. The requirement that all intersection points are marked means that the deformation $w^S \subset \widetilde{\mathcal{C}} \times S$ of the decoration w must satisfy the condition $m^s \subset w^s$. The requirement that all marked points be distinct on each C_i^s for $s \neq 0$ is the same as saying that the divisor given by w_i^s is reduced for $s \neq 0$. The condition $m^s \subset w^s$ then implies automatically that all singularities of the deformed germ $\mathcal{C}^s$ are ordinary multiple points, ie the deformed curvettas intersect transversally.

Definition 2.7 A picture deformation $\mathcal{C}^S$ of the decorated germ $(\mathcal{C}, w)$ with smooth components $C_1, \dots, C_m$ over a germ of a smooth curve $(S, 0)$ is given by a δ–constant deformation $\mathcal{C}^S \to S$ of $\mathcal{C}$ and a flat deformation $w^S \subset \widetilde{\mathcal{C}^S} = \widetilde{\mathcal{C}} \times S$ of the scheme w such that for $s \neq 0$, the divisor w^s is reduced, the only singularities of $\mathcal{C}^s$ are ordinary multiple points, and $m^s \subset w^s$.

Strictly speaking, w^S lives in the normalization, but for $s \neq 0$ we can think of w^s as the set of marked points $\{p_1, p_2, \dots, p_n\} \subset \bigcup_{i=1}^m C_i^s$ such that *all* intersection points $C_i^s \cap C_j^s$ are marked. We say that p_i is a *free* marked point if it lies on a single C_i^s (away from the intersections). (Note that these points, and the number of such points n, can generally be different for different picture deformations.)

With these definitions in place, de Jong and van Straten's results on smoothings are as stated in Theorem 1.3: every picture deformation of $(\mathcal{C}, w)$ gives rise to a smoothing

of the corresponding surface singularity $(X,0)$, and every smoothing arises in this way. Specifically, the Milnor fiber of the smoothing that corresponds to the picture deformation $\mathcal{C}^s = \bigcup_{i=1}^m C_i^s \subset \mathbb{C}^2$ with marked points $\{p_1, p_2, \dots, p_n\}$ is obtained by blowing up $\mathbb{C}^2$ at all points $p_1, p_2, \dots, p_n$ and taking the complement of the proper transforms of $C_1^s, \dots, C_m^s$ in $\mathbb{C}\#\#_{j=1}^n \overline{\mathbb{C}\mathrm{P}}^2$. Picture deformations of $\mathcal{C}$ generate all Milnor fibers, that is, each Milnor fiber of $(X,0)$ arises from some picture deformation of $(X,0)$ via this construction. Note that Theorem 1.3 makes no claim of a precise one-to-one correspondence between picture deformations and smoothings: one expects that isomorphic smoothings only come from isomorphic picture deformations (in the appropriate sense), but this has not been established. In certain cases, one can distinguish Milnor fibers by their topological invariants, or by comparing incidence matrices of the corresponding curvetta arrangements; see [27, Section 5] or [44]. We discuss this in Section 6 and use a similar technique to distinguish Stein fillings.

Remark 2.8 To be more precise, we need to consider the compact version of the construction of Milnor fibers, as follows. Fix a closed Milnor ball $B \subset \mathbb{C}^2$ for the germ $\mathcal{C}$. For sufficiently small $s \neq 0$, the deformed arrangement $\mathcal{C}^s$ will have a representative in B which meets $\partial B = S^3$ transversally, and all marked points $p_1, \dots, p_n$ are contained in the interior of B. Let $\widetilde{B}$ be the blow-up of B at $p_1, \dots, p_n$. Because in the picture deformation all the intersections between deformed curvettas are transverse, the proper transforms of $C_1^s, \dots, C_m^s$ in $\widetilde{B}$ will be disjoint smooth disks. Let $T_1, \dots, T_m$ be pairwise disjoint tubular neighborhoods of these proper transforms. As a compact 4–manifold with boundary, the Milnor fiber that corresponds to $\mathcal{C}^s$ is given by $W = \widetilde{B} \setminus \bigcup_{i=1}^m T_i$, after corners are smoothed, and the Stein structure is homotopic to the complex structure induced from the blow-up.

3 Graphical deformations of curvettas yield fillings

Let $(X,0)$ be a rational surface singularity with reduced fundamental cycle, and consider the associated decorated germ $(\mathcal{C}, w)$ of a reducible plane curve as in the previous section, with smooth branches $C_1, C_2, \dots, C_m$ equipped with weights. Our goal is to build an analog of [27] in the symplectic category: it turns out that Stein fillings of the link of $(X,0)$ can be obtained from certain *smooth* homotopies of the branches of the decorated germ $\mathcal{C}$. We will restrict to graphical homotopies to streamline our definition and constructions. (In our setting, one can always choose an appropriate coordinate system, so the graphical hypothesis leads to no loss of generality.)

Fix a closed Milnor ball B for $\mathcal{C}$ as in Remark 2.8, so that each branch C_i intersects ∂B transversally. If B is small enough, the complex coordinates (x, y) in $\mathbb{C}^2$ can be chosen so that all branches $C_1, C_2, \dots, C_m$ are graphical in B: $C_i = \{y = f_i(x)\}$. We will consider smooth graphical arrangements $\Gamma = \{\Gamma_1, \Gamma_2, \dots, \Gamma_m\}$ such that each Γ_i is a smooth graphical disk, so that $\Gamma_i = \{y = g_i(x)\}$ for a smooth function g_i, and Γ_i intersects ∂B transversally.

The following definition is given for homotopies of the branches defined for a real parameter $t \in [0, 1]$. Sometimes we will use the same notion for homotopies defined in a parameter interval $t \in [0, \tau]$, with obvious notational changes. We assume that coordinates (x, y) are chosen as above.

Definition 3.1 Let $(\mathcal{C}, w)$ be a decorated plane curve germ, with weights $w_i = w(C_i)$ of its smooth graphical branches $C_1, C_2, \dots, C_m$. A *smooth graphical homotopy* of $(\mathcal{C}, w)$ is a smooth homotopy C_i^t of the branches of $\mathcal{C}$, so that $\mathcal{C} = \bigcup_{i=1}^m C_i^0$, together with distinct marked points p_k, $k = 1, \dots, n$ (for some n), on $\bigcup_{i=1}^m C_i^1$. We assume that in a Milnor ball B the following conditions are satisfied:

(1) Each branch is given by $C_i^t = \{y = f_i^t(x)\}$ for a function $f_i^t(x) = f_i(x, t)$ smooth in (x, t), and C_i^t intersects ∂B transversally for all t.

(2) Intersections between the branches remain in the interior of B during the homotopy.

(3) At $t = 1$, all intersections of any two branches C_i^1 and C_j^1 are positive and transverse.

(4) At $t = 1$, all intersection points on each branch C_i^1 are marked, and there may be additional free marked points. Each free point lies in the interior of B on a unique branch C_i^1. The total number of marked points on C_i^1 is w_i.

The choice of Milnor ball B is unimportant as all our considerations are local. For brevity, we will often omit B from notation and talk about decorated germs and their homotopies in $\mathbb{C}^2$. In that case, we implicitly work in a fixed neighborhood of the origin, and assume that all intersections between branches which begin in this neighborhood remain in this neighborhood during the homotopy, and thus the components of the arrangement have controlled behavior near the boundary of the neighborhood.

Conditions (1) and (2) are automatically satisfied for "small" homotopies. Indeed, if t is close to 0, C_i^t is C^1–close to C_i. The reducible curve $\mathcal{C}$ with smooth branches has a

finite set of tangent directions at the origin, and the branches C_i^t will have tangent spaces lying in a small neighborhood of these directions in the Grassmannian of symplectic planes in $\mathbb{C}^2$. Therefore we can choose coordinates so that the fiber of the projection avoids these directions. We only include the intersection of the branches of $\mathcal{C}$ at 0 in the Milnor ball B, so for small t, intersections will remain in B. For larger homotopies, we require these conditions nontrivially.

Picture deformations satisfy all of the conditions (1)–(4), so a picture deformation is a special case of a smooth graphical homotopy of the germ (in appropriate coordinates). In contrast to picture deformations of [27], condition (4) on the marked points and the weight restrictions is only required at $t = 1$ for homotopies. For a closer analogy with Definition 2.7, we can consider marked points $\{p_i^j(t)\}_{j\in\{1,\dots,w_i\}}$ on C_i^t for all $0 \le t \le 1$. For $t = 0$, the marked points are concentrated at the origin on each branch, giving the decoration of $(\mathcal{C}, w)$. Suppose that $p_i^j(t)$, $0 \le t \le 1$, are smooth functions describing the motion of marked points during homotopy, so that $p_i^j(t) \in C_i^t$ for all t. For $t = 1$, the points $p_i^j(1) = p_i^j$ satisfy condition (4) above. This implies, in particular, that at $t = 1$, the branch C_i^t has no more than w_i intersection points with other branches. However, for $0 < t < 1$, the marked points $p_i^j(t)$ are not subject to any restrictions and have little significance. The homotoped curvettas C_i^t can have an arbitrary number of intersections, and intersections may be positive or negative. By contrast, for picture deformations, the weights control the number of intersection points between deformed curvettas at all times, the intersections between branches are always marked during deformation, and all intersections are positive because curvettas are deformed through complex curves.

Let (Y, ξ) be the link of the singularity $(X, 0)$ with the decorated germ $(\mathcal{C}, w)$. We will show that every smooth graphical homotopy of the germ $\mathcal{C}$ gives rise to a Stein filling of (Y, ξ).

First, we focus on the curvetta arrangement $\{C_1^1, C_2^1, \dots, C_m^1\}$ with marked points, produced at the end of homotopy at the time $t = 1$. Lemma 3.2 below produces a certain Lefschetz fibration from this input. The lemma applies to any arrangement of smooth graphical disks $\{\Gamma_1, \Gamma_2, \dots, \Gamma_m\}$ satisfying the stated hypotheses; the homotopy is not used at this stage. We use different notation to emphasize that $\{\Gamma_i\}$ need not be related to $\mathcal{C}$. Then, Lemma 3.4 uses the homotopy between the decorated germ $(\mathcal{C}, w)$ and the curvetta arrangement $\{C_1^1, C_2^1, \dots, C_m^1\}$ with its marked points $p_1, p_2, \dots, p_n$ to show that the open book on the boundary of the Lefschetz fibration supports (Y, ξ). It follows that our construction produces a Stein filling of (Y, ξ).

As a smooth 4–manifold, the filling produced by Lemma 3.2 is constructed similarly to the Milnor fibers in Theorem 1.3. Namely, we blow up at each of the intersection points of the homotoped curvettas, as well as at the free marked points, and then take the complement of the proper transforms of the curvettas. Even though C_i^1 are smooth disks (rather than complex curves), we will assume that they are locally modeled on complex curves near the intersection point, so the blow-up and the proper transforms can be understood in the usual sense. Alternatively, one could also think about the proper transform in the smooth sense, as the closure of the complement of the blown-up point; see [20, Definitions 2.2.7 and 2.2.9]. To obtain a 4–manifold with given boundary, we consider a compact version of the construction in a Milnor ball, as explained in Remark 2.8. It is convenient to consider the Milnor ball of the form $B = D_x \times D_y \subset \mathbb{C}^2$, with corners smoothed, where D_x and D_y are disks in the coordinate planes $\mathbb{C}_x$ and $\mathbb{C}_y$. For every $x_0 \in D_x$, the graphical disks Γ_i intersect $\{x_0\} \times D_y$ transversally, and the intersection with $\partial(D_x \times D_y)$ lies as a braid in $\partial D_x \times D_y$. To simplify notation, we do not mention the Milnor ball B explicitly in the first part of the lemma.

Lemma 3.2 *Let $\Gamma_1, \dots, \Gamma_m$ be smooth disks in $\mathbb{C}^2$ which are graphical with respect to the projection π_x, that is, $\Gamma_i = \{y = f_i(x)\}$. Assume that at each intersection point of two or more Γ_i, there exists a neighborhood U of the intersection such that $\bigcup_i \Gamma_i$ is cut out by complex linear equations inside U. (Up to graphical isotopy, this only requires the Γ_i to intersect transversally and positively with respect to the orientation on the graph Γ_i induced from the natural orientation on $\mathbb{C}$.) Let $p_1, \dots, p_n$ be points on the disks Γ_i which include all intersection points, and let $\alpha\colon \mathbb{C}^2 \# n\overline{\mathbb{C}\mathrm{P}}^2 \to \mathbb{C}^2$ be the blow-up at the points $p_1, \dots, p_n$. Let $\widetilde{\Gamma}_1, \dots, \widetilde{\Gamma}_m$ denote the proper transforms of $\Gamma_1, \dots, \Gamma_m$. Then $\pi_x \circ \alpha\colon (\mathbb{C}^2 \# n\overline{\mathbb{C}\mathrm{P}}^2) \setminus (\widetilde{\Gamma}_1 \cup \dots \cup \widetilde{\Gamma}_m) \to \mathbb{C}$ is a Lefschetz fibration whose regular fibers are punctured planes, where each puncture corresponds to a component $\widetilde{\Gamma}_i$. There is one vanishing cycle for each point p_j, which is a curve in the fiber enclosing the punctures that correspond to the components Γ_i passing through p_j.*

Similarly, if $B = D_x \times D_y$ is a Milnor ball that contains all the points $p_i, \dots, p_n$ and contains $(D_x \times \mathbb{C}) \cap \left(\bigcup_i \Gamma_i\right)$, and T_i is a small tubular neighborhood of $\widetilde{\Gamma}_i$, then $\pi_x \circ \alpha\colon (\alpha^{-1}(D_x \times D_y)) \setminus (T_1 \cup \dots \cup T_m) \to D_x$ is a Lefschetz fibration with compact fiber. The fiber is a disk with holes corresponding to the components Γ_i. The vanishing cycles correspond to the points p_j in the same way.

If the curvettas $C_1^s, \dots, C_m^s$ with marked points are the result of picture deformation of the germ (C, w) associated to a surface singularity, then the Lefschetz fibration

constructed as above is compatible with the complex structure on the Milnor fiber of the corresponding smoothing.

Proof Before blowing up, the projection $\pi_x\colon \mathbb{C}^2 \to \mathbb{C}$ is clearly a fibration, and the smooth disks Γ_i are sections of this fibration. If they were disjoint sections, then their complement would be a fibration whose fiber is $\mathbb{C}$ with m punctures. Since the sections intersect, we blow up at each of the intersection points, along with blow-ups at other chosen points on the curves. For each fiber containing one of the p_j where we blow up, the corresponding fiber in the blow-up is the total transform, which is a nodal curve containing the exceptional sphere and the proper transform of the fiber. More specifically, translating the coordinates (x, y) on $\mathbb{C}^2$ to be centered at p_j, the coordinates on the blow-up are

$$\mathbb{C}^2 \# \overline{\mathbb{C}\mathrm{P}}^2_{p_i} = \{((x, y), [u : v]) \mid xv = yu\}.$$

The singular fiber is the total transform of $F = \{x = 0\}$, which has two irreducible components:

$$\big(E = \{((0, 0), [u : v])\}\big) \cup \big(\widetilde{F} = \{((0, y), [0 : 1])\}\big).$$

The node occurs at the intersection of these two components at $((0, 0), [0 : 1])$. Therefore in a neighborhood of the node we can take $v = 1$, so we have local coordinates on the blow-up given by $(y, u) \in \mathbb{C}^2$ where $x = yu$. The projection $\pi_x \circ \alpha$ is given in these coordinates by

$$\pi_x \circ \alpha(y, u) = yu,$$

which is exactly the model for a Lefschetz singularity at $(y, u) = (0, 0)$.

In the coordinate chart on $\mathbb{C}^2$ centered at p_j, let $\Gamma_i = \{(x, f_i(x))\}$. The total transforms of the curves Γ_i which pass through p_j — ie which have $f_i(0) = 0$ — are given by

$$\big(E = \{((0, 0), [u : v])\}\big) \cup \left(\widetilde{\Gamma}_i = \left\{\left((x, f_i(x)), \left[1 : \lim_{a \to x} \frac{f_i(a)}{a}\right]\right)\right\}\right),$$

and those which do not pass through p_j — ie which have $f_i(0) \neq 0$ — lift isomorphically to the blow-up

$$\big\{\big((x, f_i(x)), [x : f_i(x)]\big)\big\}.$$

Note that the proper transforms do not pass through the node $((0, 0), [0 : 1])$. Moreover, since the intersections between the Γ_i were assumed to be transverse, $\lim_{a \to 0} f_i(a)/a$ have different values for different values of i where $f_i(0) = 0$. Therefore, the $\widetilde{\Gamma}_i$

are disjoint sections of the Lefschetz fibration from the blow-up of $\mathbb{C}^2$ to $\mathbb{C}$, so their complement gives a Lefschetz fibration with punctured fibers. Moreover, in the singular fibers, the sections which intersect the exceptional sphere part of the fiber are precisely the proper transforms $\widetilde{\Gamma}_i$ such that Γ_i passed through p_j.

Regular neighborhoods T_i of the $\widetilde{\Gamma}_i$ can be chosen sufficiently small to be disjoint from each other and the Lefschetz singular points, thus yielding the compact Lefschetz fibration. This changes the fiber (converting the punctures into holes) but does not change the fibration structure and the vanishing cycles. The total space of a Lefschetz fibration over a disk is a compact 4–manifold with boundary; the fibration induces a planar open book decomposition on the boundary.

In the case of a picture deformation of the germ (C, w), the deformed curvettas $C_1^s, C_2^s, \dots, C_m^s$ are smooth complex disks with marked points satisfying the hypotheses of the lemma. The Stein structure induced by the Lefschetz fibration is compatible with the complex structure on the Milnor fiber, because $\pi_x \circ \alpha$ is holomorphic. □

Consider a smooth graphical arrangement $\Gamma = \{\Gamma_1, \dots, \Gamma_m\}$ in a Milnor ball $B = D_x \times D_y$, such that each Γ_i transversally intersects the vertical part $\partial D_x \times D_y$ of ∂B and is disjoint from $D_x \times \partial D_y$. Taking the boundaries of the graphical disks, we have an m–braid $\partial\Gamma = \partial\Gamma_1 \cup \partial\Gamma_2 \cup \cdots \cup \partial\Gamma_m \subset \partial B = S^3$. (Each component $\partial\Gamma_i$ is an unknot, but the components are linked.) The monodromy of this braid is called the monodromy of the arrangement Γ. We can interpret the braid group on m strands as the mapping class group $\mathrm{MCG}(\mathbb{C}_m)$ of the m–punctured plane. Then the braid $\partial\Gamma$ is identified with the monodromy ϕ_Γ of the $\mathbb{C}_m$–bundle over S^1, given by the projection $\pi_x : \mathbb{C}^2 \setminus \bigcup_{i=1}^m \Gamma_i \to \mathbb{C}$ restricted to the preimage $\pi_x^{-1}(\partial D_x)$ of the circle $\partial D_x \subset \mathbb{C}$.

To construct the Lefschetz fibration corresponding to Γ in Lemma 3.2, we perform blow-ups at points p_i that project to the interior of D_x. These blow-ups do not affect the bundle over ∂D_x. Therefore, the noncompact version of the Lefschetz fibration (with fiber $\mathbb{C}_m$) has the monodromy ϕ_Γ given by the braid $\partial\Gamma$.

For the compact version of the Lefschetz fibration from Lemma 3.2, the general fiber P_m is the disk D_y with m holes. The fibration induces an open book on its boundary, with page P_m. The boundary of the total space of the fibration $\mathcal{L}^s$ is the union of two parts: the horizontal boundary $\partial P_m \times D$, which forms the binding of the open book, and the vertical boundary, a fiber bundle over $S^1 = \partial D_x$ with fiber P_m, which forms

the mapping torus for the open book. This fiber bundle is given by the projection $(\pi_x \circ \alpha)^{-1}(\partial D_x) \to D_x$, which is the same as the projection $\pi_x \colon B \setminus \bigcup_{i=1}^m \Gamma_i \to D_x$ restricted to $\pi_x^{-1}(\partial D_x)$, because the blow-up map α is the identity over ∂D_x. Let $\phi \colon P_m \to P_m$ denote the monodromy of this fiber bundle, ie the monodromy of the open book. We then have a commutative diagram

$$\begin{array}{ccc} P_m & \xrightarrow{\phi} & P_m \\ \downarrow & & \downarrow \\ \mathbb{C}_m & \xrightarrow{\phi_\Gamma} & \mathbb{C}_m \end{array}$$

where the vertical maps are inclusions. This proves:

Lemma 3.3 *Let $\Gamma = \{\Gamma_1, \dots, \Gamma_m\}$ be a smooth graphical arrangement with marked points $\{p_j\}$, and $B = D_x \times D_y$ a Milnor ball whose interior contains all marked points, such that $\Gamma_i \cap (D_x \times \mathbb{C}) \subset B$ and Γ_i is transverse to ∂B for all $i = 1, \dots, m$. Let ϕ_Γ be the monodromy of the braid $\partial\Gamma = \partial\Gamma_1 \cup \cdots \cup \partial\Gamma_m \subset \partial B = S^3$.*

Let $\phi \colon P_m \to P_m$ be the monodromy of the open book induced by the Lefschetz fibration constructed for $(\Gamma, \{p_j\})$ in Lemma 3.2. Then ϕ_Γ is the image of ϕ under the projection

$$\eta \colon \mathrm{MCG}(P_m) \to \mathrm{MCG}(\mathbb{C}_m)$$

induced by the inclusion $P_m \hookrightarrow \mathbb{C}_m$ of the compact disk with m holes into the m–punctured plane.

When the arrangement $(\Gamma, \{p_j\})$ is related to the decorated germ $(\mathcal{C}, w)$ by a smooth graphical homotopy, the monodromy ϕ_Γ of the braid $\partial\Gamma$ is the same as the monodromy of the braid $\partial\mathcal{C} = \partial C_1 \cup \cdots \cup \partial C_m$, because the homotopy between disks gives an isotopy of the two boundary braids. By definition, the braid monodromy of $\partial\mathcal{C}$ is the monodromy φ of the singular point of $\mathcal{C}$.

We next examine the monodromy of the open book corresponding to Γ in the case of the compact fiber, and find its relation to the monodromy of the singular curve $\mathcal{C}$.

Lemma 3.4 *Let $\{\Gamma_1, \dots, \Gamma_m\}$ and $\{\Gamma_1', \dots, \Gamma_m'\}$ be two smooth graphical arrangements, such that the boundary braid of are braid-isotopic (respecting labels) and the weights on the corresponding components agree. Let $\mathcal{L}$ and $\mathcal{L}'$ be the corresponding Lefschetz fibrations constructed in Lemma 3.2. Then the induced open book decompositions on the boundary have the same page and same monodromy.*

We will prove the lemma after pointing out its consequences. Since the plane curve arrangements at either end of a smooth graphical homotopy have braid-isotopic boundaries, and the weights on the components remain constant during the smooth graphical homotopy, it follows that the open book decomposition induced on the boundary for any Lefschetz fibration arising in this way is independent of the choice of smooth graphical homotopy.

For the case where (Γ, w) is the end point of a *picture deformation* of a plane curve germ $(\mathcal{C}, w)$, $\mathcal{L}'$ is a Lefschetz fibration on the (compactified) Milnor fiber of the associated smoothing of the surface singularity $(X, 0)$, as in Theorem 1.3. In this case the boundary of the Milnor fiber is the link Y of the singularity $(X, 0)$, and the Milnor fiber gives a Stein filling of the canonical contact structure ξ on the link, so the open book supports ξ. Because every rational singularity has a picture deformation yielding a Milnor fiber arising in such a manner (see Section 4 in our case), the open book on the boundary of any Lefschetz fibration arising from the endpoint of a smooth graphical homotopy of the same germ must support the canonical contact structure on the link of the singularity.

Combining Lemmas 3.2 and 3.4 with this discussion completes the proof of Theorem 1.4, which we summarize in the following corollary.

Corollary 3.5 *A smooth graphical homotopy of the decorated germ $(\mathcal{C}, w)$ gives rise to a Stein filling of the link (Y, ξ) of the corresponding singularity.*

Proof of Lemma 3.4 Applying the previous discussion and Lemma 3.3 to the arrangement $\Gamma = \{\Gamma_1, \Gamma_2, \dots, \Gamma_m\}$, we see that the homomorphism $\eta\colon \mathrm{MCG}(P_m) \to \mathrm{MCG}(\mathbb{C}_m)$ sends the open book monodromies ϕ and ϕ' to the same braid monodromy $\varphi \in \mathrm{MCG}(\mathbb{C}_m)$. The kernel of the map $\eta\colon \mathrm{MCG}(P_m) \to \mathrm{MCG}(\mathbb{C}_m)$ is generated by the boundary-parallel Dehn twists around the holes in the fiber P_m. (Recall that the monodromy of an open book is considered *rel* boundary of the page, so while the twists around individual strands are trivial in the braid case, the boundary twists become nontrivial for open books.) It follows that the monodromies ϕ and ϕ' of the open books on the boundaries of $\mathcal{L}$ and $\mathcal{L}'$ can differ *only* by boundary twists, since $\eta(\phi) = \eta(\phi') = \varphi$.

Let T_i denote a positive Dehn twist around the i^{th} hole. Then we have

$$\phi' = \phi \circ T_1^{\alpha_1} \circ T_2^{\alpha_2} \circ \cdots \circ T_m^{\alpha_m} \tag{3-1}$$

for some integers $\alpha_1, \alpha_2, \dots, \alpha_m$. The order is unimportant since the boundary twists are in the center of $\mathrm{MCG}(P_m)$.

It remains to pin down the boundary twists around each hole, ie to show that $\alpha_i = 0$ for every $i = 1, \dots, m$. To do so, we need to take into account the blow-ups at the free marked points p_i (the marked points that lie on the branches away from the intersections). These correspond to boundary twists. Recall a basic fact about diffeomorphisms of a planar surface *rel* boundary: for any two factorizations Ψ and Ψ' of $\psi : P_m \to P_m$, the number of Dehn twists that enclose a given hole h is the same for Ψ and Ψ'. (Here, we count all twists, not only the boundary ones.) The above statement easily follows from the fact that lantern relations generate all relations in the mapping class group of a planar surface [36], and the number of Dehn twists enclosing a given hole is unchanged under a lantern relation. This implies that the number of Dehn twists enclosing the i^{th} hole is well defined for a monodromy $\psi : P_m \to P_m$; let $n_i = n_i(\psi)$ denote this number. If two monodromies ϕ and ϕ' are related by (3-1), we have

$$n_i(\phi') = n_i(\phi) + \alpha_i. \tag{3-2}$$

On the other hand, the number n_i is determined by the vanishing cycles of the Lefschetz fibration. By construction of the fibration $\mathcal{L}^1$ associated to the homotopy $\mathcal{C}^t$, the number of Dehn twists enclosing the i^{th} hole is given by the number of blow-ups at the marked points on C_i^1, which in turn equals the weight w_i of the component C_i of the original germ $\mathcal{C}$. So $n_i(\phi) = w_i = n_i(\phi')$, and $\alpha_i = 0$ from (3-2). □

Remark 3.6 Our description of the open book monodromy for an arrangement is somewhat similar to E Hironaka's results [24] on the monodromy of complexified real line arrangements in $\mathbb{C}^2$. An important difference is that we consider Lefschetz fibrations on the complement of the proper transform of the curves in a blow-up of $\mathbb{C}^2$, while Hironaka computes the monodromy of the fiber bundle over S^1 obtained by projecting the complement of the complex lines in $\mathbb{C}^2$ to a circle of large radius; compare with the proof of Lemma 3.4. She also considers the setting with compactified fibers, by taking the complement of tubular neighborhoods of the lines, and computes the monodromy of line arrangements as an element of $\mathrm{MCG}(P_m)$. It is important to note that even in the compactified setting, her answers are different from the monodromy of the corresponding Lefschetz fibrations that we consider. (The difference is given by some boundary twists.) The discrepancy appears because when the tubular neighborhoods of the C_i^1 are removed from $\mathbb{C}^2$, their parametrization is induced from $\mathbb{C}^2$. When we blow up and take proper transforms of C_i^1, the parametrization of tubular neighborhoods is induced by the Lefschetz fibration structure on the blown-up manifold. These two

parametrizations are different in the two settings, affecting the choice of the meridian of the tubular neighborhood of a line and the framing of the boundary of the corresponding hole.

4 The Lefschetz fibration for the Artin smoothing

4.1 The Scott deformation

We can now use a specific deformation to describe the monodromy of the open book decomposition of (Y,ξ). We will use a canonical deformation, called the *Scott deformation* in [27], which yields a smoothing in the Artin component. This deformation yields a particularly nice arrangement of curvettas where the associated Lefschetz vanishing cycles are disjoint. This in turn yields a model factorization for the monodromy of the boundary open book decomposition. In Proposition 6.7, we will show that the corresponding Stein filling is uniquely recognizable from its combinatorics. Recall that $\operatorname{tang}(C_i,C_j)$ stands for the order of tangency between branches C_i and C_j of $\mathcal{C}$, and $t(C_i)=\max_j \operatorname{tang}(C_i,C_j)$.

Proposition 4.1 *Let $(X,0)$ be a rational surface singularity with reduced fundamental cycle, and $(\mathcal{C},w)$ one of its decorated reducible plane curve germs with m smooth irreducible components. Let (Y,ξ) be the contact link of $(X,0)$. Then (Y,ξ) has a planar open book decomposition whose page is a disk with m holes $h_1,\dots,h_m$, corresponding to the branches of $\mathcal{C}$. The open book monodromy admits a factorization into **disjoint** positive Dehn twists with the following properties*:

(1) *For any two branches C_i and C_j, the corresponding holes h_i and h_j are enclosed by exactly $\operatorname{tang}(C_i,C_j)$ of these Dehn twists.*

(2) *There are $w(C_i)-t(C_i)>0$ boundary Dehn twists around the hole h_i.*

(3) *There is at least one positive Dehn twist about the outer boundary component of the page.*

Proof We use the picture deformation of $(\mathcal{C},w)$ referred to as the *Scott deformation* in [27, Proposition 1.10]. This deformation arises from iteratively applying the following procedure. (We refer the reader to [27; 1] for details, including the explanation why the procedure below can be actually realized by a 1–parameter deformation.)

The input of the procedure is an isolated singular point p of a plane curve C with multiplicity m. In our case C is a union of smooth components, and the multiplicity m

is the number of components through the point p. The output of the procedure is a deformation C' whose singularities are

(I) one m–fold point where m branches intersect transversally, and

(II) the collection of singularities occurring on the proper transform of C in the blow-up of $\mathbb{C}^2$ at p.

The idea of the deformation is to blow up at p, perform a small deformation of the curves so that the singularities of the proper transform become disjoint from the exceptional divisor, and then blow down the exceptional divisor to return to the plane and obtain the curve C'.

We demonstrate this process in an example in Figure 4. The initial configuration in the bottom left consists of five curves. The curves C_1 and C_2 are tangent with multiplicity 3, and these two curves are tangent to C_3 with multiplicity 2. The curves C_4 and C_5 are transverse to C_1, C_2 and C_3 but tangent to each other with multiplicity 4. After blowing up at the common intersection point, we obtain the proper transforms together with an exceptional divisor as shown in the top left of Figure 4. Now C_1 and C_2 are tangent with multiplicity 2 and transversally intersect C_3 at the same point on the exceptional divisor. The curves C_4 and C_5 become disjoint from C_1, C_2 and C_3, and they are tangent to each other with multiplicity 3 at another point on the exceptional divisor. Next we perform the deformation of the curves, fixing the exceptional divisor, but translating the proper transforms $\widetilde{C}_1, \widetilde{C}_2, \dots, \widetilde{C}_5$ of the curvettas slightly so that the intersection of the exceptional divisor with the proper transforms now occurs away from the intersections of the proper transforms with each other, as shown in the top right of Figure 4. Finally, we blow down the exceptional divisor, which results in a transverse intersection of the resulting curvettas $C_1^s, C_2^s, \dots, C_5^s$ together with the singularities (intersections) of the proper transforms, as required.

Since the multiplicity of the orders of tangency between components decreases each time we take the proper transform, applying this procedure iteratively to the singularities of type (II) eventually yields a deformation to a plane curve with only transverse intersections. See Figure 5 for the iterations of the Scott deformation in our example, until all of the singularities are transverse intersection points. When working with a decorated germ $(\mathcal{C}, w)$, with the marked points of w initially concentrated at 0, the same blow-up procedure will separate the marked points. Indeed, if there are additional marked points which increase the weight, they can be separated by additional iterations

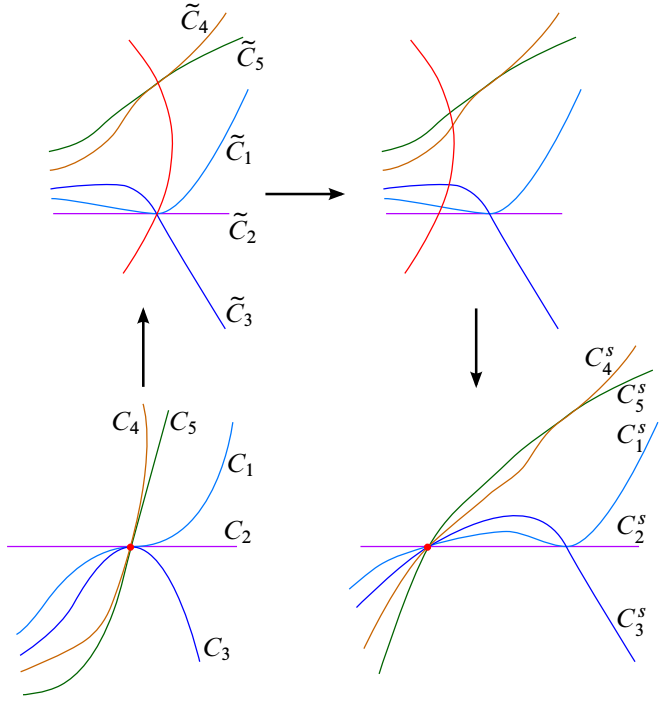

Figure 4: One iteration of the Scott deformation in an example.

of the blow-ups and translations, so that at the end all marked points are disjoint. (In this sense the scheme w^s is reduced.) Note that the total weight $w(C_i)$ of each component is equal to the total number of marked points on that component (including the intersection points).

When the components of $\mathcal{C}$ are smooth, the result of this deformation is as follows. If some components of $\mathcal{C}$ were tangent to order r_1 before the deformation, they will all

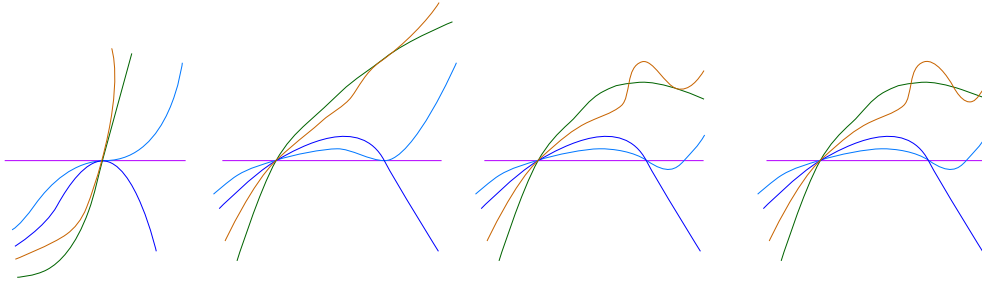

Figure 5: A Scott deformation applied iteratively until all intersections are transverse.

pass through the same r_1 transverse multipoints $p_{i_1}, \dots, p_{i_{r_1}}$. If another component of $\mathcal{C}$ intersects these components with multiplicity $r_2 < r_1$ before the deformation, this component will pass through r_2 of these points afterwards. The total number of intersection points appearing on the Scott deformation of a component C_i is precisely $t(C_i)$, the highest possible order of tangency between C_i and another branch in the original germ $\mathcal{C}$. In this sense, the intersection points are used as efficiently as possible. The number of additional marked points on C_i is $w(C_i) - t(C_i)$.

Now, consider the Lefschetz fibration constructed from the Scott deformation via Lemma 3.2. We claim that up to a curve isotopy, the vanishing cycles of this fibration are disjoint curves on the planar page. The reason for this is built into the iterative nature of the Scott deformation, which results in a nesting of the vanishing cycles as follows.

Consider the equivalence relations on the components $C_1, \dots, C_m$ of the germ $\mathcal{C}$ defined by $C_i \sim_l C_j$ if C_i and C_j intersect at 0 with multiplicity at least l. The transitivity of this relation comes from the fact that if C_1 intersects C_2 with multiplicity r at 0 and C_2 intersects C_3 with multiplicity s at 0, then C_1 must intersect C_3 with multiplicity at least $\min\{r, s\}$. These equivalence relations induce partitions of the components of $\mathcal{C}$, and $\sim_l$ refines $\sim_{l'}$ for $l > l'$.

If we apply the Scott deformation procedure iteratively, on the first iteration, we obtain one transverse intersection of all of the branches (the singularity of type (I)), which groups the components of $\mathcal{C}$ according to the (unique) block of the partition induced from $\sim_1$. Applying the Scott deformation procedure to all the singularities of type (II) generates a transverse multipoint of type (I) for every block in the partition induced by $\sim_2$. Iterating this procedure, for $l \geq 1$ we obtain a transverse intersection for every block of each partition P_l induced by $\sim_l$. For sufficiently large l, each block will consist of a single smooth component, and thus no new transverse intersections of type (I) will result from the procedure. When a block contains a single element, there may or may not be additional marked points placed. Instead of using the partition and Scott deformation to place additional marked points, we can simply use the formula that C_i must have $w(C_i) - t(C_i)$ total additional marked points.

Recall that there is one vanishing cycle in the Lefschetz fibration for each marked point of the Scott deformed curve, and this vanishing cycle encircles the punctures/holes corresponding to the components of curves which pass through the given marked point. Because the equivalence relations $\sim_l$ refine each other as l increases, the subsets

of C_i which intersect at the $(l+1)^{\text{st}}$ iteration are nested within the subsets of C_i which intersect at the l^{th} iteration. Moreover, because the isotopy in the blow-up procedure can be made arbitrarily small, we can assume that there is no braiding of the components C_i between the l^{th} and $(l+1)^{\text{st}}$ iterations; see Section 5 for more details on how braiding of the curves can occur and be understood in general. More specifically, observe that in the Scott deformation procedure, as in Figure 4, the deformation from right to left in the blow-up (at the top of the figure) can be performed by an arbitrarily small translation of the exceptional divisor. By making the translation sufficiently small, we can ensure that in each subset intersecting at the $(l+1)^{\text{st}}$ iteration, the curves stay close together and do not interact with another such subset. (In the language of Section 5, nontrivial braiding would correspond to a crossing of the wires, and a small translation ensures that the wires cannot cross in between the singularities produced iteratively by the Scott deformation.) Then, the vanishing cycles corresponding to the intersections of type (I) which are introduced at the $(l+1)^{\text{st}}$ iteration will be nested inside (and thus disjoint from) the vanishing cycles corresponding to the intersections of type (I) introduced at the l^{th} iteration. We can also assume that any two vanishing cycles introduced in this way at the l^{th} iteration are disjoint, because the application of Lemma 3.2 to the Scott deformation actually realizes these Lefschetz singularities simultaneously in the same fiber (we can later perturb so they arise in different fibers if desired). Finally, the additional marked points at smooth points of the C_i correspond to vanishing cycles which are boundary parallel to the i^{th} hole, and thus can be realized disjointly from each other and all other vanishing cycles. Thus we conclude that the Scott deformation yields a Lefschetz fibration with disjoint vanishing cycles. This means that the compatible planar open book for the link (Y,ξ) has monodromy which is a product of positive Dehn twists about the *disjoint* curves described above. Because at the first step we get a transverse intersection of *all* deformed curvettas, the corresponding vanishing cycle encloses *all* holes, ie we have a Dehn twist about the outer boundary component of the page. □

4.2 Symplectic resolution and Lefschetz fibrations

It is noted in [27] that the Scott deformation corresponds to the Artin smoothing, which in this situation is diffeomorphic to the resolution of the singularity. In fact, we can see more directly, through symplectic topological means, that the Lefschetz fibration corresponding to this Scott deformation gives a plumbing which necessarily corresponds to the resolution of the singularity.

We recall the procedure of [18, Theorem 1.1]. Starting with the plumbing graph G, this procedure produces a planar Lefschetz fibration compatible with the symplectic resolution of a rational singularity with reduced fundamental cycle. (The symplectic structure on the plumbing can be deformed to the corresponding Stein structure.) In fact, [18, Theorem 1.1] applies to a wider class of singularities (see Section 4.3 below), but we first describe it for this particular case. To construct the fiber of the Lefschetz fibration, take a sphere S_v for each vertex $v \in G$ and cut $-a(v) - v \cdot v \geq 0$ disks out of this sphere. (As before, $a(v)$ is the valency of the vertex v; the number of disks is nonnegative by (2-1).) Next, make a connected sum of these spheres with holes by adding a connected sum neck for each edge of G. For a sphere S_v corresponding to the vertex v, the number of necks equals the number of edges adjacent to v, ie its valency $a(v)$. The resulting surface S has genus 0 because G is a tree. See the top of Figure 6 for an example.

Proposition 4.2 [18, Theorem 1.1] *The surface S constructed above is the fiber of a Lefschetz fibration on a symplectic neighborhood of symplectic surfaces intersecting ω–orthogonally according to the graph G. The vanishing cycles are given by the curves parallel to the boundaries of the holes (one curve for each hole) and the cores of the necks of the connected sums.*

Let $\widetilde{X}$ be the Milnor fiber of the Artin smoothing component for a rational $(X, 0)$ with reduced fundamental cycle; $\widetilde{X}$ is a Stein filling for the contact link (Y, ξ). We now have several different Lefschetz fibration structures on $\widetilde{X}$. First, because $\widetilde{X}$ is diffeomorphic to the minimal resolution of $(X, 0)$, a Lefschetz fibration is produced by the Gay–Mark construction of Proposition 4.2. Second, for each choice of the decorated germ $(\mathcal{C}, w)$ with smooth branches, the proof of Proposition 4.1 also gives a Lefschetz fibration on $\widetilde{X}$. All these Lefschetz fibrations have planar fibers. In our construction of the Lefschetz fibration from the curvetta arrangement, the general fiber has a distinguished "outer" boundary component coming from the fibration $\pi : B \to \mathbb{C}$ on the Milnor ball $B = D_x \times D_y \subset \mathbb{C}^2$. In the Gay–Mark construction, there is no distinguished boundary component of the fiber. On the other hand, the decorated germ is not uniquely defined: recall from Proposition 2.4 that there are mult X choices of decorated germs with smooth branches representing $(X, 0)$, where some of these germs may coincide due to symmetries in the extension of the resolution graph. Of course, since the link of the singularity is independent of the choice of curvetta germs, the Stein filling arising from the Artin smoothing should not depend on these choices. We now show that the choice of curvettas

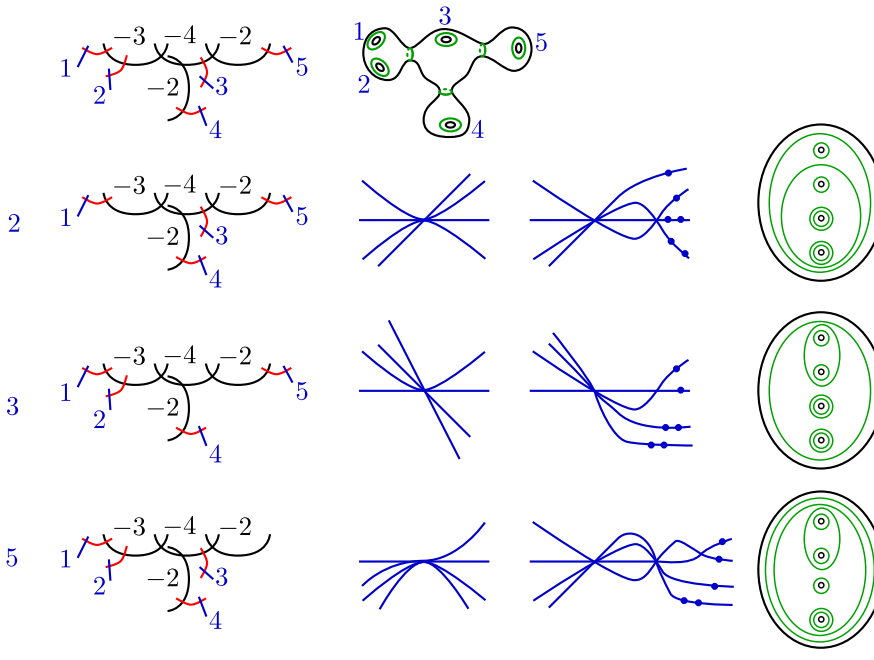

Figure 6: An example demonstrating different choices of curvettas correspond to different choices of outer boundary component for the fiber of the Lefschetz fibration. At the top we have the resolution configuration and the corresponding Gay–Mark Lefschetz fiber with vanishing cycles. The resolution configuration is augmented with red (-1) curves and blue curvettas. For each choice of curvettas we delete exactly one of these red (-1) curves and the corresponding curvetta. We show the resulting curvettas, their Scott deformation, and the corresponding planar Lefschetz fibration obtained from Lemma 3.2 in the cases of excluding the (-1) curves labeled 2, 3, and 5. Note that because of symmetries in the graph, the exclusion of 1 or 2 yield very similar looking cases, and similarly with the exclusion of 4 or 5.

corresponds precisely to the choice of the outer boundary component, so this choice only affects the presentation of the Lefschetz fibration. See Figure 6 for an example.

Lemma 4.3 *Let $\mathcal{L}$ be the planar Lefschetz fibration on $\widetilde{X}$ provided by Proposition 4.2. Then the* mult X *different choices of smooth curvetta germs for $(X,0)$ produce, via the Scott deformation, planar Lefschetz fibrations on $\widetilde{X}$ with a distinguished boundary component of the fiber. The choices of smooth curvetta germs are in one-to-one correspondence with the different choices of outer boundary component of the general fiber of $\mathcal{L}$.*

Proof As before, we associate to each vertex of the resolution graph G for the singularity the quantities $v\cdot v$ for the self-intersection and $a(v)$ for the valency. In the Gay–Mark Lefschetz fibration $\mathcal{L}$, each vertex $v\in G$ contributes $-v\cdot v-a(v)$ boundary components to the fiber. On the other hand, recall from the proof of Propositions 2.2 and 2.4 that the germ $\mathcal{C}$ of smooth curvettas is obtained from an extension of the resolution graph G to a graph G'. We attach $-v\cdot v-a(v)$ vertices with self-intersection -1 and valency 1 to each vertex v to obtain a graph G'', and then delete exactly one of these (-1) vertices to get the graph G'. This shows that the number of choices for the germ matches the number of boundary components of the fiber of $\mathcal{L}$, and this number is exactly $\operatorname{mult} X=-\sum(v\cdot v+a(v))$. The curvetta branches of the germ $\mathcal{C}$ are obtained by taking disks dual to the remaining (-1) vertices and considering their proper transform after blowing down all exceptional divisors; thus the curvettas are in one-to-one correspondence with the (-1) vertices of G'. In turn, in the Lefschetz fibration constructed by Lemma 3.2, the "inner" boundary components of the fiber are in one-to-one correspondence with the curvettas. The deleted (-1) vertex in G'' still corresponds to a boundary component in the fiber of the Gay–Mark Lefschetz fibration $\mathcal{L}$, thus we can say that it corresponds to the outer boundary component of the fiber of the planar Lefschetz fibration produced by Lemma 3.2. Note also that if we enumerate the (-1) vertices of the graph G' by $1,2,\dots,m=\operatorname{mult} X-1$, we get an enumeration of the components of $\mathcal{C}$, which in turn gives an enumeration of the holes of the fiber. □

Recall from Remark 2.6 that there may be different analytic types of singularities with the same link (Y,ξ). These singularities are all topologically equivalent and have the same graph G, so that decorated germs for each of these singularities are obtained from extensions of G. A particular choice of extension gives topologically equivalent decorated germs for all singularities with link Y. Topologically equivalent germs yield the same open book decompositions of (Y,ξ) as in Proposition 4.1, since the weights and the orders of tangency between branches are encoded by the topological type. Together with the previous proposition, this gives:

Corollary 4.4 *Let (Y,ξ) be a link of surface singularity with reduced fundamental cycle. Then for any singularity $(X,0)$ whose link is Y, and any choice of the decorated germ $\mathcal{C}$ for $(X,0)$ with smooth branches, the open book decomposition of (Y,ξ) defined by $\mathcal{C}$ is the same; namely, the open book induced by the Gay–Mark Lefschetz fibration. Different extensions G' of the resolution graph G used to construct $\mathcal{C}$ correspond to*

different choices of the outer boundary of the page of the open book. Enumeration of the branches of $\mathcal{C}$ (or equivalently, of the (-1) vertices of G') corresponds to enumeration of the holes in the page.

It is interesting to note that the Milnor fiber of the Artin smoothing is the *only* Stein filling with disjoint vanishing cycles in its Lefschetz fibration.

Proposition 4.5 *Suppose a planar Lefschetz fibration has disjoint vanishing cycles, with at least one boundary parallel vanishing cycle for each boundary component. Then this is a Lefschetz fibration for the Artin smoothing of a rational singularity with reduced fundamental cycle. In particular, the induced open book decomposition on the boundary supports the contact link of a rational singularity with reduced fundamental cycle.*

Proof As in [18], if the vanishing cycles are disjoint, we can realize all Lefschetz singularities simultaneously in the same fiber. The unique singular fiber is thus a configuration of spheres intersecting transversally according to a graph. Note that the boundary parallel twists are important to ensure that the only nonclosed components of the singular fiber are disks which retract to a point. (These disks come from the small annuli around the holes.) The nonsingular fibers provide a regular neighborhood for the configuration, so the entire 4–manifold is a symplectic plumbing. This 4–manifold gives a symplectic filling for a contact structure supported by a planar open book, thus by [15] its intersection form is negative definite, ie the plumbing graph G is negative definite. Thus, the graph can be thought of as the resolution graph of a normal surface singularity $(X, 0)$.

As in [18], $-v \cdot v \geq a(v)$ for each vertex $v \in G$, so $(X, 0)$ is a rational singularity with reduced fundamental cycle. To see this, observe that each vertex $v \in G$ corresponds to a closed component $\widehat{S}_v$ of the singular fiber. Alternatively, $\widehat{S}_v$ can be viewed as the union of a component S_v of the complement of the vanishing cycles in a regular fiber capped off by thimbles for each of its boundary vanishing cycles. Then, $v \cdot v = \widehat{S}_v \cdot \widehat{S}_v$ equals the negative number of thimbles in $\widehat{S}_v$, or equivalently the negative number of vanishing cycles on the boundary of S_v; see [19, Proposition 2.1]. The valency $a(v)$ is the number of other spheres in the singular fiber intersecting $\widehat{S}_v$. Put differently, $a(v)$ is the number of closed surfaces $\widehat{S}_{v'}$, $v' \neq v$, such that S_v and $S_{v'}$ share a vanishing cycle in their boundaries; thus $a(v)$ is the number of the vanishing cycles in ∂S_v that are not adjacent to a boundary component in the fiber. Then $-v \cdot v - a(v)$ is the number of

vanishing cycles adjacent to a boundary component in ∂S_v, so $-v\cdot v - a(v) \geq 0$, as required. Note also that $v\cdot v \leq -2$, as each S_v has at least 2 vanishing cycles on the boundary, so G is the graph of the *minimal* resolution.

The above discussion implies that if we run the construction of Proposition 4.2 for the graph G, we recover the given Lefschetz fibration. It follows that our Lefschetz fibration is compatible with the symplectic structure on the minimal resolution. For a rational singularity, the resolution is diffeomorphic to the Milnor fiber of the Artin smoothing (and the symplectic structure on the symplectic plumbing deforms to the corresponding Stein structure). This shows that the Lefschetz fibration produces the same filling as the Artin smoothing. □

4.3 A digression: some nonrational singularities and potential unexpected fillings

Although we stated Proposition 4.2 for rational singularities, Theorem 1.1 of [18] is more general: the same construction works when the normal crossings resolution has exceptional curves of higher genus, as long as condition (2-1) is satisfied. The fiber of the corresponding Lefschetz fibration is formed by taking the connected sum of surfaces given by the exceptional curves and cutting $-v\cdot v - a(v) \geq 0$ holes in the surface corresponding to $v \in G$. As before, the vanishing cycles are given by the boundary parallel curves around the holes and the curves around the connected sum necks. We can use this construction together with monodromy factorizations of [7] to construct infinite collections of Stein fillings for links of certain nonrational singularities.

Indeed, suppose that a normal surface singularity $(X, 0)$ has a good resolution such that one of the exceptional curves has genus $g \geq 2$ and self-intersection $-d$, with $d \leq 2g-4$. As before, we assume that the resolution graph has no bad vertices, ie satisfies (2-1). Then the fiber of the Lefschetz fibration from [18, Theorem 1.1] has a subsurface of genus g with some necks and holes, and a vanishing cycle around each neck and each hole. (See Figure 7.) The total number of these vanishing cycles is d. We can cut out this subsurface along the curves parallel to the vanishing cycles to get a surface of genus g with d holes, so that the product of the Dehn twists around the vanishing cycles is the boundary multitwist. For $d \leq 2g-4$, [7, Theorem A] establishes that the boundary multitwist has infinitely many positive factorizations as products of Dehn twists about nonseparating curves. These factorizations can consist of arbitrarily many Dehn twists. It follows that the monodromy of the corresponding open book on the

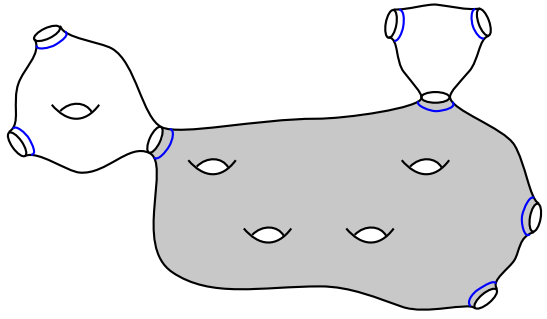

Figure 7: The Gay–Mark Lefschetz fibration for the resolution of a non-rational singularity which admits infinitely many unexpected fillings. The subsurface of genus 4 with $d = 4$ used to produce infinitely many monodromy factorizations is shaded. Vanishing cycles are drawn in blue.

link (Y, ξ) has infinitely many positive factorizations, each of which produces a positive allowable Lefschetz fibration (see [2]) and thus a Stein filling; these Stein fillings can have arbitrarily high Euler characteristic. We ask:

Question 4.6 Does the above construction produce any unexpected Stein fillings?

To answer this question, one would need to contrast these Stein fillings and the Milnor fibers of *all* surface singularities with the given link. Each fixed singularity can only have finitely many Milnor fibers. (Indeed, the Milnor fibers correspond to the components of the base of miniversal deformation; the base is a germ of an analytic space, and as such it can only have finitely many components; see eg [56, Theorem 4.10 and the discussion in Section 7].) However, because of the presence of a higher-genus surface in the resolution, every singularity as above is not (pseudo)taut [32], which means that there exist infinitely many analytic types of singularities with the same dual resolution graph, and thus the same contact link. We are interested in the Stein topology of the Milnor fibers, which is more coarse than the analytic type; in principle, it is possible that the infinite collection of analytic types of the singularity would only give rise to finitely many Stein homotopy types for the Milnor fibers. Thus, we have the following dichotomy: either

(1) there are only finitely many Stein homotopy types (or diffeomorphism types) of the Milnor fibers, which would imply existence of unexpected fillings, or

(2) an infinite collection of possible analytic types gives rise to an infinite collection of pairwise distinct Stein fillings.

Establishing either outcome would be extremely interesting, even for a single example.

It should also be noted that in the nonrational case, one should in principle consider nonnormal singularities as well, as these might generate additional Stein fillings; see [55] for a detailed discussion of this issue (which doesn't arise in the rational case).

Remark 4.7 In a related direction, it is interesting to take a closer look at a family of examples given by cones over curves. Consider a normal surface singularity whose resolution has a unique exceptional curve of genus $g \geq 2$ with self-intersection $-d$ for $d > 0$. The resolution is the total space of the complex line bundle of degree d over the corresponding Riemann surface, and the singularity can be thought of as cone point. The link is a circle bundle over the genus g surface, with Euler number $-d$. The canonical contact structure is the Boothby–Wang structure, which has an open book decomposition as described above: the page is a genus g surface with d boundary components, and the monodromy is the boundary multitwist.

As explained above, for $d \leq 2g-4$ we have an infinite collection of Stein fillings, produced by factorizations of the multitwist. Interestingly, this method no longer applies when $d > 4g+4$: in that range, the boundary multitwist admits no nontrivial positive factorizations, again by [7, Theorem A]. The singularity given by a cone over a projective curve is nonsmoothable when $d > 4g+4$ by [62]; in fact, it is also known that the resolution gives the unique Stein filling in this case [49, Proposition 8.2].

Similarly, for cones over elliptic curves, ie $g = 1$, the singularity is nonsmoothable for $d > 9$ [53], and the only Stein filling is indeed given by the resolution, while for $d \leq 9$, all Stein fillings are given by smoothings and resolutions [50].

5 Every symplectic filling comes from a symplectic deformation of curvettas

5.1 Braided wiring diagrams

A braided wiring diagram is a generalization of a braid in $\mathbb{R} \times \mathbb{C}$ (where the braid condition means that the curves should be transverse to each $\{t\} \times \mathbb{C}$). In a wiring diagram, instead of only looking at smooth braids, we allow the strands to intersect. Let $\pi_{\mathbb{R}} : \mathbb{R} \times \mathbb{C} \to \mathbb{R}$ denote the projection to the first coordinate. We will also use the natural projection from $\mathbb{C}$ to $\mathbb{R}$ sending a complex number to its real part.

Definition 5.1 A *braided wiring diagram* is a union of curves $\gamma_j\colon \mathbb{R} \to \mathbb{R}\times\mathbb{C}$, $j = 1,\dots,n$, each of which is a section of the projection $\pi_{\mathbb{R}}\colon \mathbb{R}\times\mathbb{C} \to \mathbb{R}$, ie each "wire" is given by $\gamma_j(t) = (t, h_j(t) + i\,w_j(t))$. Different wires γ_j may intersect; in this article we will assume that they are not tangent at intersections.

We say a braided wiring diagram is in *standard form* if there are disjoint intervals $I_1,\dots,I_N \subset \mathbb{R}$ such that $I_\ell \times \mathbb{C}$ contains a unique intersection point of some subcollection of the curves γ_j, and in $I_\ell\times\mathbb{C}$, the wires are given as $\gamma_j(t) = (t, k_j t + a_j + i b_j)$. If γ_j does not pass through the intersection point, we require $k_j = 0$.

Note that any braided wiring diagram can be isotoped through braided wiring diagrams to be in standard form.

We can encode a braided wiring diagram by projecting the union of the images of the γ_j to $\mathbb{R}\times\mathbb{R}$ and denoting the crossings of the projection as in a knot diagram.

A braided wiring diagram can be encoded by a sequence

$$(\beta_0, J_1, \beta_1, J_2, \dots, \beta_{m-1}, J_m, \beta_m),$$

where each β_i is a braid and $J_i = \{k_i, k_i+1, \dots, k_i+\ell_i\}$ is a consecutive sequence of integers indicating the local indices of the strands involved in the i^{th} intersection point. For brevity, we will say that J_i is a consecutive set.

Conventions Strands in a wiring diagram are numbered from bottom to top. The convention in [12] is to draw this sequence of braids and intersections from right to left. If one thinks of composing words in the braid group using group notation (left to right) instead of functional notation (right to left), then one will need to read off the braid words from left to right — this is the convention used in [12]. However, in our case since we are always thinking of braids as diffeomorphisms of the punctured plane, we will use functional notation to compose braid words, and thus read everything — the intersections and the braid words — from right to left.

Example 5.2 The braided wiring diagram shown in Figure 8 corresponds to the sequence

$$(\mathrm{id}, \{2,3\}, \mathrm{id}, \{3,4\}, \sigma_1^{-1}\circ\sigma_2^{-1}, \{3,4\}).$$

Braided wiring diagrams were introduced in [12] (inspired by foundational work of [40] and generalized from diagrams of [21]) to study configurations of complex curves,

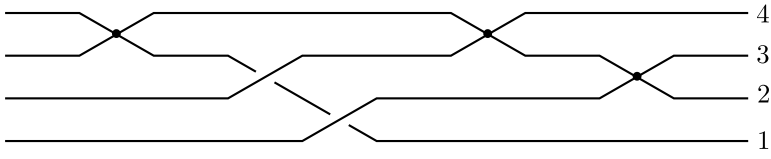

Figure 8: Braided wiring diagram.

particularly line arrangements, and the fundamental groups of their complements. The definition works just as well to study configurations of smooth graphical disks in $\mathbb{C}^2$. As in Section 3, let (x, y) be complex coordinates on $\mathbb{C}^2$, and let π_x be the projection to the first coordinate. Let $\Gamma_1, \dots, \Gamma_m$ be smooth disks in $\mathbb{C}^2$ which are graphical with respect to the projection to x, so $\Gamma_i = \{y = f_i(x)\}$. Assume that all the intersections between the Γ_i are transverse and positive (with respect to the natural orientation on the graphical disks projecting to $\mathbb{C}$).

Definition 5.3 For a graphical configuration $\Gamma = \{\Gamma_1, \Gamma_2, \dots, \Gamma_n\}$ of smooth disks in $\mathbb{C}^2$, a braided wiring diagram is obtained as follows. Choose a (real) embedded curve $\eta\colon [0,1] \to \mathbb{C}$ which passes once through the projection of each singular point of the configuration and whose real part $\operatorname{Re}\eta$ is nonincreasing. The preimage of the curve η under π_x in $\mathbb{C}^2$ is diffeomorphic to $[0,1]\times\mathbb{C}$, and the intersection of this copy of $[0,1]\times\mathbb{C}$ with the configuration Γ is the braided wiring diagram.

The transversality of each smooth disk Γ_j to the projection π_x ensures that the wiring diagram curves are transverse to the projection $\pi_{\mathbb{R}}\colon \mathbb{R}\times\mathbb{C} \to \mathbb{R}$. Note that different choices of η may result in different braided wiring diagrams, which are related by certain generalized Markov moves. See for example [12] for more details. We will show in Section 5.3 that one can always construct a configuration Γ with a given braided wiring diagram; moreover, the components Γ_j of Γ can be chosen to be symplectic.

5.2 Braided wiring diagrams to vanishing cycles

Given a configuration $\Gamma = \{\Gamma_1, \Gamma_2, \dots, \Gamma_m\}$ in $\mathbb{C}^2$ as above, Lemma 3.2 produces an associated Lefschetz fibration. Recall that a Lefschetz fibration is completely determined by its fiber and an ordered list of vanishing cycles. (Critical points are assumed to have distinct critical values.) The fiber in this situation is planar with m boundary components, where m is the number of curves in the configuration. If we are given a braided wiring diagram of Γ, we can explicitly determine the vanishing cycles, as follows.

To describe the vanishing cycles of a Lefschetz fibration $L\colon M \to \mathbb{C}$, we first need to fix certain data. Choose a regular fiber $F_0 := L^{-1}(p_0)$ as the reference fiber. Let $p_1, \dots, p_n$ denote the critical values of L. Choose paths η_j connecting p_0 to p_j in the complement of the p_j, such that the paths η_j are ordered counterclockwise from 1 to n locally around p_0. Then the j^{th} vanishing cycle V_j is the simple closed curve in F_0 which collapses to a point under parallel transport along the path η_j.

When given a braided wiring diagram, we can construct the paths η_j in a systematic manner and compute the vanishing cycles V_j in terms of the braided wiring data. The wiring diagram lies over a curve $\eta\colon [0,1] \to \mathbb{C}$ whose real part $\operatorname{Re}\eta$ is always decreasing. The Lefschetz fibration from Lemma 3.2 comes from the composition $L := \pi \circ \alpha$ of the blow-down map $\alpha\colon \mathbb{C}^2 \#_n \overline{\mathbb{C}\mathrm{P}}^2 \to \mathbb{C}^2$ with the projection map $\pi_x\colon \mathbb{C}^2 \to \mathbb{C}$. One then takes the complement of the sections given by proper transforms of the curves $\Gamma_1, \Gamma_2, \dots, \Gamma_m$ in $\mathbb{C}^2 \#_n \overline{\mathbb{C}\mathrm{P}}^2$, so that each Γ_j corresponds to a hole in the planar fiber. Thus the j^{th} hole corresponds to the wire γ_j in the diagram, and in the standard form the holes are arranged vertically in the fiber, labeled $1, \dots, m$, consecutively. Each consecutive set J_i corresponds to a subcollection of holes contained in a convex subset of $\mathbb{C}$. The Lefschetz critical points occur in $\mathbb{C}^2 \#_n \overline{\mathbb{C}\mathrm{P}}^2$ above the intersection points of the braided wiring diagram. Let $0 < t_1 < \cdots < t_n < 1$ denote the times at which the j^{th} intersection point of the wiring diagram lies over $\eta(t_j)$. We will choose our reference fiber to lie over the right endpoint $p_0 = \eta(0)$ of the curve η in $\mathbb{C}$. Strictly speaking, we need a compact version of this construction, which is obtained by working in a closed Milnor ball and taking complements of tubular neighborhoods of the $\overline{\Gamma}_i$, but for simplicity we omit the Milnor ball from the notation.

We will choose paths $\eta_j : [0, t_j] \to \mathbb{C}$ given by $\eta_j(t) = \eta(t) - \varepsilon_j \rho_j(t) i$, where $\rho_j : [0, t_j] \to [0,1]$ is a bump function which is 0 near $t = 0$ and $t = t_j$, and 1 outside a small neighborhood of 0 and t_j, and $0 < \varepsilon_1 < \varepsilon_2 < \cdots < \varepsilon_n < \varepsilon$. See Figure 9.

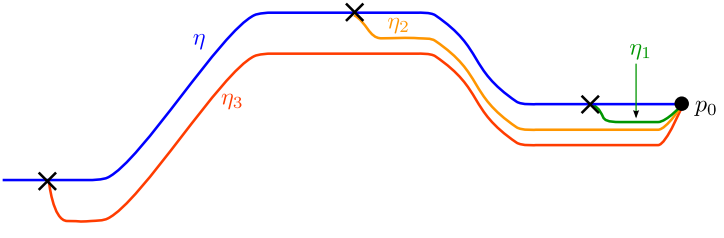

Figure 9: The vanishing paths η_j chosen to identify the vanishing cycles in the fiber over p_0 relative to the wiring diagram path η.

Our local model for the Lefschetz fibration in Lemma 3.2 shows that the curve which collapses to a point in the fiber $L^{-1}(\eta_j(t_j-\delta))$ (for small $\delta>0$) is a convex curve enclosing the holes in the set J_j. To determine the vanishing cycle in our reference fiber $F_0=L^{-1}(p_0)$, we need to track the monodromy over the path η_j for $t\in[0,t_j-\delta]$. This is the monodromy of the braid given by the intersection of the configuration with the slice of $\mathbb{C}^2$ which projects to η_j. (Note that this intersection is indeed a braid over the interior of η_j, because each curve η_j is disjoint from the critical points away from its endpoints.) By assuming ε to be sufficiently small, we see that this braid agrees with corresponding portion of the braided wiring diagram, except when passing near an intersection point. When η_j passes an interval near t_k for $k<j$, the braid resolves the intersection by separating the strands. The strands are ordered from bottom to top in decreasing order by slope in the projection $\mathbb{R}\times\mathbb{C}\to\mathbb{R}\times\mathbb{R}$ (the most positive slope is the lowest strand in the crossing). This can be verified by checking the local model for the complexification of real lines because all of our intersections are positive and transverse; see [40]. After resolving an intersection of the strands in the set $J_k=\{i_k,i_k+1,\dots,i_k+l_k\}$, the element of the mapping class group which corresponds to this portion of the braid from right to left is Δ^{-1}, where Δ is the positive half-twist of the strands $i_k,i_k+1,\dots,i_k+l_k$. (In terms of the standard generators of the braid group, $\Delta_{J_k}=(\sigma_{i_k}\cdots\sigma_{i_k+l_k-1})(\sigma_{i_k}\cdots\sigma_{i_k+l_k-2})(\sigma_{i_k}\sigma_{i_k+1})(\sigma_{i_k})$.) Therefore, the braid lying above η_j is given by

$$\phi_j=\beta_{j-1}\circ\Delta_{j-1}^{-1}\circ\cdots\circ\beta_1\circ\Delta_1^{-1}\circ\beta_0,$$

where Δ_k denotes the positive half-twist of the strands in the set J_k. Namely, Δ_k is the diffeomorphism supported in a neighborhood of the disk convexly enclosing the holes in the set J_k, which acts by rotating the disk by π counterclockwise. The j^{th} vanishing cycle is the curve which is taken to the convex curve A_j enclosing the holes in the set J_j under the braid lying above η_j. Therefore, $V_j=\phi_j^{-1}(A_j)$.

Remark 5.4 We can encode blow-ups at "free" points (as is allowed by Lemma 3.2) by adding marked points in our braided wiring diagram indicating "intersection points" that involve only a single strand (so the corresponding J will have $|J|=1$).

The total monodromy of the curve configuration around a circle enclosing all of the critical points can now be calculated in two different ways:

(1) Using the total monodromy of the curve configuration encoded by the braided wiring diagram.

(2) Taking the product of positive Dehn twists about the induced vanishing cycles.

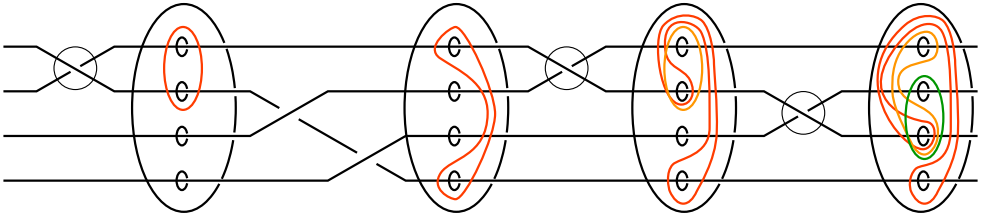

Figure 10: Vanishing cycles corresponding to the braided wiring diagram of Figure 8. The circled crossings correspond to intersections in the wiring diagram. Uncircled crossings come from braiding between intersections.

To reassure the reader that our formulas and conventions are consistent, we verify that these two different ways of calculating the monodromy agree.

The total monodromy encircling a braided wiring diagram

$$(\beta_0, J_1, \beta_1, \dots, \beta_{n-1}, J_n, \beta_n)$$

is given by following the diffeomorphisms induced by a counterclockwise rotation around the wiring interval. Such a counterclockwise circle is obtained by connecting an upward push-off of the wire interval oriented right to left with a downward push-off oriented left to right as in Figure 11. The intersections between the strands of J_j are resolved as the positive half-twist Δ_j in the upward push-off (right to left). In the downward push-off the intersection is resolved as the negative half-twist Δ_j^{-1} right to left, but since we pass through the downward push-off from left to right, each such segment contributes Δ_j to the monodromy. The braids contribute β_j when traversed right to left, and β_j^{-1} when traversed left to right. See Figure 11. The total monodromy is therefore

$$\beta_0^{-1}\circ\Delta_1\circ\beta_1^{-1}\circ\Delta_2\circ\beta_2^{-1}\circ\cdots\circ\beta_{n-2}^{-1}\circ\Delta_{n-1}\circ\beta_{n-1}^{-1}\circ\Delta_n^2\circ\beta_{n-1}\circ\Delta_{n-1}\circ\beta_{n-2}\circ\cdots\circ\beta_2\circ\Delta_2\circ\beta_1\circ\Delta_1\circ\beta_0.$$

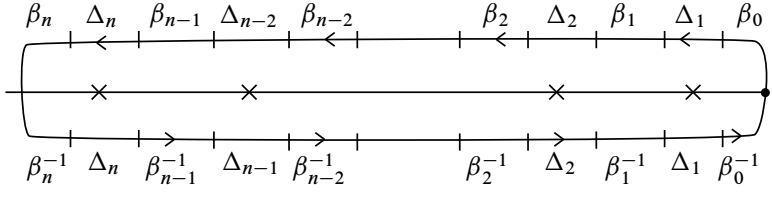

Figure 11: The total monodromy about a braided wiring diagram.

On the other hand, each vanishing cycle is given as

$$V_j = \phi_j^{-1}(A_j) = (\beta_{j-1} \circ \Delta_{j-1}^{-1} \circ \cdots \circ \beta_1 \circ \Delta_1^{-1} \circ \beta_0)^{-1}(A_j).$$

Therefore a Dehn twist τ_{V_j} about V_j is equal to

$$\tau_{V_j} = \phi_j^{-1} \circ \Delta_j^2 \circ \phi_j$$

because $\tau_{A_j} = \Delta_j^2$ and in general $\tau_{\phi(C)} = \phi \circ \tau_C \circ \phi^{-1}$. Thus, the total monodromy of the Lefschetz fibration given by the product of positive Dehn twists about the vanishing cycles is

$$\phi_n^{-1} \circ \Delta_n^2 \circ \phi_n \circ \phi_{n-1}^{-1} \circ \Delta_{n-1}^2 \circ \phi_{n-1} \circ \cdots \circ \phi_1^{-1} \circ \Delta_1^2 \circ \phi_1.$$

We can simplify $\phi_j \circ \phi_{j-1}^{-1}$ as

$$(\beta_{j-1} \circ \Delta_{j-1}^{-1} \circ \cdots \circ \beta_1 \circ \Delta_1^{-1} \circ \beta_0) \circ (\beta_0^{-1} \circ \Delta_1 \circ \beta_1^{-1} \circ \cdots \circ \Delta_{j-2} \circ \beta_{j-2}^{-1}) = \beta_{j-1} \circ \Delta_{j-1}^{-1}.$$

Therefore $\tau_{V_n} \circ \cdots \circ \tau_{V_1}$ is equal to

$$\phi_n^{-1} \circ \Delta_n^2 \circ (\beta_{n-1} \circ \Delta_{n-1}^{-1}) \circ \Delta_{n-1}^2 \circ \cdots \circ (\beta_1 \circ \Delta_1^{-1}) \circ \Delta_1^2 \circ \beta_0,$$

which equals

$$\beta_0^{-1} \circ \Delta_1 \circ \beta_1^{-1} \circ \cdots \circ \Delta_{n-1} \circ \beta_{n-1}^{-1} \circ \Delta_n^2 \circ \beta_{n-1} \circ \Delta_{n-1} \circ \cdots \circ \beta_1 \circ \Delta_1 \circ \beta_0.$$

This coincides with the total monodromy of the braided wiring diagram given above, as required.

5.3 Wiring diagrams to symplectic configurations

Given any braided wiring diagram, we interpret it as a collection of intersecting curves in $\mathbb{R} \times \mathbb{C}$. We will extend each of these curves to a symplectic surface in $\mathbb{C} \times \mathbb{C}$.

Proposition 5.5 *Given a braided wiring diagram $\bigcup_j \gamma_j \subset \mathbb{R} \times \mathbb{C}$ in standard form, there exists a configuration of symplectic surfaces $\bigcup_j \Gamma_j$ in $\mathbb{C} \times \mathbb{C}$ such that Γ_j extends γ_j, that is,*

$$\left(\bigcup_j \Gamma_j \right) \cap (\mathbb{R} \times \{0\} \times \mathbb{C}) = \bigcup_j \gamma_j,$$

and all intersections $\Gamma_j \cap \Gamma_k$ lie in the original wiring diagram in $(\mathbb{R} \times \{0\} \times \mathbb{C})$ and are transverse and positive.

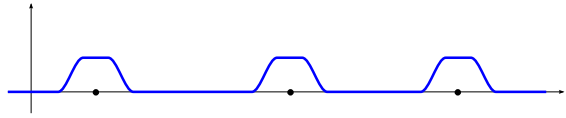

Figure 12: The graph of $\rho\colon \mathbb{R} \to [0,1]$. The marked points on $\mathbb{R}$ are the t_i.

Proof Let $t_1 = \pi_{\mathbb{R}}(p_1), \dots, t_n = \pi_{\mathbb{R}}(p_n)$ denote the $\mathbb{R}$ coordinates of the intersection points $p_1, \dots, p_n$ in the wiring diagram. Braid crossings in the wiring diagram can be viewed as additional intersections that appear in the image of the diagram under the projection $\mathbb{R} \times \mathbb{C} \to \mathbb{R} \times \mathbb{R}$. Choose $\delta > 0$ sufficiently small that there are no crossings in the braided wiring diagram in $\pi_{\mathbb{R}}^{-1}([t_i - 4\delta, t_i + 4\delta])$ (except the intersection at p_n). Let $\rho_i\colon \mathbb{R} \to [0,1]$ be a smooth bump function such that

$$\rho_i(t) = \begin{cases} 1 & \text{for } t \in [t_i - \delta, t_i + \delta], \\ 0 & \text{for } t \notin (t_i - 2\delta, t_i + 2\delta). \end{cases}$$

Let $\rho = \sum_{i=1}^{n} \rho_i$. See Figure 12.

Let $\eta > 0$. Let $\chi\colon \mathbb{R} \to [-\eta, \eta]$ be a smooth function such that

$$\chi(s) = \begin{cases} -\eta & \text{for } s \le -2\eta, \\ s & \text{for } -\frac{1}{2}\eta \le s \le \frac{1}{2}\eta, \\ \eta & \text{for } s \ge 2\eta, \end{cases} \qquad \chi'(s) \ge 0 \quad \text{for all } s \in \mathbb{R}.$$

See Figure 13.

For each wire, we will define its extension to a symplectic surface. Suppose the wire is parametrized as

$$\gamma_j(t) = (t, h_j(t) + i\, w_j(t)) \in \mathbb{R} \times \mathbb{C}.$$

Define $\Gamma_j(t,s)\colon \mathbb{R}^2 \to \mathbb{C}^2$ by

$$\Gamma_j(t,s) = \big(t + i\, s, h_j(t) + i\,(w_j(t) + \rho(t)\chi(s)h_j'(t))\big).$$

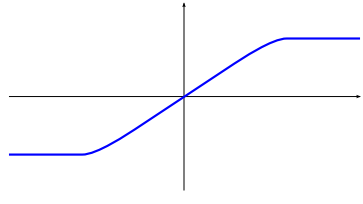

Figure 13: The graph of $\chi\colon \mathbb{R} \to [-\eta, \eta]$.

The tangent space of the image of Γ_j is spanned by

$$\frac{\partial \Gamma_j}{\partial t} = d\Gamma_j\Big(\frac{\partial}{\partial t}\Big) \quad \text{and} \quad \frac{\partial \Gamma_j}{\partial s} = d\Gamma_j\Big(\frac{\partial}{\partial s}\Big).$$

The previous formulas use complex coordinates (x, y) on $\mathbb{C}^2$; now we pass to real coordinates (x_1, x_2, y_1, y_2), so that $x = x_1 + ix_2$, $y = y_1 + iy_2$. In these coordinates, the standard symplectic form is given by $\omega = dx_1 \wedge dx_2 + dy_1 \wedge dy_2$. We have

$$\frac{\partial \Gamma}{\partial t} = \frac{\partial}{\partial x_1} + h_j'(t)\frac{\partial}{\partial y_1} + \big(w'(t) + \rho'(t)\chi(s)h_j'(t) + \rho(t)\chi(s)h_j''(t)\big)\frac{\partial}{\partial y_2},$$
$$\frac{\partial \Gamma_j}{\partial s} = \frac{\partial}{\partial x_2} + \rho(t)\chi'(s)h_j'(t)\frac{\partial}{\partial y_2}.$$

Evaluating the symplectic form gives

$$\omega\left(\frac{\partial \Gamma_j}{\partial t}, \frac{\partial \Gamma_j}{\partial s}\right) = 1 + \rho(t)\chi'(s)(h_j'(t))^2 > 0,$$

so the image of Γ_j is a symplectic surface.

To verify that these extensions do not intersect outside of the original intersections of the wiring diagram, we observe that any intersection between Γ_j and Γ_k would occur at the same parameters (t_0, s_0) and must have

$$h_j(t_0) = h_k(t_0) \quad \text{and} \quad w_j(t_0) + \rho(t_0)\chi(s_0)h_j'(t_0) = w_k(t_0) + \rho(t_0)\chi(s_0)h_k'(t_0).$$

If $h_j(t_0) = h_k(t_0)$, this means that the wires γ_j and γ_k project to the same point under the projection $\mathbb{R} \times \mathbb{C} \to \mathbb{R} \times \mathbb{R}$. This means there is either a crossing or an intersection between wires γ_j and γ_k at t_0.

If t_0 is an intersection point of the wires, $w_j(t_0) = w_k(t_0)$. Additionally, at t_0, the projections of the wires have different slopes, so $h_j'(t_0) \neq h_k'(t_0)$. We also have $\rho(t) \equiv 1$ near t_0. Using this, the intersection assumption that

$$w_j(t_0) + \rho(t_0)\chi(s_0)h_j'(t_0) = w_k(t_0) + \rho(t_0)\chi(s_0)h_k'(t_0)$$

implies that

$$\chi(s_0)(h_k'(t_0) - h_j'(t_0)) = w_j(t_0) - w_k(t_0) = 0.$$

Therefore, $\chi(s_0) = 0$, so $s_0 = 0$ by definition of χ.

If t_0 is a crossing between wires, $w_j(t_0) \neq w_k(t_0)$. Because ρ is supported only near the intersection times, and we assume the crossings occur outside of these intervals, $\rho \equiv 0$. Therefore, the assumption that $w_j(t_0) + \rho(t_0)\chi(s_0)h_j'(t_0) = w_k(t_0) + \rho(t_0)\chi(s_0)h_k'(t_0)$ gives a contradiction.

Finally, we check that Γ_j and Γ_k intersect positively. If we assume that the wiring diagram is in standard form near the intersection points $h_j(t) = k_j t + a_j$ and constant coordinate $w_j(t) \equiv b_j$, then near $(t_i, 0)$ where $\rho(t) \equiv 1$ and $\chi(s) \equiv s$, we have that

$$\Gamma_j(t,s) = (t + is, k_j t + a_j + i(b_j + k_j s)),$$

so the image of Γ_j agrees with the complex line $y = k_j x + a_j + b_j i$, and the intersection of Γ_j and Γ_k locally agrees with an intersection of complex lines. □

5.4 Stein fillings correspond to symplectic configurations

Given a contact structure supported by a planar open book, a theorem of Wendl [65] says that every Stein filling is symplectic deformation equivalent to a Lefschetz fibration with the same planar fiber; Niederkrüger and Wendl [48] extend this result to minimal weak symplectic fillings. Thus, Stein fillings are essentially in one-to-one correspondence with positive factorizations of the monodromy of the given planar open book (and the same is true even for weak symplectic fillings, up to blow-up). The following statement is equivalent to Theorem 1.5.

Proposition 5.6 *Let (Y, ξ) be the link of a rational singularity $(X, 0)$ with reduced fundamental cycle. Fix a decorated germ $(\mathcal{C}, w)$ for $(X, 0)$, with smooth branches $C_1, C_2, \dots, C_m$.*

Then every Stein filling of (Y, ξ) is supported by a Lefschetz fibration built from a configuration of m symplectic disks $\{\Gamma_1, \Gamma_2, \dots, \Gamma_m\}$ in $\mathbb{C}^2$ with marked points, via Lemma 3.2.

Proof Because the contact manifold is planar, any Stein filling is supported by a planar Lefschetz fibration with the same fiber. We will reverse-engineer the required configuration of symplectic disks. Let F_0 be a fixed identification of the planar fiber, where the holes are lined up vertically and labeled by numbers $1, 2, \dots, m$. Let $V_1, \dots, V_n$ be the ordered list of vanishing cycles for the Lefschetz fibration. We begin by producing a collection $(\psi_0, \dots, \psi_{n-1})$ of diffeomorphisms $\psi_i : F_0 \to F_0$ and $(J_1, \dots, J_n)$ of consecutive subsets of $\{1, \dots, m\}$. Here, "consecutive" means that $J_j = \{i, i+1, \dots, i+k\}$ for some i and k.

Choose a diffeomorphism $\beta_0 : F_0 \to F_0$ so that $\beta_0(V_1)$ is isotopic to a curve convexly enclosing a consecutive collection of holes; let J_1 be the corresponding consecutive subset. Let Δ_1 be the counterclockwise half-twist of the convex disk that contains

precisely the holes indexed by J_1. Recursively, choose a diffeomorphism $\beta_j : F_0 \to F_0$ such that $\beta_j \circ \Delta_j^{-1} \circ \cdots \circ \beta_1 \circ \Delta_1^{-1} \circ \beta_0(V_{j+1})$ is isotopic to a curve convexly enclosing a consecutive collection of holes that corresponds to the set J_{j+1}, and let Δ_{j+1} denote the corresponding half-twist.

Consider the braided wiring diagram determined by $(\beta_0, J_1, \beta_1, J_2, \ldots, \beta_{n-1}, J_n)$. By Proposition 5.5, we can construct a configuration of symplectic surfaces $\Gamma_1, \ldots, \Gamma_m$ in $\mathbb{C}^2$ extending this diagram. Using Lemma 3.2, we obtain a planar Lefschetz fibration. We need to use the compact version of the construction to get a fibration whose general fiber is a disk with m holes; for this, we start with a Milnor ball of the form $B = D_x \times D_y$, such that D_x is a neighborhood of η, and D_y is a disk of sufficiently large radius to include the wires above D_x.

As explained in Section 5.2, the vanishing cycles of this Lefschetz fibration will be given by

$$V_j' = (\beta_{j-1} \circ \Delta_{j-1}^{-1} \circ \cdots \circ \beta_1 \circ \Delta_1^{-1} \circ \beta_0)^{-1}(A_j)$$

for $j = 1, \ldots, n$, where A_j is a convex curve enclosing the consecutive holes in the set J_j. The choice of the β_j ensures that these vanishing cycles are identical to our original ones: $V_j' = V_j$.

Along with the symplectic disk configuration $\{\Gamma_1, \ldots, \Gamma_m\}$, we also obtain a collection of marked points on these disks. The marked points include all the intersections as well as additional free marked points, as in Remark 5.4. Each free marked point can be chosen anywhere on the corresponding disk, as long as all marked points are distinct. As in Lemma 3.4, counting multiplicities of pairwise Dehn twists in the monodromy shows that the number of marked points on each disk Γ_j is the same as the weight $w(C_j)$ of the corresponding curvetta C_j of the defining decorated germ (C, w) of the singularity. □

Remark 5.7 The diffeomorphisms β_j are not unique. Any choice will suffice to produce an appropriate braided wiring diagram and corresponding symplectic configuration.

To show that every Stein filling is generated by a symplectic analog of the de Jong–van Straten theorem, it remains to prove that different symplectic configurations with the same monodromy are related by deformations. The role of de Jong and van Straten's picture deformations is played by graphical homotopies.

Proposition 5.8 *Let $(X,0)$ be a rational singularity with reduced fundamental cycle, and (C,w) its decorated plane curve germ with smooth branches $C_1,\dots,C_m$. Let (Y,ξ) be the contact link of $(X,0)$. Suppose that $\Gamma=\{\Gamma_1,\Gamma_2,\dots,\Gamma_m\}$ is a configuration of symplectic disks with marked points $p_1,\dots,p_n$, constructed for a given Stein filling of (Y,ξ) as in Proposition 5.6. Then $(\Gamma,\{p_j\})$ can be connected to (C,w) by a smooth graphical homotopy.*

Lemma 5.9 *Suppose $C_1^0,\dots,C_m^0$ and $C_1^1,\dots,C_m^1$ are two configurations of graphical disks in a Milnor ball $B=D_x\times D_y$, such that $\partial C_j^0=\partial C_j^1$ for $j=1,\dots,m$. Then there is a family of graphical disks $C_1^t,\dots,C_m^t$ (potentially with negative intersections) interpolating between these two configurations with fixed boundary link $\partial C_1^t\cup\cdots\cup\partial C_m^t\subset\partial B$. Here, $\partial C_j^t=C_j^t\cap\partial B=C_j^t\cap(\partial D_x\times D_y)$.*

Proof Because we are not limiting the behavior of the intersections of the components, it suffices to check that there is a family C_j^t interpolating between C_j^0 and C_j^1 for one component. For simplicity of notation we will drop the j. For this, because both C^0 and C^1 are graphical, we can write them as $C^s=\{(x,f^s(x))\}$ for $s=0,1$. Then since $\partial C^0=\partial C^1$, we have that $f^0(x)=f^1(x)$ for $x\in\partial D_x$. Let $C^t=\{(x,tf^1(z)+(1-t)f^0(x)\}$. Then C^t interpolates smoothly between C^0 and C^1, and its boundary is fixed. □

Lemma 5.10 *Suppose $C_1\cup\cdots\cup C_m$ is a configuration of graphical disks, so its boundary $\partial C_1\cup\cdots\cup\partial C_m$ is a braid. Let $L_1,\dots,L_m$ be the components of a braid $L_1\cup\cdots\cup L_m$ which is braid isotopic (with corresponding indices) to $\partial C_1\cup\cdots\cup\partial C_m$. Then there is a homotopy of graphical disks $C_1^t,\dots,C_m^t$ such that $C_j^0=C_j$ and $\partial C_j^1=L_j$.*

Proof If $C_1,\dots,C_m$ are graphical over a disk D_x, choose a larger disk D_x' containing D_x. Then we can extend $C_1,\dots,C_m$ to graphical disks $C_1',\dots,C_m'$ over D_x' so that $\partial C_1',\dots,\partial C_m'$ is the braid L_j, by realizing the trace of the braid isotopy over the annulus $D_x'\setminus D_x$. Next, we can shrink D_x' to D_x continuously via a family of embeddings $\phi_t\colon D_x'\to D_x'$ where $\phi_0=\mathrm{id}$, $\phi_1(D_x')=D_x$, and ϕ_1 identifies points in $\partial D_x'$ with points in ∂D_x according to the same identification used to realize the trace. Then if $C_j'=\{(x,f_j(x))\}$ for $x\in D_x'$, we can let

$$C_j^t=\{(\phi_t(x),f_j(x)\mid x\in D_x'\}\cap(D_x\times\mathbb{C}).$$

Then $C_j^0=C_j$ and $\partial C_j^1=L_j$, as required. □

Proof of Proposition 5.8 When we fix the germ (C, w) and apply the method of Proposition 5.6 to a given Stein filling for (Y, ξ), we first consider the open book on (Y, ξ) induced by the decorated germ as in Proposition 4.1. The Stein filling then carries a Lefschetz fibration that induces the same open book on the boundary, and the arrangement $(\Gamma, \{p_j\})$ is constructed from the monodromy of this Lefschetz fibration. The smooth disks $\Gamma_1, \dots, \Gamma_m$ are contained in the Milnor ball B for $\mathcal{C}$ and are transverse to its boundary S^3, so that $S^3 \cap (\Gamma_1 \cup \cdots \cup \Gamma_m)$ is a braid. By Lemma 3.3, the monodromy of this braid is the image of the monodromy of the open book under the projection $\mathrm{MCG}(P_m) \to \mathrm{MCG}(\mathbb{C}_m)$ of the mapping class group of the compact disk with holes to the mapping class group of the punctured plane, so the two braids are braid-isotopic. Therefore, we can apply Lemma 5.10 to perform a graphical homotopy to $\Gamma_1, \dots, \Gamma_m$ so that its boundary agrees with that of $C_1, \dots, C_m$. Next, apply Lemma 5.9 to continue the graphical homotopy from $C_1, \dots, C_m$ to $\Gamma_1, \dots, \Gamma_m$. □

Remark 5.11 For our construction of a Lefschetz fibration, it is not important that the C_i^t are symplectic disks, we only care that they are graphical. However, by performing a rescaling in the y direction, we can ensure that all of the graphical disks are symplectic if the partial derivatives of the function f are sufficiently small. More specifically, if $C = \{(x, f(x))\}$, where $x = x_1 + ix_2$ and

$$\left|\frac{\partial f}{\partial x_1}\right|, \left|\frac{\partial f}{\partial x_2}\right| < \frac{\sqrt{2}}{2},$$

then C will be symplectic. This bound is sufficient although not necessary; it can be achieved by rescaling f, which itself is a graphical homotopy. Moreover, if f^0 and f^1 both satisfy these bounds, then their convex combination $tf^0 + (1-t)f^1$ also satisfies the bound for all $t \in [0, 1]$, so the interpolation between the two disks will also be symplectic.

6 Incidence matrix and topology of fillings

6.1 Basic topological invariants

It is shown in [27] that the basic topological invariants of the Milnor fibers obtained from the picture deformations can be easily computed from the deformed curvetta arrangement. Moreover, the incidence matrix of the arrangement can be reconstructed from the Milnor fiber [44]. We now review these facts briefly and adapt and generalize

them in our context: the goal is to show that exactly the same results hold for more general Stein fillings, constructed from smooth disk arrangements as in Section 5.

As we have shown in Section 5, every Stein filling W can be described by an arrangement $\Gamma = \{\Gamma_i\}$ of symplectic curvettas with marked points $\{p_j\}_{j=1}^n$, related to the plane curve germ $\mathcal{C} = C_1 \cup \cdots \cup C_m$ by a smooth graphical homotopy. We always assume that curvettas intersect positively. We also treat the components of $\mathcal{C}$ as labeled, so the ordering of components $C_1, \ldots, C_m$ is fixed. The set of marked points $\{p_j\}_{j=1}^n$ contains all intersection points between the Γ_i and possibly a number of free points. The *incidence matrix* $\mathcal{I}(\Gamma, \{p_j\})$ has m rows and n columns, defined so that its entry a_{ij} at the intersection of the i^{th} row and the j^{th} column equals 1 if $p_j \in \Gamma_i$, and 0 otherwise. Note that there is no canonical labeling of the points p_j, so the incidence matrix is defined only up to permutation of columns. We will say that two arrangements $(\Gamma, \{p_j\})$ and $(\Gamma', \{p'_j\})$ are *combinatorially equivalent* if their incidence matrices coincide (up to permutation of columns, ie up to relabeling of the marked points).

Let $\mathcal{L}$ be the Lefschetz fibration constructed for the arrangement $(\Gamma, \{p_j\})$ as in Lemma 3.2. Its general fiber is a disk with m holes that correspond to the curvettas $\Gamma_1, \ldots, \Gamma_m$ of Γ; in particular, the number of holes equals the number of rows in the matrix $\mathcal{I}(\Gamma, \{p_j\})$. The vanishing cycles of $\mathcal{L}$ correspond to the marked points $\{p_j\}_{j=1}^n$ and enclose sets of holes that correspond to curvettas passing through that point: if $\Gamma_{i_1}, \ldots, \Gamma_{i_k}$ are all curvettas that intersect at p_j, the vanishing cycle V_j encloses the holes $h_{i_1}, \ldots, h_{i_k}$. It follows that *homology classes* of the vanishing cycles of $\mathcal{L}$ can be determined from the incidence matrix $\mathcal{I}(\Gamma, \{p_j\})$, and we have:

Proposition 6.1 *Let $\mathcal{L}$ be the Lefschetz fibration for the arrangement $(\Gamma, \{p_j\})$ with incidence matrix $\mathcal{I}(\Gamma, \{p_j\})$. If the j^{th} column of $\mathcal{I}(\Gamma, \{p_j\})$ has 1s in rows $i_1, i_2, \ldots, i_k$, the corresponding vanishing cycle V_j of $\mathcal{L}$ encloses the holes $h_{i_1}, \ldots, h_{i_k}$ in the fiber.*

Corollary 6.2 *Let $(\Gamma, \{p_j\})$ and $(\Gamma', \{p'_j\})$ be two combinatorially equivalent arrangements, and $\mathcal{L}$ and $\mathcal{L}'$ the corresponding Lefschetz fibrations. Then the vanishing cycles of $\mathcal{L}$ and $\mathcal{L}'$ are in one-to-one correspondence, so that the two vanishing cycles that correspond to one another are given by homologous curves in the fiber.*

Because smooth graphical homotopies do not allow intersections to escape through the boundary, the number of pairwise intersections of Γ_i and Γ_j is given by $\operatorname{tang}(C_i, C_j) = \rho(v_i, v_j; v_0)$; see Remark 2.6. The weight of Γ_i (the total number of intersection points and the free marked points on Γ_i) is given by $w(C_i) = 1 + l(v_0, v_i)$. The intersections

between Γ_i and Γ_j correspond to the points among $p_1, p_2, \dots, p_n$ contained in both lines, and each such point gives a 1 in the same column for the i^{th} row and the j^{th} row of the incidence matrix. Therefore we have:

Lemma 6.3 *Let $(\mathcal{C}, w)$ be a decorated germ corresponding to $(X, 0)$, with branches $C_1, C_2, \dots, C_m$. Consider any arrangement $\{\Gamma_i\}_{i=1}^m$ of smooth curvettas encoding a Stein filling of the link of $(X, 0)$. The incidence matrix $\mathcal{I}(\Gamma, \{p_j\})$ has the following properties*:

(i) *The number of 1s in the i^{th} row of $\mathcal{I}(\Gamma, \{p_j\})$ is $w(C_i) = 1 + l(v_0, v_i)$.*

(ii) *The number of 1s which appear in the same columns for the i^{th} row and the j^{th} row is $\operatorname{tang}(C_i, C_j) = \rho(v_i, v_j; v_0)$.*

Here, $l(v_0, v_i)$ and $\rho(v_i, v_j; v_0)$ are the length and overlap functions on the resolution graph G, defined in Remark 2.6, and v_0 is the choice of root.

We now describe how the incidence matrix $\mathcal{I}(\Gamma, \{p_j\})$ determines basic algebraic topology of the filling W, namely $H_1(W)$, $H_2(W)$, the intersection form of W, and the first Chern class $c_1(J)$ of the Stein structure. (Homology is taken with $\mathbb{Z}$ coefficients throughout.) The statements about the homology and the intersection form of W are proved in [27, Section 5] for the algebraic case, but the proofs are entirely topological and apply in the more general settings as well. Alternatively, the same invariants can be computed from the vanishing cycles of the Lefschetz fibration [6, Lemma 16]. For Lefschetz fibrations with planar fiber, detailed proofs for the intersection form and $c_1(J)$ calculations are given in [19]. We write $\mathbb{Z}\langle\{p_j\}\rangle$ for the free abelian group generated by $\{p_j\}_{j=1}^n$, and $\mathbb{Z}\langle\{\Gamma_i\}\rangle$ is defined similarly. The incidence matrix $\mathcal{I}(\Gamma, \{p_j\})$ defines a map between the corresponding lattices.

Proposition 6.4 *There is a short exact sequence*

$$0 \to H_2(W) \to \mathbb{Z}\langle\{p_j\}\rangle \xrightarrow{\mathcal{I}} \mathbb{Z}\langle\{\Gamma_i\}\rangle \to H_1(W) \to 0.$$

Proof Let W be the total space of a Lefschetz fibration over a disk D, with planar fiber P. (We always assume that W, P and D are compatibly oriented.) If $D' \subset D$ is a small disk that contains no critical points, then W is obtained from $P \times D'$ by attaching 2–handles to copies of the vanishing cycles contained in the vertical boundary $P \times \partial D'$, so that distinct handles are attached along knots contained in distinct fibers.

We use the exact sequence of the pair $(W, P \times D')$; since $P \times D'$ retracts onto P, we can replace the former with the latter. Notice also that $H_1(W, P) = 0$, so we get

$$0 \to H_2(W) \xrightarrow{j_*} H_2(W, P) \xrightarrow{\partial_*} H_1(P) \to H_1(W) \to 0.$$

The group $H_2(W, P)$ is freely generated by the cores of the attached 2–handles; we can identify these generators with the vanishing cycles. By construction of the Lefschetz fibration, each vanishing cycle corresponds to a blow-up at some marked point, so we can identify the vanishing cycles with the set $\{p_j\}$. The free abelian group $H_2(W, P)$ is then identified with the lattice $\mathbb{Z}\langle\{p_j\}\rangle$. The generators for the free abelian group $H_1(P)$ can be given by loops around the holes in the planar fiber. The holes correspond to the branches of $\mathcal{C}$, thus $H_1(P)$ can be identified with the lattice $\mathbb{Z}\langle\{\Gamma_i\}\rangle$. The map ∂_* is evaluated as follows: to compute $\partial_*(p_j)$, we take the boundary of the core of the corresponding 2–handle, given by the vanishing cycle associated with p_j, and express this vanishing cycle in terms of the generators of $H_1(P) = \mathbb{Z}\langle\{\Gamma_i\}\rangle$. Since the vanishing cycle is a simple closed curve on the planar page, its first homology class equals the sum of the boundaries of the holes it encloses, which in turn correspond to the branches Γ_i passing through p_j. Therefore, $\partial_*(p_j)$ is given precisely by the j^{th} column of the incidence matrix $\mathcal{I}(\Gamma, \{p_j\})$, as required. □

Remark 6.5 Since the link Y of a rational singularity $(X, 0)$ is always a rational homology 3–sphere, a standard argument shows that $b_1(W) = 0$ for any Stein filling W of Y. Indeed, W has no 3–handles, so $H^3(W; \mathbb{Q}) = 0$; then for the pair $(W, Y) = (W, \partial W)$ we have

$$0 = H_1(\partial W; \mathbb{Q}) \to H_1(W; \mathbb{Q}) \to H_1(W, \partial W; \mathbb{Q}) \cong H^3(W; \mathbb{Q}) = 0.$$

It follows that the matrix $\mathcal{I}(\Gamma, \{p_j\})$ always has full rank.

Note that $H_2(W)$ is isomorphic to $\operatorname{Im} j_*$, which in turn equals $\ker \partial_*$. So $H_2(W)$ can be identified with null-homologous linear combinations of vanishing cycles (thought of as 1–chains in P). One can explicitly describe an oriented embedded surface in W representing a given second homology class, as follows [19, Section 2]. First, one constructs an oriented embedded surface in $P \times D'$ whose boundary is the given null-homologous linear combination of the vanishing cycles, and then the vanishing cycles are capped off in W. A similar construction is given in [27] without Lefschetz fibrations, for Milnor fibers obtained by blowing up the 4–ball at the marked points and taking the complement of the proper transforms of curvettas; exactly the same

argument works for a smooth curvetta arrangement $(\Gamma, \{p_j\})$. After blowing up the 4–ball B at the points $p_1, p_2, \dots, p_n$, we have the 4–manifold $\widetilde{B}$, the blow-up of B, with generators of $H_2(\widetilde{B})$ given by the fundamental classes E_{p_i} of the exceptional divisors. We identify $H_2(\widetilde{B}) = \mathbb{Z}\langle\{p_j\}\rangle$. The intersection form of $\widetilde{B}$ is standard negative definite in the given basis, as $E_p \cdot E_p = -1$. The manifold W is obtained from $\widetilde{B}$ by removing the tubular neighborhoods T_i of the proper transforms $\widetilde{\Gamma}_i$ of the curvettas Γ_i. The inclusion induces a map $H_2(W) \to H_2(\widetilde{B})$, which is in fact the same map as j_* above, under obvious identifications. Every homology class in $H_2(W)$ is represented by an embedded oriented surface which can be constructed by taking the collection of the corresponding exceptional spheres E_{p_i}, punctured at their intersections with $\widetilde{\Gamma}_j$, and connected by tubes running inside the cylinders T_i. The intersection of two such surfaces can be computed by taking the intersections of the corresponding collections of exceptional spheres, as the tubes can be arranged to be disjoint. For the Stein structure J on W associated to the given Lefschetz fibration, we can compute $c_1(J)$ using the same inclusion $H_2(W) \to H_2(\widetilde{B})$. Indeed, J is homotopic to the restriction of the complex structure j on $\widetilde{B}$, and $c_1(j)[E_{p_i}] = 1$ for every E_{p_i}. Therefore we have:

Proposition 6.6 *The intersection form on $H_2(W) \subset \mathbb{Z}\langle\{p_j\}\rangle$ is the restriction of the standard negative definite form given by $p_i \cdot p_j = -\delta_{ij}$ for $i, j = 1, \dots, n$. The first Chern class $c_1(J)$ of the Stein structure is the restriction of the linear form on $\mathbb{Z}\langle\{p_j\}\rangle$ given by $c_1[p_i] = 1$ for $i = 1, \dots, n$.*

See also [19, Propositions 2.1 and 2.4] for a detailed calculation (in terms of the vanishing cycles) of the intersection form and $c_1(J)$ for an arbitrary Lefschetz fibration (W, J) with planar fiber.

6.2 Uniqueness of the Artin filling and proof of Theorem 1.2

In general, the topology of the filling might not be fully determined by the incidence matrix of the corresponding curvettas arrangement; Proposition 6.1 gives the homology classes of the vanishing cycles but not their isotopy classes. However, it turns out that the incidence matrix completely determines the smoothing for picture deformations that are combinatorially equivalent to the Scott deformation, so that one gets the Artin smoothing component [27, Cases 4.13]. We prove that an analogous result holds for Stein fillings as well. Note that the argument in [27] uses simultaneous resolutions and

only works in the algebraic setting, while we work with mapping class groups instead. Our argument works because the Artin filling has a Lefschetz fibration with *disjoint* vanishing cycles in the fiber.

Proposition 6.7 *Let $(X,0)$ be a rational surface singularity with reduced fundamental cycle, with contact link (Y,ξ) and decorated germ $(\mathcal{C},w)$. Let Γ be an arrangement of smooth graphical curves with positive intersections and marked points $\{p_j\}$, related to the germ $(\mathcal{C},w)$ by a smooth graphical homotopy, so that $(\Gamma,\{p_j\})$ gives rise to a Stein filling W of (Y,ξ).*

Suppose that $(\Gamma,\{p_j\})$ is combinatorially equivalent to the Scott deformation $(\mathcal{C}^s,w^s)$ of $(\mathcal{C},w)$. Then the Stein filling given by $(\Gamma,\{p_j\})$ is Stein deformation-equivalent to the Artin filling of (Y,ξ).

Proof Let $\mathcal{L}$ be the Lefschetz fibration for $(\Gamma,\{p_j\})$, constructed as in Lemma 3.2, and let $\mathcal{L}_A$ be the Lefschetz fibration for the Artin smoothing, given in Proposition 4.2. We know that $\mathcal{L}_A$ is given by the monodromy factorization as in Proposition 4.1; let ϕ denote the monodromy of the open book as in the lemma.

Both fibrations $\mathcal{L}$ and $\mathcal{L}_A$ have the same fiber S, and the fibration $\mathcal{L}$ corresponds to some factorization of the same monodromy ϕ. By Corollary 6.2, the vanishing cycles $\{V_j\}$ and $\{V_j^A\}$ of the two fibrations are in one-to-one correspondence, so that the curves V_j and V_j^A are homologous in the fiber. We need to show that V_j and V_j^A are isotopic.

There are two types of vanishing cycle in the fibration $\mathcal{L}_A$: (1) boundary-parallel curves that enclose a single hole each, and (2) the curves that go around the necks connecting the spheres, as shown at the top of Figure 6. The isotopy class of a boundary-parallel curve in the fiber is uniquely determined by its homology class, so if V_j^A is boundary-parallel, then $V_j = V_j^A$. Now, because the total monodromy of $\mathcal{L}$ and $\mathcal{L}_A$ is the same, and the Dehn twists around the boundary-parallel curves are in the center of the mapping class group of the fiber, we see that the products of the Dehn twists around the vanishing cycles homologous to necks are the same for both $\mathcal{L}$ and $\mathcal{L}_A$. In other words, if N denotes the set of vanishing cycles homologous to necks, we have

$$\prod_{V_j\in N}\tau_{V_j}=\prod_{V_j^A\in N}\tau_{V_j^A}. \tag{6-1}$$

Let ψ denote the diffeomorphism of the fiber given by the product (6-1).

To prove that each vanishing cycle V_j is indeed isotopic to the vanishing class V_j^A homologous to V_j, we proceed by induction on the number of necks in the fiber S (this is the same as the number of edges in the dual resolution graph G). Equivalently, we can induct on the number of vertices, since G is a tree. When G has only one vertex, there are no necks, so all the vanishing cycles are boundary-parallel, and $V_j = V_j^A$ for all pairs of vanishing cycles. Assume that the claim is established for all graphs with k vertices or fewer. Consider a graph G with $k+1$ vertices and pick a leaf vertex v of G. We will be able to remove v to reduce the question to a graph G' with k vertices.

In the Lefschetz fibration of Proposition 4.2, the leaf v corresponds to the sphere S_v with holes, connected to the rest of the fiber S by a single neck. The fibration $\mathcal{L}_A$ has a vanishing cycle V^A that goes around this neck, and $\mathcal{L}$ has a vanishing cycle V in the same homology class. Since v is a leaf, S_v is separated from its complement $S \setminus S_v$ by the curve V^A. Observe that all the other nonboundary parallel vanishing cycles of $\mathcal{L}_A$ lie outside S_v. A priori, nonboundary parallel vanishing cycles of $\mathcal{L}$ may belong to different isotopy classes and intersect S_v; we want to show that they can be isotoped to lie outside S_v.

If the self-intersection $v \cdot v = -2$, then in fact V^A encloses only one hole, so it is boundary-parallel, and we can immediately conclude that V and V^A are isotopic, and S_v is a boundary-parallel annulus disjoint from all the other vanishing cycles.

Suppose now that $v \cdot v \leq -3$, so that V^A encloses $r = -1 - v \cdot v > 1$ holes. Connect these holes by $r-1$ disjoint arcs $\alpha_1, \dots, \alpha_{r-1}$ in the sphere S_v, so that if the fiber S is cut along these arcs, the r holes will become a single hole; see Figure 14.

By construction, the arcs $\alpha_1, \dots, \alpha_{r-1}$ are disjoint from all nonboundary parallel vanishing cycles V_j^A of $\mathcal{L}_A$. It follows that each α_i is fixed by the diffeomorphism ψ. As in [7, Proposition 3] and [17, Section 2], we now make the following key observation: after an isotopy removing nonessential intersections, all arcs $\alpha_1, \dots, \alpha_{r-1}$ must be also disjoint from all non-boundary-parallel vanishing cycles V_j of $\mathcal{L}$. To see this, we recall that each right-handed Dehn twist is a right-veering diffeomorphism of the oriented surface S [25]. If α and β are two arcs with the same endpoint $x \in \partial S$, we say that β lies to the right of α if the pair of tangent vectors $(\dot{\beta}, \dot{\alpha})$ at x gives the orientation of S. The right-veering property of a boundary-fixing map $\tau\colon S \to S$ means that for every simple arc α with endpoints on ∂S, the image $\tau(\alpha)$ is either isotopic to α or lies to the right of α at both endpoints, once all nonessential intersections between α and $\tau(\alpha)$ are removed. Now, suppose that $\mathcal{L}$ has a vanishing cycle $V_j \in N$ that

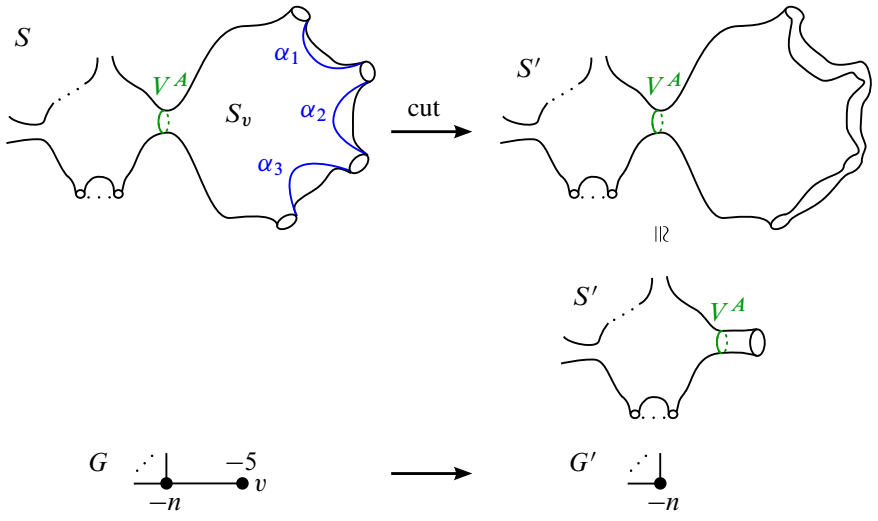

Figure 14: After cutting the fiber S, the vanishing cycle V^A becomes boundary-parallel in S'.

essentially intersects one of the arcs, say α_1. Then the curve $\tau_{V_j}(\alpha_1)$ is not isotopic to α (see eg [16, Proposition 3.2]), so $\tau_{V_j}(\alpha_1)$ lies to the right of α_1. Since the composition of right-veering maps is right-veering, we can only get curves that lie further to the right of α after composing with the other nonboundary parallel vanishing cycles of $\mathcal{L}$. However, the composition $\psi = \prod_{V_j \in N} \tau_{V_j}$ fixes α_1, a contradiction.

Once we know that no vanishing cycles of $\mathcal{L}$ or $\mathcal{L}_A$ intersect any of the arcs $\alpha_1, \dots, \alpha_{r-1}$, we can cut the fiber S along these arcs, and consider the image of the relation (6-1) in the resulting cut-up surface S'. In S', V^A becomes a boundary-parallel curve, and since V lies in the same homology class, we see that V and V^A are isotopic in S' (and therefore in S). We then have

$$\prod_{V_j \in N,\, V_j \neq V} \tau_{V_j} = \prod_{V_j^A \in N,\, V_j^A \neq V^A} \tau_{V_j^A}.$$

Now observe that cutting up S along the arcs as above has the same effect as removing the sphere S_v with its neck from the set of subsurfaces forming the fiber S in Proposition 4.2. Then the cut-up fiber S' with its non-boundary-parallel vanishing cycles $\{V_j\}$ and $\{V_j^A\}$ corresponds to the fibrations for the graph G' obtained by deleting the leaf v and its outgoing edge from the graph G. By the induction hypothesis, we can conclude that all pairs of homologous vanishing cycles V_j, V_j^A are isotopic in S', and

thus in S. It follows that the Lefschetz fibrations $\mathcal{L}$ and $\mathcal{L}_A$ are equivalent, and therefore the Stein filling given by $\mathcal{L}$ is Stein deformation equivalent to the Artin filling. □

The above results have the following interesting application, related to conjectures of Kollár on deformations of rational surface singularities. Suppose that a rational singularity $(X, 0)$ has a dual resolution graph G such that $v \cdot v \leq -5$ for every vertex $v \in G$. In this case, Kollár's conjecture asserts that the base space of a semiuniversal deformation of X has just one component, the Artin component; in particular, there is a unique smoothing, up to diffeomorphism. In the special case of reduced fundamental cycle, this conjecture was proved by de Jong and van Straten via their picture deformations method. We establish the symplectic version of this result, proving Theorem 1.2.

Proof of Theorem 1.2 We can focus on Stein fillings: by [65] and [48], every weak symplectic filling of a planar contact manifold is a blow-up of a Stein filling, up to symplectic deformation. By Section 5, Stein fillings are given by arrangements of symplectic curvettas. The argument in [27, Theorem 6.23] shows that under the given hypotheses on the resolution of $(X, 0)$, there is a unique *combinatorial* solution to the smoothing problem, namely, any arrangement of curvettas must have the same incidence matrix as the Artin incidence matrix given by the Scott deformation. The argument of De Jong and van Straten is somewhat involved, so we will not summarize it here, but we emphasize that the proof of this fact is completely combinatorial and does not use the algebraic nature of arrangements. The same claim holds for an arbitrary smooth arrangement subject to the same hypotheses. The only input used in [27] is the properties of the incidence matrix determined by the resolution graph as in Lemma 6.3, together with the following observation: if all vertices of the resolution graph G have self-intersection -5 or lower, each end vertex of G (except the root) gets at least three (-1) vertices attached in the augmented graph G', so that there are at least three corresponding curvettas. An important step in the inductive proof is that the matrix must have a column where all entries are 1, ie all the Γ_i must have a common point.

Once we know that all arrangements corresponding to possible Stein fillings are combinatorially equivalent to the arrangement given by the Scott deformation, Theorem 1.2 follows from Proposition 6.7. □

In the case where, additionally, the graph G is star-shaped with three legs, uniqueness of minimal symplectic filling (up to symplectomorphism and symplectic deformation) was proved by Bhupal and Stipsicz [9]. (They give a detailed proof under the hypothesis

that the self-intersection of the central vertex is at most -10, but mention that one can go up to -5 with similar techniques.) Their method relies on McDuff's theorem [38] and was previously used by Lisca [34]: one finds a concave symplectic cap which is a plumbing of spheres that completes an arbitrary filling to a rational surface, which must be a blow-up of $\mathbb{C}\mathrm{P}^2$, analyzes possible configurations of (-1) curves, and then verifies that the configurations in the image of the cap plumbing under the blow-down is a pencil of symplectic lines which has a unique symplectic isotopy class. To our knowledge, this strategy has not been applied to non-star-shaped graphs in the existing literature. The difficulty in the non-star-shaped case is that there is not an obvious concave symplectic plumbing which can serve as a cap. Our proof works for completely arbitrary trees.

6.3 Distinguishing Stein fillings

We now turn to constructions that will be needed in the next section, and explain how to use incidence matrices to distinguish Stein fillings, at least relative to certain boundary data. Indeed, as shown by Némethi and Popescu-Pampu [44], the incidence matrix is "remembered" by the Milnor fiber of the corresponding smoothing, which allows us to show that certain Milnor fibers are not diffeomorphic (in the strong sense, ie relative to a boundary marking). The argument in [44] is purely topological, so we can generalize it to arbitrary Stein fillings. While [44] applies more generally to sandwiched singularities, we only consider the case of reduced fundamental cycle.

Instead of the boundary marking used in [44], we will keep track of the boundary data via a choice of a compatible embedded open book for (Y,ξ). As in Section 2, we fix a choice of extension G' of the dual resolution graph G of a singularity with link (Y,ξ), to fix the topological type of the associated decorated germ $(\mathcal{C},w)$ with labeled branches $C_1,\dots,C_m$. Each branch C_j corresponds to a hole h_j of the open book as, explained in Section 4; fixing the embedded open book, up to isotopy, is equivalent to fixing the topological type of the decorated germ. In fact, this open book decomposition provides the data of the "markings" of [44], where the solid tori components of the binding correspond to "pieces" of the marking data which allow one to fix the gluing of the smooth cap of [44] to the filling using the open book instead of the markings.

By Wendl's theorem [65], all Stein fillings of a planar contact 3–manifold are given, up to symplectic deformation, by Lefschetz fibrations with same fiber, so that these fibrations are encoded by monodromy factorizations of the fixed open book as above. Suppose

that Stein fillings W and W' arise from symplectic curvetta arrangements $(\Gamma, \{p_j\})$ and $(\Gamma', \{p'_j\})$ as in Propositions 5.6 and 5.8. On the boundaries ∂W and $\partial W'$, these arrangements induce open books which are isomorphic, because both are isomorphic to the open book induced by the germ $(\mathcal{C}, w)$. Fix these two open books, $\mathcal{OB}$ on ∂W and $\mathcal{OB}'$ on $\partial W'$, defined up to isotopy; as part of the open book data, we also label the binding components (with the exception of the outer boundary of the disk, the boundary components of the page correspond to the branches of the decorated germ).

We will say that W and W' are *strongly diffeomorphic* if there is an orientation-preserving diffeomorphism $W \to W'$ whose restriction to ∂W maps the open book $\mathcal{OB}$ on ∂W to an open book on $\partial W'$ which is isotopic to the given one, $\mathcal{OB}'$. If the open book on $\partial W'$ is isotopic to the image of the open book on ∂W, we can compose the diffeomorphism $W \to W'$ with a self-diffeomorphism of W' which extends the isotopy of $\partial W'$ to obtain a diffeomorphism matching the open books. Therefore, we can equivalently say that W and W' are *strongly diffeomorphic* if there is an orientation-preserving diffeomorphism $W \to W'$ that identifies the open books $\mathcal{OB}$ on ∂W and $\mathcal{OB}'$ on $\partial W'$. This identification is required to preserve the labeling of the binding components. (We will discuss a slightly weaker condition in Remark 6.9.)

Rephrasing the theorem of [44] in our context, we have:

Proposition 6.8 [44, Theorem 4.3.3] *Let (Y, ξ) be the contact link of a rational singularity with reduced fundamental cycle, and fix the isotopy class of an embedded open book as above. Let two strongly diffeomorphic Stein fillings W and W' arise from arrangements $(\Gamma, \{p_j\})$ and $(\Gamma', \{p'_j\})$ of symplectic curvettas with marked points, as in Section 5. Then the incidence matrices $\mathcal{I}(\Gamma, \{p_j\})$ and $\mathcal{I}(\Gamma', \{p'_j\})$ are equal, up to permutation of columns.*

Proof We outline the proof briefly, referring the reader to [44] for details, as we use exactly the same topological argument in a slightly different (in fact, simpler) context.

Let $(\mathcal{C}, w)$ be the decorated germ with labeled smooth branches $C_1, \dots, C_m$, determined up to topological equivalence by the open book data for (Y, ξ). Unlike [44], we only work with the case of smooth components of $\mathcal{C}$; therefore, all δ–invariants of the branches C_i are 0, and the formulas of [44] become simpler.

As in [44], we construct a cap U, which is a smooth manifold with boundary that can be attached to any Stein filling W of (Y, ξ), so that $W \cup U$ is a blow-up of a 4–sphere. To construct U, let $B \subset \mathbb{C}^2$ be a closed Milnor ball as in Section 3, so that

B contains both the branches of the germ $\mathcal{C}$ and the arrangement Γ together with all intersection points between curvettas Γ_i. Let $(B', \mathcal{C}')$ be another copy of this ball with the germ $\mathcal{C}$ inside, with reversed orientation. After an isotopy of the boundaries of the curvettas Γ_i to match ∂C_i, we can glue (B, Γ) and $(B', \mathcal{C}')$ so that the boundary of Γ_i is glued to the boundary of the corresponding germ branch C_i'. Each disk Γ_i is oriented as a graph over $\mathbb{C}$, so the result of gluing is a smooth 4–sphere $B \cup B'$ containing the embedded smooth 2–spheres $\Sigma_i = \Gamma_i \cup C_i'$. Blowing up at the points $p_1, \dots, p_n$, we get $\#_{i=1}^n \overline{\mathbb{C}\mathrm{P}}^2$, represented as the blow-up $\widetilde{B}$ of the ball B glued to B'. Let T_i be a thin tubular neighborhood of the proper transform of Γ_i in $\widetilde{B}$. By Lemmas 3.2 and 3.4, we have $W = \widetilde{B} \setminus \bigcup_{i=1}^m T_i$. Set $U = B' \bigcup_{i=1}^m T_i$, so that we have $U \cup W = \#_{i=1}^n \overline{\mathbb{C}\mathrm{P}}^2$. As in [44, Lemma 4.2.4], the cap U is independent of W and is determined by the boundary data. Indeed, to form U, we attach 2–handles to the 4–ball B'. The attaching circles are given by the boundaries of the Γ_i, and the link $\bigcup_i \partial\Gamma_i$ is isotopic to the link given by the boundaries of the branches of the original decorated germ. The framing for $\partial\Gamma_i$ is $-w_i$, the negative weight on the branch C_i of the decorated germ. The proof of Lemma 3.4 shows that the weight w_i is given by the number of Dehn twists enclosing the i^{th} hole in (any decomposition of) the monodromy of the open book. Thus, the cap U and the way it is glued to W is determined by the decorated germ defining the singularity, together with the fixed open book data of (Y, ξ). Finally, as in [44], we see that there is a unique basis $\{e_j\}_{j=1}^n$ for $H_2\big(\#_{i=1}^n \overline{\mathbb{C}\mathrm{P}}^2\big)$ of classes of square -1 such that the intersection numbers $\Sigma_i \cdot e_j$ are all positive. It follows that these numbers depend only on W and the open book data. On the other hand, the numbers $\Sigma_i \cdot e_j$ form the incidence matrix $\mathcal{I}(\Gamma, \{p_j\})$, as $\Sigma_i \cdot e_j = 1$ if $p_j \in \Gamma_i$, and 0 otherwise. It follows that the incidence matrices $\mathcal{I}(\Gamma, \{p_j\})$ and $\mathcal{I}(\Gamma', \{p_j'\})$ are the same, up to relabeling the marked points, which amounts to permutation of columns. □

Remark 6.9 Our definition of a strong diffeomorphism and the above proof assumes that the binding components of the open book are labeled, and that the diffeomorphism preserves this labeling. In other words, we think of the page of the open book(s) as a disk with holes, where each hole h_i corresponds to the i^{th} branch of the fixed decorated germ; the diffeomorphism matches the i^{th} hole of the page for ∂W to the i^{th} hole for $\partial W'$. It is in fact possible to consider a less restrictive definition of strong diffeomorphism, by allowing permutations of binding components, and to prove a sightly stronger version of Proposition 6.8 and Theorem 7.8. More precisely, the proposition still holds if there is a diffeomorphism $f : W \to W'$ that sends the chosen open book $\mathcal{OB}$ on ∂W to an open book on $\partial W'$ which is isotopic to $\mathcal{OB}'$, in the sense

of isotoping the binding and the pages, but the isotopy matches the binding components in a wrong order. Moreover, it is plausible that the proposition still holds if we only have a diffeomorphism $W \to W'$ whose restriction to ∂W takes the binding of the open book $\mathcal{OB}$ to an oriented link which is isotopic to the binding of $\mathcal{OB}'$ on $\partial W'$ — because $\partial W = Y$ is a link of rational singularity, and thus a rational homology sphere, it seems possible to use [63] to construct an isotopy of pages of the open books if their bindings are isotopic, perhaps under some mild additional hypotheses. We leave most of the details to the motivated reader, only indicating below why the proposition should hold if the identification of the open books permutes the binding components. It should be emphasized that these arguments would yield only a mild generalization of Proposition 6.8: fixing appropriate boundary data is crucial for our proof. Note that by Wendl's theorem, all Stein fillings of a planar contact manifold fill *the same* open book; so in this sense, it is reasonable to think of the boundary open book as fixed.

To consider the case where the diffeomorphism between the fillings permutes the binding components of the open book, assume that there is an orientation-preserving self-diffeomorphism σ of the page of the open book that commutes with the monodromy. We do not assume that σ fixes the boundary of the page; in particular, we are interested in the case where σ permutes the boundary components. It can be shown that if σ acts nontrivially on the set of boundary components, then the decorated germ and/or the resolution graph of the singularity has the corresponding symmetry. For example, if σ exchanges holes h_1 and h_2, these holes must be enclosed by the same number of Dehn twists (in any positive factorizations of the open book); this implies, in particular, the equality of weights for the corresponding curvetta branches,

$$w_1 = w(C_1) = w(C_2) = w_2.$$

Additionally, for any other hole h_i, the number of Dehn twists enclosing the pair h_1, h_i must be the same as the number of Dehn twists enclosing the pair h_2, h_i. Because the Artin factorization is determined by combinatorial data (see Proposition 6.7), it follows that the Artin factorization admits a symmetry interchanging holes h_1 and h_2. Then, we can argue as in Proposition 4.5 to reconstruct the resolution graph of the singularity, and to see that the graph must have a symmetry, and the corresponding curvetta arrangement must admit a symmetry interchanging curvettas C_1 and C_2 (up to a topological equivalence). Similar reasoning would work for a more general self-diffeomorphism σ; we do not give the complete argument to avoid setting up complicated notation. If σ exchanges the boundary of a hole with the outer boundary of

the page (thought of as a disk with holes), there must be a symmetry of the resolution graphs and the corresponding extended graphs; see Section 2.

Since the self-diffeomorphism σ of the page commutes with the monodromy, it induces a self-diffeomorphism of the supporting 3–manifold Y, which is not necessarily isotopic to the identity. We will use the same notation for this self-diffeomorphism of Y, $\sigma : Y \to Y$.

Now, suppose that fillings W and W' are as in Proposition 6.8, and that there is an orientation-preserving diffeomorphism $f : W \to W'$ that maps the open book $\mathcal{OB}$ on W to the open book $f(\mathcal{OB})$ on W' that is isotopic to $\sigma(\mathcal{OB}')$ rather than to $\mathcal{OB}'$. As explained above, the decorated germ admits a symmetry induced by σ; in turn, it follows that the cap U admits a self-diffeomorphism that restricts to the map $\sigma : Y \to Y$ on the boundary, after an orientation reversal. Using this self-diffeomorphism to glue the cap to W', and comparing $W \cup_{\mathrm{id}} U$ and $W' \cup_{\sigma} U$, we can argue as in Proposition 6.8 to conclude that the incidence matrices $\mathcal{I}(\Gamma, \{p_j\})$ and $\mathcal{I}(\Gamma', \{p'_j\})$ are the same.

7 Milnor fibers and unexpected Stein fillings: examples

We now construct examples where the link of a rational singularity with reduced fundamental cycle has Stein fillings that are not realized by Milnor fibers of any smoothing.

Our examples build on results of the previous sections: by [27], Milnor fibers of smoothings correspond to (algebraic) picture deformations of the decorated germ, while Stein fillings of the link can be constructed from arbitrary smooth graphical homotopies of the curvettas. During the picture deformation, the decorated germ $\mathcal{C}$ is *immediately* deformed into an arrangement of curvettas yielding a Milnor fiber, so that the arrangement appears as the deformation $\mathcal{C}^s$ for small s (and for a given deformation, all values of s close to 0 produce diffeomorphic Milnor fibers and equivalent Lefschetz fibrations). Indeed, for an algebrogeometric 1–parameter deformation of the germ $\mathcal{C}$, the general fibers of the deformation all "look the same" (up to diffeomorphism). By contrast, during the course of a smooth graphical homotopy, we are allowed to change the topology of the arrangement of curvettas, and thus will produce Stein fillings whose topology varies during the homotopy. We emphasize that *immediate deformation* vs *long-term homotopy* of the branches of $\mathcal{C}$ makes the key difference between Milnor fillings and Stein fillings of links of rational singularities with reduced

fundamental cycle. In Section 8, we explain why this is the key aspect and compare picture deformations and smooth graphical homotopies in more detail. In this section, we exploit the difference between immediate deformations and long-term homotopies to produce examples of Stein fillings that are not diffeomorphic (rel boundary) to any Milnor fibers.

7.1 Arrangements of symplectic lines and pseudolines

To construct links of singularities that admit unexpected Stein fillings, we first consider decorated germs given by pencils of lines (with weights) and focus on their associated singularities. In this section, we will use the following terminology: several points are *collinear* if they all lie on the same line, and several lines are *concurrent* if they all pass through the same point. Concurrent lines form a *pencil*; we will refer to an arrangement of concurrent lines as a *pencil of lines*. We will also talk about concurrent pseudolines or concurrent smooth disks, with the same meaning.

Note that any two pencils of complex lines in $\mathbb{C}^2$ are isotopic through pencils, therefore the corresponding singularities are topologically equivalent and have contactomorphic links. Let $\mathcal{C} = \{C_1, C_2, \dots, C_m\}$ be a pencil of m complex lines, with each line C_k decorated by a weight $w_k = w(C_k)$. Consider the surface singularity that corresponds to the decorated germ $(\mathcal{C}, w)$, and let $Y(m, w) = Y(m; w_1, \dots, w_m)$ denote its link with the canonical contact structure ξ. Note that $Y(m, w)$ is a Seifert fibered space over S^2 with at most m singular fibers. Indeed, consider the dual resolution graph of the singularity; the graph gives a surgery diagram for the link. This graph has m legs emanating from the central vertex. Legs correspond to the lines of the pencil, so that the k^{th} leg has $w_k - 1$ vertices (including the central vertex).

Note that legs of length 1 consist only of the central vertex and thus will appear invisible. However, in the examples we focus on, every leg will have length greater than 1. The central vertex has self-intersection $-m - 1$, all the other vertices have self-intersection -2. See Figure 16 for an example. The decorated pencil $\mathcal{C}$ can be recovered from the graph as in Section 2: we add (-1) vertices at the end of each leg, take the corresponding collection of curvettas, and blow down the augmented graph.

To construct Stein fillings of $Y(m, w)$, we will use curvetta homotopies taking the pencil of complex lines to a symplectic line arrangement in $\mathbb{C}^2$. We define these arrangements as follows.

Definition 7.1 A *symplectic line arrangement* in $\mathbb{C}^2$ is a collection of m symplectic graphical disks $\Gamma_1, \dots, \Gamma_m$ in $\mathbb{C}^2$ with respect to a projection $\pi : \mathbb{C}^2 \to \mathbb{C}$ such that

(i) for every pair $i, j \in \{1, \dots, m\}$ with $i \neq j$, Γ_i intersects Γ_j positively transversally exactly once, and

(ii) for R sufficiently large, $(\Gamma_1 \cup \cdots \cup \Gamma_m) \cap \pi^{-1}(S_R)$ is isotopic to the braid given by one full twist on m strands in the solid torus $\pi^{-1}(S_R)$, where $S_R \subset \mathbb{C}$ is the circle of radius R.

Equivalently, we can view the symplectic line arrangement in a Milnor ball $B = D_x \times D_y \subset \mathbb{C}^2$ containing all intersections. The intersection of the arrangement with ∂B is then the braid of one full twist in $\partial D_x \times D_y$. A symplectic line arrangement in the closed ball B can always be extended to an arrangement in $\mathbb{C}^2$, so we will give all statements about symplectic line arrangements in $\mathbb{C}^2$.

Example 7.2 A pencil of complex lines intersecting at the origin in $\mathbb{C}^2$ is a symplectic line arrangement. Clearly every pair of lines intersects at a single point (the origin) transversally (and positively because they are complex). That the monodromy in $\pi^{-1}(S_R)$ is one full twist on m strands can be computed directly from a model as in [40].

More generally, any complex line arrangement of m lines in $\mathbb{C}^2$ such that no intersections between lines occur at infinity (ie every complex line has a different complex slope) gives a symplectic line arrangement. This can be seen by compactifying the line arrangement in $\mathbb{C}\mathrm{P}^2$ and looking at the intersection of the lines with the boundary of a regular neighborhood of the $\mathbb{C}\mathrm{P}^1$ at infinity. These intersections form an m component link with one component for each line, such that the link components are isotopic to disjoint fibers of the ε–neighborhood (which can be identified with a subset of the normal bundle) of the $\mathbb{C}\mathrm{P}^1$ at infinity. After changing coordinates from the perspective of the $\mathbb{C}\mathrm{P}^1$ at infinity to the perspective of the complementary ball, the components of the link obtain one full twist. From the Kirby calculus perspective, the boundary of the ε–neighborhood of $\mathbb{C}\mathrm{P}^1$ is presented as $(+1)$ surgery on the unknot, and the link is m parallel meridians of this surgery curve. After reversing orientation to get the boundary of the complementary ball, the surgery coefficient on the unknot becomes a (-1) surgery, and blowing down this surgery curve induces one full twist in the m unknotted meridians.

Since any symplectic line arrangement has the same monodromy as the pencil of complex lines, Lemmas 5.9 and 5.10 imply they are related to the pencil by a smooth graphical homotopy.

Our primary source of examples of noncomplex symplectic line arrangements is given by pseudoline arrangements as described below. However, symplectic line arrangements are more general and can include braiding in the associated wiring diagram.

Example 7.3 A *pseudoline arrangement* is a collection $\ell_1, \dots, \ell_m$ of smooth graphical curves in $\mathbb{R}^2$ where for every pair i, j, the curves ℓ_i and ℓ_j intersect transversally at exactly one point. Such a pseudoline arrangement can be considered a braided wiring diagram as in Definition 5.1, but in the particular case where there is no braiding. In particular, we can apply Proposition 5.5 to extend the pseudoline arrangement to an arrangement of symplectic graphical disks $\Gamma_1, \dots, \Gamma_m$; the extension produces a symplectic line arrangement. Indeed, condition (i) in the definition of a symplectic line arrangement is satisfied because any two pseudolines intersect transversally at one point, and their extensions intersect positively by construction. Condition (ii) follows from the calculation of the total monodromy as in Section 5.2 and a classical theorem of Matsumoto and Tits [37] about uniqueness of reduced factorizations in the braid group.

Alternatively, we can refer to the results of [57, Section 6], where pseudoline arrangements in $\mathbb{R}\mathrm{P}^2$ are extended to symplectic line arrangements in $\mathbb{C}\mathrm{P}^2$ (extensions in $\mathbb{C}\mathrm{P}^2$ are strictly harder to construct than extensions in $\mathbb{C}^2$). Additionally, using the same theorem of Matsumoto and Tits, [57, Proposition 6.4] provides a homotopy of pseudoline arrangements connecting the given arrangement to the pencil. After applying Proposition 5.5, we get a homotopy of the corresponding symplectic line arrangements. Note that by construction, this homotopy of symplectic line arrangements keeps all intersections positive at all times, whereas the smooth graphical homotopy given by Lemmas 5.9 and 5.10 may introduce negative intersections.

We use symplectic line and pseudoline arrangements to construct Stein fillings of Seifert fibered spaces $(Y(m; w), \xi)$ via Lemmas 3.2 and 3.4.

Proposition 7.4 *Let $(\mathcal{C}, w)$ be a decorated pencil of m lines. Suppose that $\Gamma = \{\Gamma_1, \dots, \Gamma_m\}$ is a symplectic line arrangement such that each disk Γ_i has at most w_i distinct intersection points with the other disks of the arrangement. Then, $(\Gamma, \{p_j\})$ yields a Stein filling of $(Y(m; w_1, w_2, \dots, w_m), \xi)$.*

In particular, a pseudoline arrangement $\Lambda = \{\ell_1, \dots, \ell_m\}$ gives a Stein filling of $(Y(m; w_1, w_2, \dots, w_m), \xi)$ via an extension to a symplectic line arrangement, provided that ℓ_i has at most w_i distinct intersection points with the other pseudolines.

7.2 Unexpected line arrangements yield unexpected fillings

Now we will show that some of the Stein fillings as above do not arise as Milnor fibers. In the next lemma, we consider analytic deformations of reducible plane curve germs, associated to a singularity by the de Jong–van Straten theory, and establish a property that will play a key role in our construction of unexpected arrangements.

The term *δ–constant* deformation in the next lemma refers to an algebrogeometric property: the deformation is required to preserve the δ–invariant of a singular plane curve. We keep this terminology since it is used in [27] and [44]; however, under the hypothesis that the germ has smooth branches, the δ–constant condition simply means that the deformation changes the germ componentwise, without merging different components. Intuitively, the δ–invariant counts the number of double points "concentrated" in each singular point [39, Section 10]; for example, an ordinary d–tuple point (where d smooth components meet transversely) contributes $\delta = \frac{1}{2}d(d-1)$, since it can be perturbed to $\frac{1}{2}d(d-1)$ double points. Thus, we can deform a triple point to three double points by a δ–constant deformation, but we are not allowed to deform two transversely intersecting lines into a smooth conic (such a deformation would kill a double point).

Lemma 7.5 *Consider the germ of a reducible plane curve $\mathcal{C}$ in $\mathbb{C}^2$ with m smooth graphical branches $C_1, C_2, \dots, C_m$ passing through 0, and let $\mathcal{C}^s = \bigcup_{k=1}^m C_k^s$ be a δ–constant deformation of $\mathcal{C}$.* (Here, *δ–constant* means that each branch of the germ is deformed individually, ie the deformation is not allowed to merge different branches.) *Suppose that all the branches $C_1, \dots, C_m$ have distinct tangent lines at 0, and that not all deformed branches $C_1^s, \dots, C_m^s$ are concurrent for $s \neq 0$.*

Then there exists a complex line arrangement $\mathcal{A} = \{L_1, \dots, L_m\}$ in $\mathbb{C}^2$ such that not all lines in $\mathcal{A}$ are concurrent, no two lines are equal, and $\mathcal{A}$ satisfies all the incidence relations of $\mathcal{C}^s$. Namely, for any collection of the deformed branches $C_{i_1}^s, C_{i_2}^s, \dots, C_{i_k}^s$ that intersect at one point, the corresponding lines $L_{i_1}, L_{i_2}, \dots, L_{i_k}$ also intersect, ie

$$C_{i_1}^s \cap C_{i_2}^s \cap \cdots \cap C_{i_k}^s \neq \varnothing \implies L_{i_1} \cap L_{i_2} \cap \cdots \cap L_{i_k} \neq \varnothing. \tag{7-1}$$

Note that the incidence pattern for branches of $\mathcal{C}^s$ is the same for all $s \neq 0$, because the definition of a 1–parameter deformation implies that all nearby fibers "look the same". It is important to keep in mind that the complex line arrangement $\mathcal{A}$ may satisfy additional incidences, so that certain intersection points coincide in $\mathcal{A}$ but are distinct

for the arrangement $\{C_1^s, C_2^s, \dots, C_m^s\}$. In particular, a pencil of lines would satisfy incidence relations of any other arrangement, but we postulate that $\mathcal{A}$ cannot be a pencil (the lines in $\mathcal{A}$ are not all concurrent).

Proof of Lemma 7.5 Since any two curvettas intersect positively in the original germ $\mathcal{C}$, any two deformed branches C_i^s, C_j^s intersect for $s \neq 0$. We can make an s–dependent translation to ensure that the first two branches always intersect at the origin, $C_1^s \cap C_2^s = \{0\}$; strictly speaking, this means passing to a slightly different deformation of the germ $\mathcal{C}$.

All components of the reducible curve $\mathcal{C}$ pass through 0 and are graphical analytic disks with respect to the projection to the x–coordinate. Thus we can define the germ of $\mathcal{C}$ near 0 by an equation of the form

$$\prod_{i=1}^{m}(a_i x + c_i(x) - y) = 0,$$

where $c_i(x) = \sum_{k\geq 2} c_{i,k} x^k$ are analytic functions in x with $\operatorname{ord}_x c_i > 1$ at 0. We can also assume that $a_i \neq 0$ for all $i = 1, \dots, m$.

The 1–parameter deformation $\mathcal{C}^s$ is then given, for s close to 0, by an equation of the form

$$\prod_{i=1}^{m}(a_i(s)x + b_i(s) + c_i(x,s) - y) = 0.$$

Here a_i and b_i are analytic functions in s, and at the origin $(0,0)$ we have $\operatorname{ord}_s a_i = 0$ and $\operatorname{ord}_s b_i > 0$; additionally, $c_i(x,s)$ is analytic in x and s, and $\operatorname{ord}_x c_i > 1$. The i^{th} component C_i^s of the deformed curve at time s is given by $a_i(s)x + b_i(s) + c_i(x,s) - y = 0$. Because the branches C_1^s and C_2^s pass through 0 for all s, we have $b_1 \equiv b_2 \equiv 0$. At $s = 0$ all components pass through the origin, so $b_i(0) = 0$ for all i.

Let $r = \min_i(\operatorname{ord}_s b_i)$, where the order is always taken at the origin. Because $b_i(0) = 0$ for all i, we have $r > 0$, and $r = \operatorname{ord}_s b_{i_0}$ for some $3 \leq i_0 \leq m$. Notice also that $r < +\infty$, since otherwise all the components C_i^s would pass through 0 for all $s \neq 0$. We write $b_i(s) = s^r \overline{b}_i(s)$; then $\overline{b}_{i_0}(0) \neq 0$.

Now make a change of variables for $s \neq 0$,

$$x = s^r x' \quad \text{and} \quad y = s^r y'.$$

Since $\operatorname{ord}_x c_i(x,s) \geq 2$, we have $c_i(x,s) = s^{2r}\overline{c}_i(x',s)$ for some analytic function $\overline{c}_i$. Thus, the equation for the deformation becomes

$$\prod_{i=0}^{m}\left(a_i(s)s^r x' + s^r \overline{b}_i(s) + s^{2r}\overline{c}_i(x',s) - s^r y'\right) = 0.$$

Equivalently, for $s \neq 0$ and $i = 1,\dots,m$, the deformed components C_i^s are given by the equations

$$a_i(s)x' + \overline{b}_i(s) + s^r\overline{c}_i(x',s) - y' = 0.$$

When we pass to the limit as $s \to 0$, the equations become

$$a_i(0)x' + \overline{b}_i(0) - y' = 0,$$

so in the limit we obtain an arrangement of straight lines in $\mathbb{C}^2$. Not all of these lines are concurrent, since $\overline{b}_{i_0}(0) \neq 0$ while $\overline{b}_1(0) = \overline{b}_2(0) = 0$.

The curves C_i^s satisfy the same incidence relations for all $s \neq 0$. Since intersection points between curves vary continuously with s, the incidence relations must be preserved in the limit, so (7-1) holds. □

Our examples of unexpected Stein fillings are given by pseudoline arrangements with the following special property.

Definition 7.6 Let $\Lambda = \{\Gamma_1,\dots\Gamma_m\} \subset \mathbb{R}^2$ be a symplectic line arrangement where not all lines are concurrent. We say that Λ is *unexpected* if the only complex line arrangements that satisfy all the incidence relations of Λ are pencils of lines. Namely, whenever a complex line arrangement $\mathcal{A} = \{L_1, L_2, \dots, L_m\} \subset \mathbb{C}^2$ has the property

$$\Gamma_{i_1} \cap \Gamma_{i_2} \cap \cdots \cap \Gamma_{i_k} \neq \varnothing \implies L_{i_1} \cap L_{i_2} \cap \cdots \cap L_{i_k} \neq \varnothing,$$

all the lines $L_1, L_2, \dots, L_m$ of $\mathcal{A}$ must be concurrent.

If an unexpected symplectic line arrangement comes from a pseudoline arrangement, we will say that the pseudoline arrangement is unexpected.

Remark 7.7 It is important to note that unexpected symplectic line arrangements are not the same as symplectic line arrangements not realizable by complex lines. Being an unexpected arrangement is a stronger condition: we want to rule out not only complex line arrangements with the same incidence relations as those of Λ, but also complex line arrangements that satisfy all the incidence relations of Λ and possibly additional incidence relations (without being a pencil). For instance, the pseudo-Pappus

arrangement (Example 8.1 in the next section) is not realizable by complex lines but it is not unexpected, because the classical Pappus arrangement has all of the same incidences and an additional one.

Theorem 7.8 *Suppose that $\Gamma = \{\Gamma_1, \dots, \Gamma_m\}$ is an arrangement of smooth graphical disks with marked points $\{p_j\}$, related by a smooth graphical homotopy to a decorated germ $(\mathcal{C}, w)$. Let (Y, ξ) be the link of the surface singularity that corresponds to $(\mathcal{C}, w)$. Suppose that a subcollection of disks $\{\Gamma_1, \Gamma_2, \dots, \Gamma_r\}$ of Γ forms an unexpected symplectic line arrangement.*

Then the Stein filling W given by $(\Gamma, \{p_j\})$ is not strongly diffeomorphic to any Milnor filling of (Y, ξ). If the weights on $\mathcal{C}$ are large enough, W is simply connected.

By Proposition 7.4, unexpected line arrangements yield unexpected fillings of Seifert fibered spaces of the form $Y(m, w)$.

Corollary 7.9 *Let $\Gamma = \{\Gamma_1, \dots, \Gamma_m\}$ be an unexpected symplectic line arrangement, and for $k = 1, \dots, m$, let $w(\Gamma_k)$ denote the number of intersection points of Γ_k with the disks Γ_i, $i \neq k$. Then for every weight $w = (w_1, w_2, \dots, w_m)$ with $w_k \geq w(\Gamma_k)$ for $k = 1, \dots, m$, the Seifert fibered space $(Y(m, w), \xi)$ has a Stein filling not strongly diffeomorphic to any Milnor filling. This Stein filling is given by a Lefschetz fibration constructed from the arrangement Γ with the appropriate choice of marked points. When strict inequalities $w_k > w(\Gamma_k)$ hold for all k, we get a simply connected unexpected Stein filling.*

Proof of Theorem 7.8 Observe that when the number of intersection points on each Γ_i is smaller than the weight of the corresponding branch of the decorated germ, each Γ_i has a free marked point. Then the Lefschetz fibration constructed from $(\Gamma, \{p_j\})$ has a boundary-parallel vanishing cycle around every hole in the disk fiber, so that the corresponding thimbles kill all generators of $\pi_1(\text{fiber})$, and therefore, in this case $\pi_1(W) = 0$.

Let W_M be a Milnor filling that arises from a smoothing of some surface singularity with the link Y. By Theorem 1.3, W_M corresponds to a picture deformation $\mathcal{C}'^s$ of a decorated germ $\mathcal{C}' = \bigcup_{i=1}^m C_i'$ with weight w, topologically equivalent to $(\mathcal{C}, w)$.

Although the germs $\mathcal{C}$ and $\mathcal{C}'$ may differ analytically, they are topologically equivalent and thus have isotopic boundary braids. Therefore by Lemma 3.4 the open book decomposition naturally induced by the Lefschetz fibration in Lemma 3.2 for W agrees with that for W_M, so comparing them via strong diffeomorphism makes sense.

By Proposition 6.8, if W is strongly diffeomorphic to W_M, the incidence matrix of the deformed curvetta arrangement $\{C_1'^s, \dots, C_m'^s\}$, $s \neq 0$, with its marked points must be the same as the incidence matrix for the arrangement $(\Gamma, \{p_j\})$, up to permutation of columns. In particular, we see that the subarrangement $\{\Gamma_1, \dots, \Gamma_r\}$ of symplectic lines satisfies the same incidence relations as the subarrangement $\{C_1'^s, \dots, C_r'^s\}$ of the deformed curvettas of $\mathcal{C}'$. By assumption, in each of these arrangements not all curvettas are concurrent. Because pairs of curves $\Gamma_1, \dots, \Gamma_r$ intersect algebraically positively once, $C_1', \dots, C_r'$ have distinct tangent lines. Now by Lemma 7.5, there exists a complex line arrangement $\mathcal{A}$ that satisfies all the incidence relations of $\{C_1'^s, \dots, C_r'^s\}$, and thus all the incidence relations of Γ. This is a contradiction because Γ is an unexpected arrangement. □

7.3 Constructing unexpected pseudoline arrangements

We now give examples of unexpected pseudoline arrangements; these will yield concrete examples of unexpected Stein fillings. We start with classical projective geometry constructions.

Example 7.10 Recall that the classical Pappus arrangement in $\mathbb{R}^2$ is constructed as follows. Take two lines, ℓ_1 and ℓ_2, and mark three distinct points a, b, c on L_1 and three distinct points A, B, C on ℓ_2, avoiding the intersection $\ell_1 \cap \ell_2$. Consider the following lines through pairs of marked points:

$$\ell_3 = aB, \quad \ell_4 = aC, \quad \ell_5 = bA, \quad \ell_6 = bC, \quad \ell_7 = cA, \quad \ell_8 = cB.$$

The Pappus theorem asserts that the three intersection points $\ell_3 \cap \ell_5$, $\ell_4 \cap \ell_7$, and $\ell_6 \cap \ell_8$ are collinear; the classical Pappus arrangement consists of the lines $\ell_1, \dots, \ell_8$, together with the line through these three points. We modify this last line to make an unexpected pseudoline arrangement, as follows. Let ℓ_9 be a line through C, distinct from ℓ_4 and ℓ_6. Consider the intersection point $\ell_8 \cap \ell_9$ and let ℓ_{10} be a pseudoline passing through points $\ell_3 \cap \ell_5$, $\ell_4 \cap \ell_7$ and $\ell_8 \cap \ell_9$, as shown in Figure 15. Let $\mathcal{P} = \{\ell_1, \ell_2, \dots, \ell_{10}\}$.

Notice that in this case, it is clear that the pseudoline ℓ_{10} can be homotoped to the classical Pappus line through the points $\ell_3 \cap \ell_5$, $\ell_4 \cap \ell_7$ and $\ell_6 \cap \ell_8$. The resulting arrangement of straight lines in $\mathbb{R}^2$ can be homotoped to a pencil by linear homotopy. (We already know from discussion in Example 7.3 that $\mathcal{P}$ is homotopic to the pencil, but here we have a very simple explicit homotopy.)

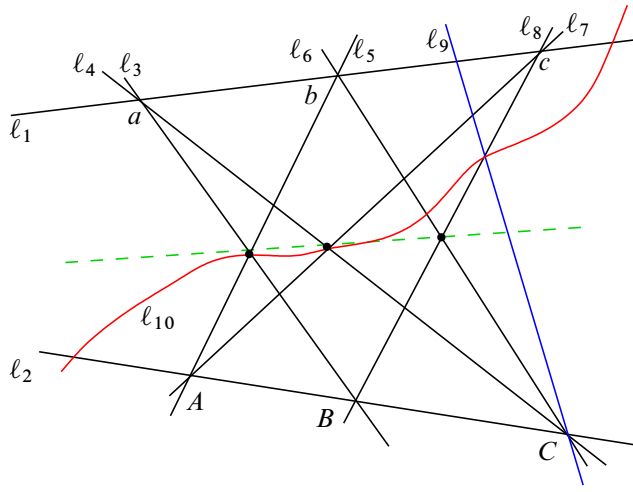

Figure 15: The pseudoline arrangement $\mathcal{P} = \{\ell_1, \ell_2, \dots, \ell_{10}\}$ is given by the black lines, the blue line, and the red line in the figure. The dotted line in the middle is not included. The dotted line and the eight black lines give the classical Pappus arrangement. The intersection points $\ell_1 \cap \ell_2$, $\ell_3 \cap \ell_6$, $\ell_3 \cap \ell_9$, $\ell_5 \cap \ell_8$ and $\ell_5 \cap \ell_9$ are not shown in the figure.

Proposition 7.11 *The arrangement $\mathcal{P}$ is unexpected.*

Proof As already stated, the classical Pappus theorem asserts that for the given arrangement, the intersection points $\ell_3 \cap \ell_5$, $\ell_4 \cap \ell_7$, and $\ell_6 \cap \ell_8$ are collinear. Collinearity holds both in the real and in the complex projective geometry settings, so that if $L_1, L_2, \dots, L_7, L_8 \subset \mathbb{C}^2$ are complex lines with given incidences, then $L_3 \cap L_5$, $L_4 \cap L_7$, and $L_6 \cap L_8$ are collinear. From this, we can immediately see that the arrangement $\mathcal{P}$ is not realizable by complex lines $\{L_1, L_2, \dots, L_{10}\}$: since $L_6 \cap L_8$ and $L_8 \cap L_9$ are distinct points on L_8, the points $L_3 \cap L_5$, $L_4 \cap L_7$ and $L_8 \cap L_9$ cannot be collinear.

To show that $\mathcal{P}$ is unexpected, we need to prove that no complex line arrangement satisfies all the incidence relations of $\mathcal{P}$ even if some (but not all) of the intersection points coincide. Indeed, we show that if a complex line arrangement $\mathcal{A} = \{L_1, L_2, \dots, L_{10}\}$ satisfies the incidence relations of $\mathcal{P}$ and two of the intersection points coincide, then $\mathcal{A}$ must be a pencil. Remember that we always assume that all the lines in the arrangement are distinct.

The following trivial fact, applied systematically, greatly simplifies the analysis of cases:

Observation 7.12 *Let L_1, L_2, L_3, L_4 be four lines in $\mathbb{C}^2$, which are not necessarily distinct. Suppose that two of the pairwise intersection points coincide: $L_1 \cap L_2 = L_3 \cap L_4$. Then L_1, L_2, L_3 and L_4 are concurrent, so that they all intersect at the point $L_1 \cap L_2 = L_1 \cap L_3 = L_1 \cap L_4 = L_2 \cap L_3 = L_2 \cap L_4 = L_3 \cap L_4$.*

In the case of three lines, if $L_1 \cap L_2 = L_3 \cap L_1$, then $L_2 \cap L_3 = L_1 \cap L_2 = L_3 \cap L_1$. Visually, if two vertices of a triangle coincide, the third vertex of the triangle coincides with the first two.

Assuming that some of the intersection points in Figure 15 coincide, we mark these points by "O", and then use Observation 7.12 to chase vertices that coincide: starting with two marked vertices, we look for additional vertices that coincide with the first two, further mark these by "O", and continue. When every line contains a marked intersection point, we know that all lines in the arrangement are concurrent: they form a pencil though O.

We begin this process. First, assume that the intersection points $L_3 \cap L_5 \cap L_{10}$ and $L_4 \cap L_7 \cap L_{10}$ are distinct. By the Pappus theorem, the complex line arrangement $\mathcal{A} = \{L_1, L_2, \dots, L_{10}\}$ can satisfy all the incidence relations of $\mathcal{P}$ only if $L_6 \cap L_8 = L_8 \cap L_9 \cap L_{10}$. Setting $\mathrm{O} = L_6 \cap L_8 = L_8 \cap L_9 \cap L_{10}$, by Observation 7.12 we have $\mathrm{O} = C = L_4 \cap L_6 \cap L_9 \cap L_2$, then $\mathrm{O} = B = L_8 \cap L_2 \cap L_3$, then $\mathrm{O} = a = L_3 \cap L_4 \cap L_1$, then $\mathrm{O} = b = L_5 \cap L_6 \cap L_1$ and $\mathrm{O} = c = L_7 \cap L_8 \cap L_1$. Now, O appears on every line at least once, so the arrangement degenerates to a pencil.

(This can be seen quickly if in the above diagram, you highlight the lines passing through intersection points marked by O, in order. You can mark a new intersection by O if it contains at least two highlighted lines, and then highlight all the lines through that point O. When all the lines are highlighted, you have a pencil.)

For the second case, assume that the intersection points $L_3 \cap L_5 \cap L_{10}$ and $L_4 \cap L_7 \cap L_{10}$ coincide. Set $\mathrm{O} = L_3 \cap L_5 \cap L_{10} = L_4 \cap L_7 \cap L_{10}$. Then $\mathrm{O} = a = L_3 \cap L_4 \cap L_1$ and $\mathrm{O} = A = L_5 \cap L_7 \cap L_2$. Then $\mathrm{O} = c = L_7 \cap L_8 \cap L_1$ and $\mathrm{O} = C = L_4 \cap L_6 \cap L_2 \cap L_9$. Again, every line contains a point marked O, so the arrangement degenerates to a pencil. □

Corollary 7.13 *Let $Y = Y(10; w)$ be a Seifert fibered space given by a star-shaped plumbing graph with 10 legs, as in Figure 16, such that eight of the legs of the graph have at least 5 vertices each, including the central vertex, and two remaining legs have at least 4 vertices each. (Equivalently, two components of w are 5 or greater, and the*

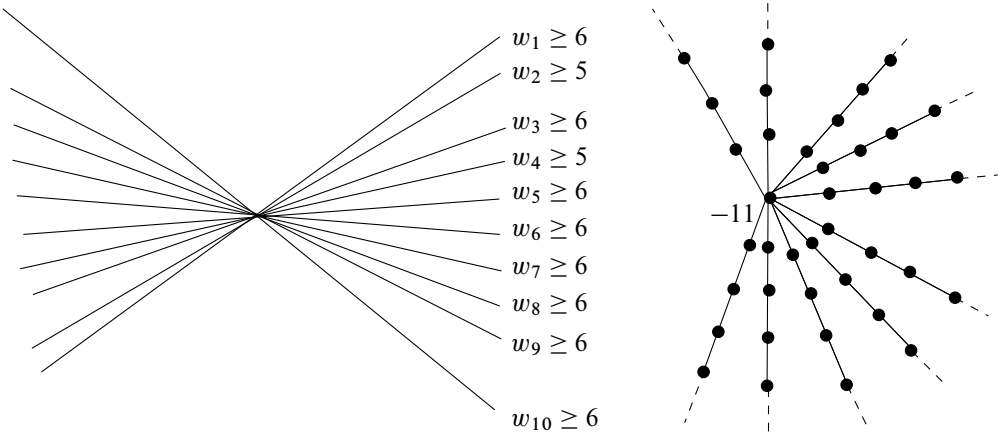

Figure 16: Left, a pencil of 10 lines decorated with weights. Right, the plumbing graph for Y: the central vertex has self-intersection -11, all the rest have self-intersection -2. Eight of the legs have at least 5 vertices each (including the central vertex), and two remaining legs have at least 4 vertices each.

rest are 6 or greater.) Observe that Y is the link of a rational singularity, and let ξ be the Milnor fillable contact structure on Y. Then (Y, ξ) admits a Stein filling which is not strongly diffeomorphic to any Milnor filling.

Proof We count the intersection points on each line in the arrangement $\mathcal{P}$: $w(\ell_2) = w(\ell_4) = 5$, $w(\ell_k) = 6$ for $k \neq 2, 4$. Then for any collection of integers $w_1, w_2, \dots, w_{10}$ such that $w_2 \geq 5$, $w_4 \geq 5$ and $w_k \geq 6$ for $k \neq 2, 4$, we can mark the lines of the arrangement $\mathcal{P}$ as required in Corollary 7.9. The corresponding singularity has the dual resolution graph as shown in Figure 16, with one leg of length $w_k - 1$ for each line L_k in the arrangement, so the link is the Seifert fibered space $Y(10, w)$. The result now follows from Corollary 7.9 and Proposition 7.11. □

A different example comes from a version of the Desargues theorem; we use complete quadrangles and harmonic conjugates. The example in Figure 17 was pointed out to us by Stepan Orevkov. He suggested an approach to proving that this arrangement cannot appear as an algebraic deformation of a pencil. We are grateful for his input, which inspired us to define unexpected line arrangements and prove Lemma 7.5.

Example 7.14 In the standard $\mathbb{R}^2 \subset \mathbb{R}\mathrm{P}^2$, we take four vertical lines $\ell_1, \ell_2, \ell_3, \ell_4$, three horizontal lines ℓ_5, ℓ_6, ℓ_7, the two parallel diagonal lines ℓ_8, ℓ_9, and a "bent"

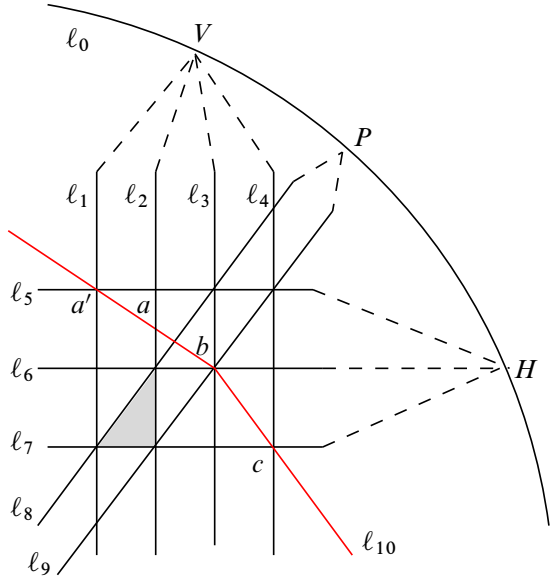

Figure 17: An arrangement of real pseudolines. The intersection of ℓ_0 and ℓ_{10} is not shown.

pseudoline ℓ_{10}, as shown in Figure 17. Let ℓ_0 be the line at infinity. Note that because $\ell_1, \ell_2, \ell_3, \ell_4$ are all parallel in $\mathbb{R}^2$, they intersect at a point V on ℓ_0. Similarly, the lines ℓ_5, ℓ_6, ℓ_7 have a common intersection with ℓ_0 at a point H, and the lines ℓ_8 and ℓ_9 intersect on ℓ_0 at a point P. Removing from $\mathbb{R}\mathrm{P}^2$ a line which is different from all the ℓ_i and intersects them generically, we can consider $\mathcal{Q} = \{\ell_i\}_{i=0}^{10}$ as a pseudoline arrangement in $\mathbb{R}^2$. (See Figure 18 for a version where ℓ_0 is no longer the line at infinity.)

Proposition 7.15 *The pseudoline arrangement $\mathcal{Q}$ is unexpected.*

Proof Suppose that a complex line arrangement $\mathcal{A} = L_0, L_1, \dots, L_{10}$ satisfies all the incidence relations of $\mathcal{Q}$. This means that for all intersections between the pseudolines in Figure 17, the corresponding lines of $\mathcal{A}$ intersect. We claim that unless $\mathcal{A}$ is a pencil, all of these intersection points must be distinct — that is, no two distinct intersection points in Figure 17 can coincide for the arrangement $\mathcal{A}$. To see this, we use Observation 7.12 repeatedly, as in Proposition 7.11. Recall that $V = L_1 \cap L_2 \cap L_3 \cap L_4 \cap L_0$ and $H = L_5 \cap L_6 \cap L_7 \cap L_0$.

If $H = V = \mathrm{O}$, then we have $L_i \cap L_j = \mathrm{O}$ for all $1 \le i \le 4$ and $5 \le j \le 7$, so $\mathcal{A}$ is a pencil.

If one of the intersection points $L_i \cap L_j$ with $1 \le i \le 4$ and $5 \le j \le 7$ coincides with V or H, then we have two intersection points marked with O on a vertical or horizontal line in Figure 17; then $O = V = H$, and all lines are concurrent.

If any two intersection points $L_i \cap L_j$ with $1 \le i \le 4$ and $5 \le j \le 7$ coincide, Observation 7.12 implies that they will both coincide with at least one of V or H, so we revert to the previous case.

Finally, if all the points V, H and $L_i \cap L_j$ with $1 \le i \le 4$ and $5 \le j \le 7$ are distinct, all remaining intersection points which do not coincide with one of these are necessarily generic double points (otherwise we would have a pair of lines intersecting more than once).

Once we know that all the distinct intersections for $\mathcal{Q}$ are distinct for $\mathcal{A}$, it remains to show that $\mathcal{Q}$ cannot be realized as a complex line arrangement $\mathcal{A} = \{L_i\}_{i=0}^{10}$. Suppose that it is, for the sake of contradiction.

We will show that the intersection points

$$a = L_2 \cap L_5, \quad b = L_3 \cap L_6 \quad \text{and} \quad c = L_4 \cap L_7$$

are collinear. (See Figure 18.) Then we can conclude that the points $a' = L_1 \cap L_5$, b and c cannot be collinear. Indeed, $a \neq a'$, since all intersection points in the diagram are distinct. If all four points a, a', b and c were collinear, then the line L_5 through a and a' would coincide with the line L_{10} through a', b and c, but we assume that L_5 and L_{10} are distinct.

To see that the points a, b and c are collinear, we will use some notions of classical projective geometry, namely complete quadrangles and harmonic conjugates. (In Remark 7.16 below, we also indicate an alternative proof, in the more familiar Euclidean terms.) Observe that the lines L_5, L_6, L_2, L_3, L_8 and the line L through a and b form the four sides and the two diagonals of a complete quadrangle. Then the point $Q = L \cap L_0$ is the harmonic conjugate of the point $P = L_8 \cap L_0$ with respect to the points $V = L_2 \cap L_3$ and $H = L_5 \cap L_6$. Now, consider the lines L_2, L_4, L_5, L_7, L_9 and the line L' through a and c. Again these form a complete quadrangle, so that the point $Q' = L' \cap L_0$ is the harmonic conjugate of the point $P = L_9 \cap L_0$ with respect to $V = L_2 \cap L_4$ and $H = L_5 \cap L_7$. Since the harmonic conjugate of P with respect to V and H is unique, it follows that $Q = Q'$. Since the lines L and L' both pass through $Q = Q'$ and a, we must have $L = L'$, and so all three points a, b and c lie on this line. □

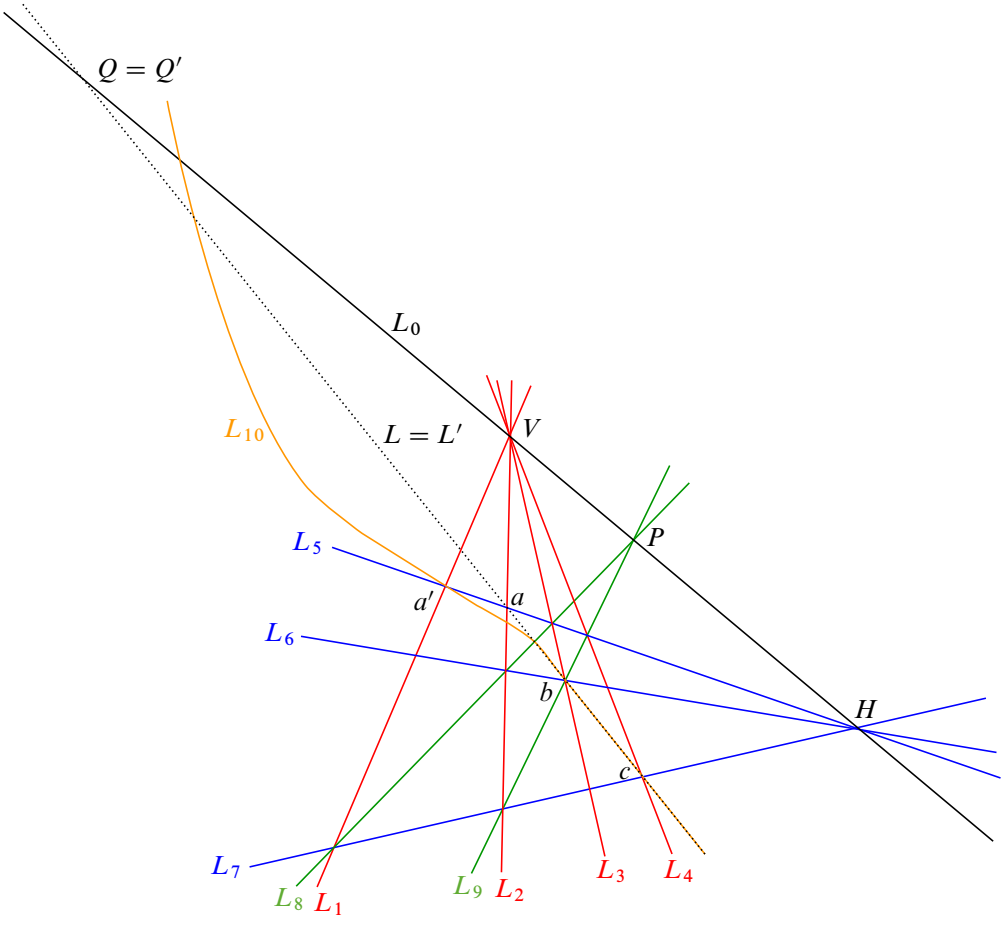

Figure 18: An arrangement of lines $L_0, L_1, \dots, L_9$ and pseudoline L_{10} with incidences as in Figure 17. We show that the line L through a and b and the line L' through a and c coincide (with the dotted line shown), so the points a, b and c are collinear. Therefore a', b and c cannot be collinear.

Remark 7.16 The above statement also has an easy Euclidean geometry proof, after some projective transformations. Indeed, we can find an automorphism of $\mathbb{C}\mathrm{P}^2$ such that

$$L_1 \cap L_5 \mapsto (0:0:1), \quad L_1 \cap L_6 \mapsto (1:0:1),$$
$$L_2 \cap L_5 \mapsto (0:1:1), \quad L_2 \cap L_6 \mapsto (1:1:1).$$

Then $H \mapsto (1:0:0)$ and $V \mapsto (0:1:0)$, and it is not hard to see that all the lines in the figure must be complexifications of real lines. The line L_0 is the line at infinity; the remaining lines are (complexifications of) the corresponding real lines in $\mathbb{R}^2$. We use the same notation for the real lines. Now we see that L_1, L_2, L_3, L_4 are parallel

vertical lines, L_5, L_6, L_7 are parallel horizontal lines, etc. So the arrangement looks like Figure 17. The lines in the figure form a number of triangles that are similar to the shaded triangle; it then follows that the points a, b, c are collinear, so a', b, c are not.

Note, however, that the above proof is somewhat incomplete: Figure 17 assumes a particular position of the lines L_3, L_4, L_7 relative to L_1, L_2, L_5, L_6. For a complete proof, an additional analysis of cases is required, with slightly different figures for other possible relative positions of the lines. Our projective argument with harmonic conjugates allows us to avoid this analysis, and also to emphasize the projective nature of the statement and the proof.

Corollary 7.17 *Let $Y = Y(11; w)$ be the Seifert fibered space given by a star-shaped plumbing graph with 11 legs such that two legs have at least 5 vertices each, two legs have at least 3 vertices, and the remaining 7 legs have at least 4 vertices each (including the central vertex). In other words, two components of the multiweight w are 4 or greater, two are 6 or greater, and the remaining seven are 5 or greater. Let ξ be the Milnor fillable contact structure on Y. Then (Y, ξ) admits a Stein filling which is not strongly diffeomorphic to any Milnor filling.*

Proof Exactly as in Corollary 7.13, this follows from Corollary 7.9 and Proposition 7.15. The picture is similar to Figure 16, with the obvious minor changes. Indeed, the pseudoline arrangement of Proposition 7.15 has two lines ℓ_0 and ℓ_3 with weight 4, two lines ℓ_9 and ℓ_{10} with weight 6, and seven remaining lines with weight 5. Note that a permutation of the components of w does not change the contact manifold, so we avoided labeling the components of w in the statement of the corollary. □

It is easy to generalize the above examples to star-shaped graphs with higher negative self-intersection values of the central vertex. Indeed, by Theorem 7.8, we can construct unexpected Stein fillings from an arbitrary arrangement of smooth graphical disks that contains an unexpected symplectic line arrangement. We turn to the general case later in this section; for now, we create more unexpected pseudoline arrangements simply by adding extra lines.

Lemma 7.18 *Suppose that Λ is an unexpected symplectic line arrangement. Let ℓ be a symplectic line that passes through at least one intersection point of two or more lines in Λ. Then the pseudoline arrangement $\Lambda \cup \{\ell\}$ is also unexpected.*

Proof If there exists a complex line arrangement $\mathcal{A}\cup\{L\}$ that satisfies all the incidence relations of $\Lambda\cup\{\ell\}$, and L corresponds to ℓ, then $\mathcal{A}$ satisfies all incidences of Λ, and so $\mathcal{A}$ is a pencil. The line L must pass through the intersection of two or more lines of $\mathcal{A}$, so $\mathcal{A}\cup\{L\}$ is also a pencil. □

Theorem 7.19 *For any $m\geq 10$, consider the Seifert fibered space $Y_m = Y(m,w)$ with $m\geq 10$, with weights $w=(w_1,\dots,w_m)$ such that $w_i\geq m-1$ for all $i=1,\dots,m$. The space Y_m is given by a star-shaped graph with $m\geq 10$ legs, such that the length of each leg is at least $m-1$. The central vertex has self-intersection $-m-1$, and all other vertices have self-intersection -2. Let ξ be the Milnor fillable contact structure on Y. Then (Y,ξ) admits a simply connected Stein filling not strongly diffeomorphic to any Milnor fiber.*

Proof We can add lines to the arrangement $\mathcal{P}$ to form unexpected arrangements of $m\geq 10$ pseudolines. Since any pseudolines intersect at most once, each pseudoline has at most $m-1$ intersections with other lines. By Corollary 7.9, $Y=Y(n,w)$ is an unexpected Stein filling if $w_i\geq m-1$ for all $i=1,\dots,m$, which is simply connected if all inequalities are strict. □

Varying the positions of the additional lines and/or applying a similar procedure to different arrangements such as $\mathcal{P}$ and $\mathcal{Q}$, it is possible to construct a variety of pairwise nonhomeomorphic Stein fillings of the same link, so that none of the Stein fillings is strongly diffeomorphic to a Milnor filling. We give one such construction below to prove the first part of Theorem 1.1. The second part of Theorem 1.1 follows from the discussion at the end of this section, where we extend star-shaped graphs that correspond to unexpected arrangements to a much wider collection of graphs of rational singularities with reduced fundamental cycle.

Theorem 7.20 *For every $N>0$ there exists a rational singularity with reduced fundamental cycle whose link (Y,ξ) admits at least N pairwise nonhomeomorphic simply connected Stein fillings, none of which is strongly diffeomorphic to any Milnor fiber. The link Y is given by a Seifert fibered space $Y=Y(2N+5,w)$ with sufficiently large weights w.*

Proof We will start with the arrangement $\mathcal{Q}$ of Figure 17 and augment it to other unexpected arrangements, using Lemma 7.18. First, we add more "vertical" and "horizontal" lines to the arrangement, so that it has N vertical and N horizontal lines, creating a

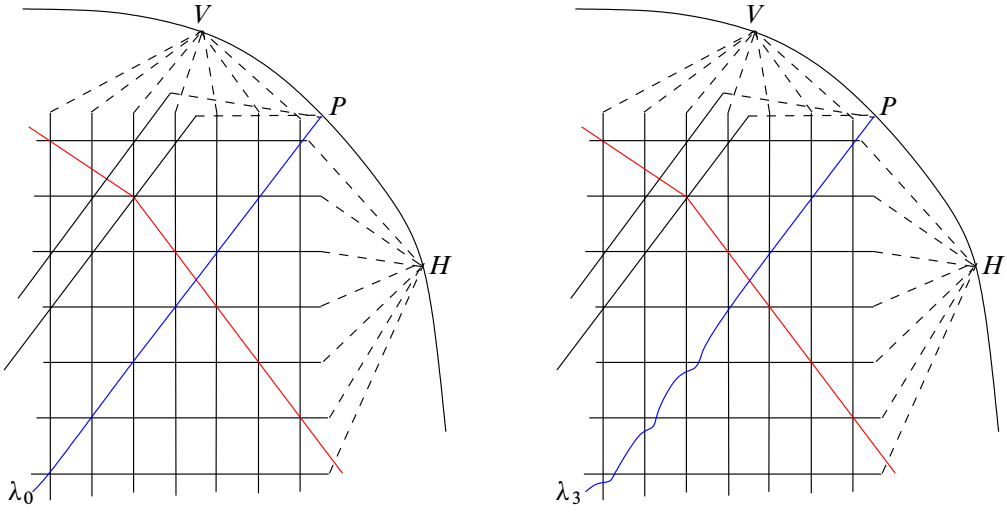

Figure 19: Pseudoline arrangements and fillings with different topology.

grid as shown in Figure 19. (We assume $N \geq 4$ as the $N = 4$ case fulfills the statement for lower values of N.) All "vertical" lines intersect at the point V, all horizontal lines intersect at the point H. The two diagonal lines ℓ_8 and ℓ_9 intersecting at P, the bent pseudoline ℓ_{10}, and the line at infinity ℓ_0 are present as in the arrangement $\mathcal{Q}$. Let $\mathcal{Q}'$ denote this arrangement. We will now produce $N+1$ unexpected arrangements $\mathcal{Q}'_k = \mathcal{Q}' \cup \lambda_k$ for $k = 0, 1, \ldots, N$, by adding to $\mathcal{Q}'$ different additional "diagonal" pseudolines $\lambda_0, \lambda_1, \ldots, \lambda_N$ passing through P; see Figure 19. Each arrangement $\mathcal{Q}'_k$ consists of $2N+5$ pseudolines. The pseudoline λ_0 is taken to be the main diagonal of the grid formed by the vertical and horizontal lines; it is a straight line in $\mathbb{R}\mathrm{P}^2$ passing through the point P. The pseudoline λ_1 differs from λ_0 in a small neighborhood of a single grid intersection: while λ_0 passes through the chosen intersection point of a vertical and a horizontal line, λ_1 intersects these two lines at distinct points. Similarly, λ_k differs from λ_0 in neighborhoods of k grid intersections and meets the corresponding vertical and horizontal lines at distinct points. Figure 19 shows the arrangements $\mathcal{Q}'_0 = \mathcal{Q}' \cup \lambda_0$ and $\mathcal{Q}'_3 = \mathcal{Q}' \cup \lambda_3$.

Now, consider the decorated germ given by a pencil of $2N+5$ lines, each with a weight greater than $2N+4$. We choose the weights to be greater than the number of intersection points on each line in any of the arrangements $\mathcal{Q}'_k$; obviously, taking weights greater than $2N+4$ suffices because each line intersects the other $2N+4$ lines once (in fact, $w \geq 2N+2$ suffices for this arrangement). Let (Y_N, ξ) be the contact link of the corresponding singularity. Similarly to the previous examples, Y_N is the

Seifert fibered space given by a star-shaped plumbing graph with $2N+5$ sufficiently long legs, with the central vertex having the self-intersection $-2N-6$ and all the other vertices self-intersection -2. By Corollary 7.9, each arrangement $\mathcal{Q}'_k$ yields a Stein filling W_k of (Y_N, ξ) which is not strongly diffeomorphic to any Milnor filling.

Finally, we argue that all fillings $W_0, W_1, \dots, W_N$ have different Euler characteristic. Each W_k has the structure of a Lefschetz fibration with the same planar fiber (a disk with $2N+5$ holes), but these Lefschetz fibrations have different numbers of vanishing cycles. Every time we replace a triple intersection of pseudolines in the arrangement by three double points (and arrange the marked points on the lines accordingly), the number of vanishing cycles decreases by 1. Indeed, three double points correspond to three vanishing cycles in the Lefschetz fibration (each enclosing two holes), while a triple intersection together with an additional free marked point on each of three lines corresponds to four vanishing cycles (one vanishing cycle enclosing three holes, the remaining three enclosing a single hole each). Thus, replacing a triple point by three double points corresponds to a lantern relation monodromy substitution, which in turn corresponds to a rational blow-down of a (-4) sphere. Therefore, $\chi(W_0) > \chi(W_1) > \cdots > \chi(W_N)$, as required. □

7.4 Generalizations

All our previous examples were given by singularities with star-shaped graphs where most vertices have self-intersection -2. It is not hard to obtain examples with much more general graphs, using the full power of Theorem 7.8: we add more smooth disks to an unexpected symplectic line arrangement.

Example 7.21 In the arrangement $\mathcal{Q}$ of Figure 17, replace the line ℓ_3 by several pseudolines that all pass through the same four intersection points. Note that because of multiple intersections, the result is no longer a pseudoline arrangement, but we still have a braided wiring diagram and can apply Proposition 5.5 to extend it to an arrangement of symplectic disks. In Figure 20, we take three curves replacing ℓ_3. In the decorated germ, the complex line corresponding to ℓ_3 will be replaced by 3 curvettas that are tangent to order 4 (and transverse to the other 10 branches of the germ). By (2-2), the weight of each new curvetta must be 5 or greater. We take the weights to be exactly 5 for the three new curvettas. Consider the symplectic curve arrangement given by the extension of the diagram in Figure 20, with marked points at all intersections and one additional free marked point on each of the three new curves (to account for higher weights). The resolution graph for $\mathcal{Q}$ is star-shaped with 11 legs. The

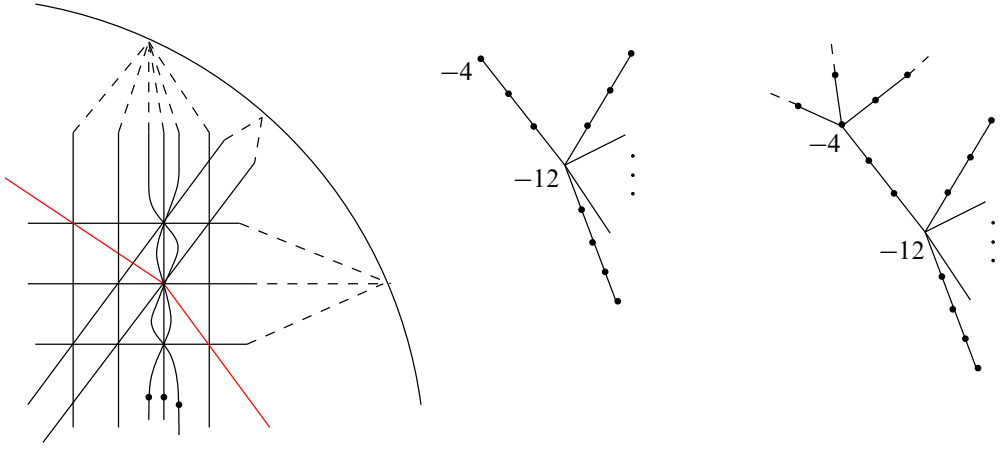

Figure 20: The pseudoline arrangement $\mathcal{Q}$ of Figure 17 is modified: the pseudoline ℓ_3 is replaced by three smooth curves with 4 intersections, as shown. There are 3 free marked points, one on each of the new curves; the rest of the marked points are the intersections in the diagram. The germ of the corresponding singularity has three curvettas tangent to order 4, each of weight 5, replacing one of the lines. The resolution graph of the corresponding singularity is shown in the middle of the figure. If the weights of the three tangent curvettas are taken to be higher, the graph will have additional branching as shown on the right. All unlabeled vertices have self-intersection -2.

self-intersection of the central vertex is -12 and all other self-intersections are -2. The legs of the resolution graph for $\mathcal{Q}$ with minimal weights had two legs of length 3, two of length 5, and seven of length 4. For this revised arrangement, the corresponding singularity has an augmented graph. Specifically, one of the legs of length 3 (which corresponded to ℓ_3) gains an additional vertex of self-intersection -4. If the three tangent curvettas have higher weights, so they have additional free marked points in the deformed arrangement, the -4 vertex becomes a branching point with 3 additional legs (each vertex on these legs has self-intersection -2). See Figure 20. By Theorem 7.8, the links of the corresponding singularities have unexpected Stein fillings.

In general, if we replace ℓ_3 with k curves commonly intersecting at the four points where ℓ_3 intersected other pseudolines as above, the additional vertex will have self-intersection $-k-1$ and increased weights will yield k additional legs with (-2) vertices.

Further, we can replace each of the k pseudolines by a bundle of curves that go through the same intersections.

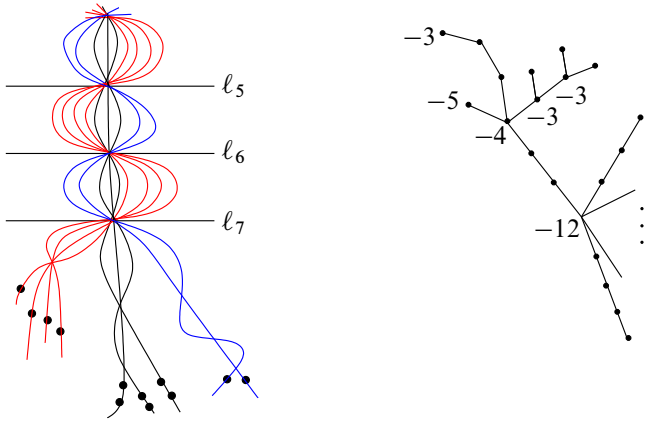

Figure 21: In the pseudoline arrangement $\mathcal{Q}$ of Figure 17, we replace ℓ_3 with a bundle of curves passing through the existing intersections of ℓ_3 with ℓ_5, ℓ_6, ℓ_7 and ℓ_0. (Only part of the arrangement is shown.) The additional curves create no extra intersections with the pseudolines of $\mathcal{Q}$. All the intersection points are marked, and there are additional free marked points that correspond to higher weights. In the resolution graph of the singularity, the leg corresponding to ℓ_3 is replaced by a tree with additional branching, as shown. All unlabeled vertices have self-intersection -2.

Example 7.22 Figure 21 shows a possible bundle replacing ℓ_3, instead of the bundle of three curves in the previous arrangement of Figure 20. All the new curves run C^1–close to and are isotopic to the original pseudoline, and they pass through the same intersection points with the other pseudolines. Within each bundle, the curves may have additional intersections, which lead to higher-order tangencies between the corresponding curvettas in the decorated germ. In particular, for the arrangement in Figure 21, the bundle of curves replacing ℓ_3 will have three subbundles of curves intersecting each other 4 times, and intersecting each of the other pseudolines once. One of these subbundles has four curves which intersect each other a total of 5 times, another has two curves which intersect a total of 7 times, and the third has two curves intersecting each other a total of 6 times, with an additional curve intersecting these two 5 times.

The corresponding decorated germ (with the weights given by the number of intersection points in the disk arrangement) encodes the singularity whose graph has more branching and some vertices with higher negative self-intersections, as shown in Figure 21. If we vary the incidence pattern of the additional curves (subject to the weight restrictions), we can obtain a number of unexpected Stein fillings with different topology.

Example 7.22 demonstrates how, once we have an unexpected symplectic line arrangement $\Gamma = \{\Gamma_i\}$, the star-shaped graph G of the corresponding singularity can be extended to arbitrarily complicated graphs of rational singularities with reduced fundamental cycle. The following proposition explains how to form these bundles in general from a given extension of the graph, completing the proof of Theorem 1.1. It is not hard to see that under the hypotheses of the proposition, the extended graph H corresponds to a singularity with reduced fundamental cycle.

Proposition 7.23 *Let G be the star-shaped resolution graph corresponding to the surface singularity associated to an unexpected symplectic line arrangement with minimal possible weights. Let I be the set of leaves of G, and let $\{G_i\}_{i\in I}$ be a collection of (possibly empty) negative definite rooted trees; assume that G and G_i have no (-1) vertices.*

Consider a graph H constructed by attaching to G the rooted trees G_i, $i \in I$, so that the root of G_i is connected to the leaf u_i by a single edge. Assume that the resulting graph H satisfies condition (2-1). Let (Y,ξ) be the link of a rational surface singularity with reduced fundamental cycle whose dual resolution graph is H.

Then (Y,ξ) admits a Stein filling which is not strongly diffeomorphic to any Milnor filling.

Remark 7.24 Proposition 7.23 provides a fairly general class of rational surface singularities with reduced fundamental cycle which admit unexpected fillings. The construction can be further generalized to include variations in the bundling structure and to apply to more general graphs G as the input. Despite all variations, getting rid of the (-2) vertices in the resolution graph seems difficult. Indeed, we could add a curve intersecting ℓ_3 only twice in Example 7.22, which would lower the self-intersection to (-3) for one of the vertices on the leg of the star-shaped graph G. However, such a curve would intersect the other pseudolines in the arrangement $\mathcal{Q}$ at new points. This would increase the weights on the curvettas corresponding to these other pseudolines, producing free marked points and yielding additional (-2) vertices elsewhere in the graph. In fact, we already know from Theorem 1.2 that our strategy must have limitations, as there are no unexpected fillings when each vertex of the resolution graph has self-intersection -5 or lower.

Proof of Proposition 7.23 The initial unexpected symplectic line arrangement $\{L_i\}$ consists of symplectic lines associated to the legs of the star-shaped graph G. As above,

let u_i denote the valency 1 vertex of the leg that corresponds to L_i. Choose a braided wiring diagram for the symplectic line arrangement such that a symplectic line L_i corresponds to the wire γ_i. The braided wiring diagram should be chosen so that γ_i contains all the marked points of L_i (including free points). We will replace each wire γ_i with a bundle of curves (with intersections but no braiding between the components of the bundle) constructed according to the tree G_i, as follows.

All curves in the i^{th} bundle must intersect at all marked points on γ_i. We will specify the additional intersections and explain how to determine the number of curves and free marked points in the bundle. The bundle will be described recursively, via its subbundles and iterative (sub)^k–bundles, which we determine by moving through the graph G_i. We start at the root and move upward in the graph G_i with respect to the partial order induced by the root, stopping when we either reach either a vertex v_0 of self-intersection number $-s_0$ for $s_0 \geq 3$, or exhaust the graph G_i.

By condition (2-1), (-2) vertices can only occur in a linear chain. Thus, if we never reach a vertex with self-intersection $-s_0$ for $s_0 \geq 3$, then all vertices of G_i have self-intersection -2 (and G_i is a linear chain). Suppose there are $r_0 \geq 0$ such (-2) vertices. In that case, the bundle for G_i should consist of only a single curve, but with $r_0 \geq 0$ additional free points. (The weights of the decorated germ increase accordingly.)

If there exists a vertex v_0 of self-intersection $-s_0$ for $s_0 \geq 3$ after passing through a linear chain of r_0 vertices of self-intersection -2, then the bundle will consist of exactly $s_0 - 1$ nonempty subbundles. The subbundles will be described as we travel further along G_i. We require that all curves in the bundle intersect exactly r_0 additional times (where each of these r_0 intersection points gets marked) and increase the weight of each curve by $r_0 + 1$, yielding one additional free marked point on each curve. Two curves in different subbundles will not intersect at any additional points beyond those specified so far.

Note that v_0 can have at most $s_0 - 1$ vertices directly above it in G_i, since its valency is at most s_0. In particular, G_i itself is built by attaching $s_0 - 1$ (potentially empty) trees onto the subgraph $\{v \leq v_0\} \subset G_i$. We associate the $s_0 - 1$ subbundles to these $s_0 - 1$ rooted trees $G_1^1, \ldots, G_{s_0-1}^1$, which may be empty or nonempty. (The partial order on G induced by its root induces a partial order and root on each G_j^1.)

Now we will create subbundles and their subsubbundles by iteratively repeating a slight modification of the process above. For each tree G_j^1, we construct a subbundle as follows. Starting at the root of G_j^1, we again have a linear chain of $r_1 \geq 0$ vertices

with self-intersection -2, which either exhausts the graph G_j^1 or ends in a vertex v_1 of self-intersection number $-s_1$ for $s_1 \geq 3$. (Note that r_1 and s_1 depend on j, but we drop this index to avoid further notational clutter.) If we are in the first case, where there is no such vertex v_1, the subbundle associated to G_j^1 will consist of a single curve with r_1 additional free marked points. If we are in the second case, where the chain of length r_1 of (-2) vertices ends at a vertex v_1 with self-intersection $-s_1$ with $s_1 \geq 3$, the subbundle itself will be a union of $s_1 - 1$ nonempty subsubbundles, intersecting at $r_1 + 1$ additional points. (Accordingly, the weights increase by $r_1 + 1$, but no new free marked points are added.) Two curves in different subsubbundles will not intersect at any additional points beyond those previously specified.

The $s_1 - 1$ subsubbundles correspond to the $s_1 - 1$ potentially empty trees $G_1^2, \dots, G_{s_1-1}^2$ attached above v_1. We determine these subsubbundles by iteratively repeating this process, where G_l^2 takes the role of G_j^1 and the subsubbundle takes the role of the subbundle. The $(\text{sub})^k$–bundles will generally have $(\text{sub})^{k+1}$–bundles, leading to additional iterations of the procedure. The situation where a $(\text{sub})^k$–bundle does not have a $(\text{sub})^{k+1}$–bundle is when the $(\text{sub})^k$–bundle consists of a single component (as in the first case of the procedure). Since the graph is finite, there will be a finite number of iterations, so this process will eventually describe the bundle completely.

Having constructed such bundles individually for each G_i, we now superimpose them onto the wires γ_i as satellites to get a new braided wiring diagram by inserting them into a small neighborhood of γ_i so that each wire of the bundle is C^1–close to the original wire γ_i. Recall that all intersection points between wires are marked in the original diagram, and all curves from the i^{th}–bundle are required to intersect at all marked points. It follows that curves from the different bundles are allowed to intersect *only* at the marked points of the original diagram.

We can apply Proposition 5.5 to extend the new braided wiring diagram to an arrangement Γ of symplectic disks. We claim that via Lemma 3.2, the resulting arrangement Γ provides a Stein filling for the link of the singularity with the resolution graph H. To check the claim, we need to show that the open book decomposition on the boundary of the Lefschetz fibration constructed from Γ supports the canonical contact structure for the link associated to H. Recall that H is associated to a decorated germ $\mathcal{C}^H$ with smooth branches, by attaching (-1) vertices and curvettas and blowing down. We will show that Γ is related by a smooth graphical homotopy to another decorated germ $\mathcal{C}$, which is topologically equivalent to $\mathcal{C}^H$. The topological type of $\mathcal{C}$ will be determined by the intersections and marked points in Γ: the order of tangency between

two components in $\mathcal{C}$ is equal to the number of intersections between the corresponding components of Γ. The weight on each curve is the total number of marked points on the corresponding disk of Γ, including intersections and free marked points. After showing that Γ and $\mathcal{C}$ are related by a smooth graphical homotopy, we will verify that $\mathcal{C}$ and $\mathcal{C}^H$ are topologically equivalent (with corresponding weights), to conclude that the open book decompositions are equivalent.

To relate Γ and $\mathcal{C}$, we first construct a smooth graphical homotopy from Γ to a "pencil of the bundles". In the pencil of the bundles, all curves will intersect at one point, and curves from different bundles do not intersect anywhere else, but curves from the same bundle may intersect at other points along the corresponding line. We can use a smooth graphical homotopy of the original symplectic line arrangement $\{L_i\}$ to a pencil as a guide to build the required homotopy of Γ, because each bundle is C^1–close to the corresponding symplectic line inside the chosen Milnor ball. Essentially, at this step we treat each bundle as a whole, bringing different bundles together without perturbing curves inside each bundle. More precisely, we satellite the bundle onto the family of wiring diagrams corresponding to the smooth graphical homotopy of the symplectic lines to the pencil. The intersection points within a bundle will remain distinct in this smooth graphical homotopy. At intermediate times during the homotopy, we allow many additional intersection points in the arrangement, as curves from different bundles will intersect outside the common marked intersections.

Next, we show that each bundle can be homotoped so that all the intersections come together to high-order tangencies. Let Γ^i denote the i^{th} bundle constructed above, and let $\mathcal{C}^i$ denote the curves in the germ $\mathcal{C}$ corresponding to those in Γ^i. To show that Γ^i and $\mathcal{C}^i$ are related by a smooth graphical homotopy, it suffices to check that they have the same boundary braid. To verify this, we observe that the subbundling structure looks like the nested structure produced by the Scott deformation of $\mathcal{C}^i$ as in the proof of Proposition 4.1. The bundle, as drawn in $\mathbb{R}^2$, provides a wiring diagram which is planar isotopic to the wiring diagram of the Scott deformation, and thus their braid monodromy is the same. As a consequence, each bundle Γ^i is related by a smooth graphical homotopy to $\mathcal{C}^i$. Applying these homotopies to all bundles, we see that Γ is related to $\mathcal{C}$ by a smooth graphical homotopy, and their induced open books agree.

Now, we need to check that $\mathcal{C}$ and $\mathcal{C}^H$ are topologically equivalent. To this end, we will compare the weights and the pairwise orders of tangency between curvettas in the two germs. For $\mathcal{C}$, these quantities are computed from the intersections and marked points in Γ, while Remark 2.6 shows how to compute them from the graph H.

First, we make a few observations to relate the curvettas on the graph H to the bundling construction above. Before the star-shaped graph G is extended, the lines L_i correspond to the legs of the graph. For each i, the i^{th} leg is a chain of (-2) vertices, with an end vertex u_i. We attach a single (-1) vertex to u_i and put a curvetta on this vertex; this curvetta gives rise to the line L_i. By Remark 2.6, the weight of L_i is $1 + l(u_0, u_i)$, where u_0 is the root of G. In this case, the root has been chosen to be the center of the star-shaped graph.

When G_i is nonempty, the symplectic line L_i is replaced by a collection of m_i curves (we compute m_i below) in the germ associated to H. These new curves come from curvettas on the additional (-1) vertices attached to G_i. For each $v \in G_i$, $(v \cdot v + a(v))$ additional (-1) vertices are attached to v, and each (-1) vertex has a curvetta attached, thus

$$m_i = -\sum_{v \in G_i} (v \cdot v + a(v)),$$

as in Proposition 2.4. Note that m_i agrees with the number of curves in the bundle Γ_i constructed above for the graph G_i. This is because the subbundling process terminates when you reach a $(\text{sub})^k$–bundle which is a single component. This occurs when the $(\text{sub})^k$–bundle corresponds to a $(\text{sub})^k$–tree consisting of only $r \geq 0$ vertices of self-intersection -2. When $r > 0$, this means that there is a (-2) vertex leaf which contributes one to m_i, and when $r = 0$, this means there is a $(-s)$ vertex v with fewer than $(s-1)$ branches above it, and there are correspondingly $-(v \cdot v + a(v)) = s - a(v)$ such $(\text{sub})^k$–bundles, each consisting of a single curve.

Now, let C_x be one of the curvettas for the graph H, and let $\widetilde{v}_x$ be a vertex of G such that C_x intersects a (-1) vertex attached to $\widetilde{v}_x$. According to Remark 2.6, the weight of C_x according to the graph H is $1 + l(\widetilde{v}_x, u_0)$, where $l(\widetilde{v}_x, u_0)$ counts the number of vertices in the path from the root u_0 of G to the vertex $\widetilde{v}_x$. This path consists of several parts. From the original graph G, the path contains the $l(u_i, u_0)$ vertices connecting the root u_0 to the vertex u_i where G_i is attached. Next, there are vertices from G_i, which can be organized into $(K+1)$ chains as shown in Figure 22. For $0 \leq k \leq K-1$, the k^{th} chain consists of $r_k \geq 0$ vertices of self-intersection (-2), followed by a vertex of self-intersection $-s_k < -2$. Finally, there may be a last chain of (-2) vertices, of length $r_K \geq 0$, such that $\widetilde{v}_x$ is its last vertex. (If $\widetilde{v}_x \cdot \widetilde{v}_x < -2$, then $r_K = 0$.) Therefore,

$$1 + l(\widetilde{v}_x, u_0) = 1 + l(u_i, u_0) + r_K + \sum_{k=0}^{K-1} (r_k + 1).$$

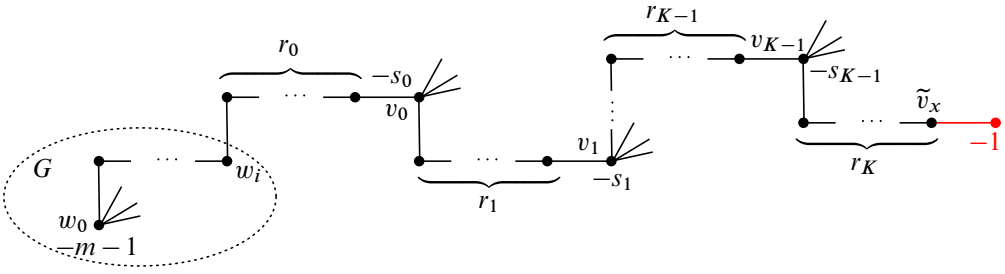

Figure 22: How to compute the weights from the graph G following the proof of Proposition 7.23.

On the other hand, in the construction of the bundle, the initial weight on each curve begins at $1 + l(u_i, u_0)$. For each iterative $(\text{sub})^k$–bundle it is included in, the weight is increased by $r_k + 1$, until we reach a stage K where the $(\text{sub})^K$ graph consists of $r_K \geq 0$ vertices, all of self-intersection -2. For this K^{th} stage, the weight is increased by r_K (the increase is associated to free marked points). Therefore, the total weight on C_x will be

$$w(C_x) = 1 + l(u_i, u_0) + r_K + \sum_{k=0}^{K-1} (r_k + 1),$$

which agrees with $1 + l(\widetilde{v}_x, u_0)$, as required.

Next, we compare the orders of tangency between the curves. According to Remark 2.6, the order of tangency between two components C_x and C_y is $\rho(\widetilde{v}_x, \widetilde{v}_y; u_0)$, the number of common vertices in the path from $\widetilde{v}_x$ to u_0 with the path from $\widetilde{v}_y$ to u_0. By condition (2-1), the vertex v_L where these two paths diverge has self-intersection $-s_L$ for $s \geq 3$. See Figure 23. The path from u_0 to v_L includes the path from u_0 to u_i in G. This contributes $l(u_i, u_0)$ vertices. The path continues into G_i, with sequential chains of r_k vertices of self-intersection (-2), each ending in a vertex v_k of self-intersection $-s_k < -2$, for $0 \leq k \leq L$. Therefore,

$$\rho(\widetilde{v}_x, \widetilde{v}_y; v_0) = l(u_i, u_0) + \sum_{k=0}^{L} (r_k + 1).$$

On the other hand, in the bundle construction, the curves C_x and C_y lie in two distinct $(\text{sub})^{L+1}$–bundles created for two of the distinct trees lying above vertex v_L. No intersections between C_x and C_y will be created after the L^{th} stage. At the beginning of the bundle construction, all curves are required to intersect $1 + l(u_i, u_0)$ times. All other intersections between C_x and C_y are created in the procedure above at some

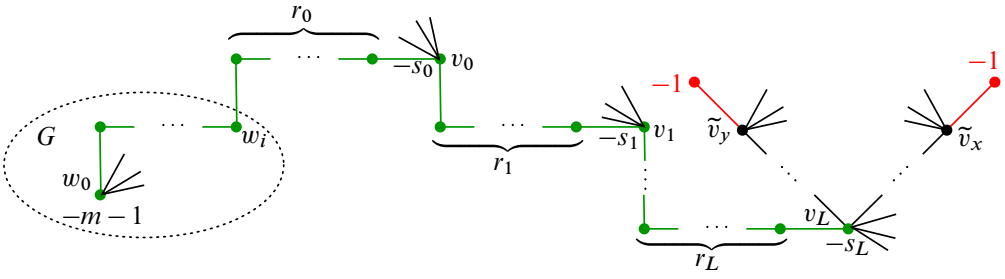

Figure 23: How to compute the tangencies from the graph G following the proof of Proposition 7.23.

iteration k, $0 \le k \le L$. At the $k = 0$ stage, we add r_0 intersections between C_x and C_y. At stage k for $1 \le k \le L$, we add additional $r_k + 1$ intersections between C_x and C_y. Therefore the total number of intersections between C_x and C_y is

$$1 + l(u_0, u_i) + r_0 + \sum_{k=1}^{L} (r_k + 1),$$

which agrees with $\rho(\widetilde{v}_x, \widetilde{v}_y; v_r)$.

To complete the proof, observe that the arrangement Γ contains the original unexpected symplectic line arrangement as a subarrangement (choose a single component of each bundle). By Theorem 7.8, we obtain unexpected Stein fillings of the link of the singularity corresponding to the graph H. □

8 Further comments and questions on curvetta homotopies

In the previous section we showed that Stein fillings of the link of a singularity do not always arise from the Milnor fibers, even for the simple class of rational singularities with reduced fundamental cycle. Our examples of unexpected Stein fillings come from curvetta arrangements that do not arise as picture deformations of the decorated germ representing the singularity, although these arrangements are still related to the decorated germ through a smooth graphical homotopy. In this section, we make a detailed comparison of de Jong and van Straten's picture deformations (Definition 2.7) with smooth graphical homotopies (Definition 3.1). Observe that the two notions differ in several essential ways. Indeed, the curvetta branches are required to be algebraic in the former, and just smooth in the latter; positivity of all intersections and the weight restrictions must hold at all times during a picture deformation but only at the end of a graphical homotopy; the topology of the arrangement may change at nonzero times

	smooth graphical homotopy	picture deformation
type of curvetta branch C_j^t	smooth graphical disk	disk given by (germ of) algebraic curve
topology of curvetta arrangement	may change with time	remains the same
weight restrictions: C_j^t has at most w_j intersections	only hold for final arrangement, may be violated during homotopy	hold at all times
positivity of intersection points: $C_i^t \cdot C_j^t > 0$	only hold for the final arrangement, may be violated during homotopy	hold at all times

Table 1

during graphical homotopy but not during a picture deformation. This is summarized in Table 1. We will explore each of these aspects and their role in differentiating Stein fillings from Milnor fibers. The most important aspect seems to be the topology of the curvetta arrangement, and whether it is allowed to vary during the homotopy.

8.1 Algebraic versus smooth

The first difference between picture deformations and homotopies is that a smooth graphical homotopy includes curvettas which need not be complex algebraic curves, either during the course of the homotopy or at the end of the homotopy. It turns out that this is not the key aspect contributing to the difference between Milnor fillings and Stein fillings in our examples. Indeed, adding higher-order terms, one can produce some surprising curvetta arrangements. Because the curvettas are open algebraic disks, possibly given by high-degree algebraic equations, curvetta arrangements can be more general than arrangements of complex lines or global algebraic curves. To illustrate, we recall the example of the pseudo-Pappus arrangement from [27]; see Figure 24.

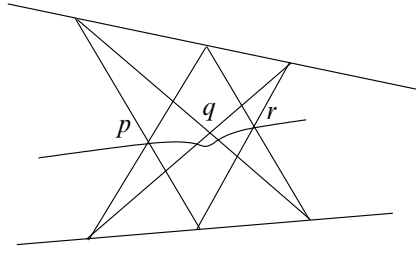

Figure 24: The pseudo-Pappus arrangement.

Example 8.1 [23; 27] The classical Pappus arrangement consists of 9 lines; we have already discussed this arrangement in Example 7.10. By the Pappus theorem, the points p, q, r in the middle of Figure 24 are collinear. In the pseudo-Pappus arrangement, the line through these three points is replaced by a bent pseudoline that passes through two points but not through the third. The pseudo-Pappus arrangement cannot be realized by complex lines. However, the bent pseudoline can be given by a graph of a high-degree polynomial whose additional intersections with the other lines occur sufficiently far outside the ball we restrict to. Thus, the pseudo-Pappus arrangement can be realized by higher-degree open algebraic curves. In fact, as mentioned in [27], the pseudo-Pappus arrangement arises as a picture deformation of the pencil of 9 lines, with the weights of each line given by the number of intersection points on the corresponding line in the arrangement. The picture deformation can be obtained by adding small higher-order terms to the linear deformation of the pencil to the classical Pappus arrangement. Thus, the pseudo-Pappus arrangement gives rise to Milnor fibers of smoothings of the singularities given by the corresponding decorated pencil of 9 lines.

In fact, all of the fillings produced via arrangements of real pseudolines can be obtained from an algebraic curvetta arrangement which can be deformed by a polynomial homotopy (through algebraic curves) to a pencil of lines. (However, this family does not constitute a picture deformation because the topology may vary at different $t \neq 0$, and the weight constraints may fail at intermediate times.) Note that we only consider a portion of the algebraic curves in a chosen ball surrounding the origin. In particular, the algebraic curves may intersect additional times outside of this ball, but we do not need to count such intersections in the incidence data of our arrangement.

Proposition 8.2 *Let $\Lambda = \{\ell_1, \dots, \ell_m\}$ be an arrangement of real pseudolines in $\mathbb{R}^2$. Then there exists a family of complex algebraic curves $\{\Gamma_1^t, \dots, \Gamma_m^t\}$, given by polynomial equations*

$$\Gamma_i^t = \{y = p(x,t)\}$$

and a smoothly embedded closed 4–ball $B \subset \mathbb{C}^2$, such that $\{\Gamma_1^t, \dots, \Gamma_m^t\}$ is a symplectic line arrangement in B (with intersections in the interior of B) for every $t \in [0,1]$, where

- *$B \cap (\Gamma_1^0 \cup \cdots \cup \Gamma_m^0)$ has the incidences of a pencil of lines, and*
- *$B \cap (\Gamma_1^1 \cup \cdots \cup \Gamma_m^1)$ is isotopic in B to the symplectic extension of the pseudoline arrangement $\ell_1 \cup \cdots \cup \ell_m$ given by Proposition 5.5.*

Before proving the proposition, we discuss its consequences.

Remark 8.3 Consider an arbitrary pseudoline arrangement $\ell_1, \dots, \ell_m$ and the corresponding symplectic line arrangement $\{\Gamma_1, \dots, \Gamma_m\}$. By Proposition 7.4, this arrangement gives Stein fillings of the spaces $(Y(m; w_1, \dots, w_k), \xi)$ whenever the weights satisfy inequalities $w_k \geq w(\Gamma_k)$ for $k = 1, \dots, m$. Let $\Gamma^t = \{\Gamma_1^t, \dots, \Gamma_m^t\}$ be a polynomial homotopy between a pencil of lines and the arrangement $\{\Gamma_1, \dots, \Gamma_m\}$; such a homotopy always exists by Proposition 8.2. A priori, the homotopy may violate the weight constraints: at some moment t, the number of intersections may increase, so that $w(\Gamma_k^t) > w_k$. (In fact, the homotopy constructed in Proposition 8.2 converts all multiple intersections into double points and thus creates a lot of additional intersections.) However, since Γ_k^t intersects each of the other $m-1$ components exactly once, $w(\Gamma_k^t)$ will never exceed $m-1$. Thus, if $w_k \geq m-1$ for all k, any homotopy as above will satisfy the weight constraints. By construction, intersections between any two components Γ_i^t and Γ_j^t remain positive for all t. Thus, the homotopy Γ^t satisfies the requirements of the first, third and fourth lines in Table 1, sharing these properties with picture deformations, but it changes the topology of the arrangement. Accordingly, the arrangement $\{\Gamma_1^t, \dots, \Gamma_m^t\}$ gives a Stein filling W_t of $(Y(m; w_1, \dots, w_k), \xi)$ for every t, and W_t carries a Lefschetz fibration as in Lemma 3.2, but the topology of the fillings W_t changes with t. Note also that for small $t > 0$, the defining polynomials for Γ_k^t give an unfolding, and thus a 1–parameter deformation of $\mathcal{C}$. Equipped with marked points, this gives a picture deformation. Therefore, for small $t > 0$ the Stein filling W_t is given by a Milnor fiber. As t increases and the topology of the arrangement changes, we obtain new fillings W_t, which may not be realizable by Milnor fibers. We will consider a specific example of such a topology change in Section 8.3.

The conclusion we wish to draw here is that the difference between algebraic curves and smooth curves is not essential to our counterexamples, as we can realize the corresponding symplectic line arrangements by complex algebraic curves and construct polynomial homotopies. The positivity of intersections and the weight constraints can often be trivially satisfied, although we further discuss the role of weights in Section 8.4. In fact, the important difference comes from the second aspect in Table 1, namely smooth graphical homotopies can vary their topology and singularities in various different ways during the homotopy, whereas picture deformations must maintain the same topology for all nonzero parameters t.

We now turn to the proof of Proposition 8.2. Given any pseudoline arrangement, it can be isotoped in $\mathbb{R}^2$ to be in a standard wiring diagram form, with the following properties. Each pseudoline is graphical, $\ell_i = \{y = f_i(x)\}$. Away from intersection

points, each pseudoline is horizontal with $f_i(x) = 2\delta n$ for some integer $1 \le n \le m$ and a fixed constant $\delta > 0$. There are disjoint intervals $(a_1, b_1), \dots, (a_r, b_r)$ at which $f_i(x)$ is nonconstant, such that there is a unique point in each interval (a_k, b_k) at which ℓ_i intersects other pseudolines. Furthermore, we ask that f_i and f_j are linear whenever $|f_i(x) - f_j(x)| < \delta$, and each $f_i(x)$ is monotonic in each interval (a_k, b_k). We will assume after a planar isotopy of Λ that our pseudoline arrangement is initially given in this form. To construct our algebraic family, we first require a smooth family of pseudolines connecting this given pseudoline arrangement in standard wiring diagram form to a pencil, and satisfying a quantitative transversality property, as follows.

Lemma 8.4 *Let $\Lambda = \{\ell_1, \dots, \ell_m\}$ be an arrangement of real pseudolines in $\mathbb{R}^2$ in standard wiring diagram form with constant δ, such that all intersections occur in $[-M, M] \times \mathbb{R}$. Then there exist smooth functions $f_i : [-M, M] \times [0, 1] \to \mathbb{R}$ with the following properties*:

(1) *$\ell_i = \{y = f_i(x, 1)\}$, ie at time 1 the graphs of the functions give the chosen pseudoline arrangement.*

(2) *$f_i(x, 0) = c_i x$, ie at time 0 the graphs of the functions give a linear pencil.*

(3) *For any $t_0 \in [0, 1]$ and any $i \neq j$, there is a unique point $\overline{x} \in [-M, M]$ such that $f_i(\overline{x}, t_0) = f_j(\overline{x}, t_0)$ and an interval $(a, b) \subset [-M, M]$ containing $\overline{x}$ such that $|f_i(x, t_0) - f_j(x, t_0)| < \delta$ if and only if $x \in (a, b)$, ie the pseudolines remain at least distance δ apart except in a neighborhood of their unique intersection.*

(4) *For any $t_0 \in [0, 1]$ and any $x_0 \in [-M, M]$ such that $|f_i(x_0, t_0) - f_j(x_0, t_0)| < \delta$, we have that*

$$\left| \frac{\partial f_i}{\partial x}(x_0, t_0) - \frac{\partial f_j}{\partial x}(x_0, t_0) \right| > \eta := \frac{\delta}{2M},$$

ie whenever the pseudolines become close enough to intersect, their slopes are quantitatively far enough from each other to ensure isolated transverse intersections.

Proof Note that when the original pseudoline arrangement $\{\ell_i\}$ is in standard wiring diagram form, it does satisfy property (4) of the lemma when $t_0 = 1$. This is because whenever $|f_i(x, 1) - f_j(x, 1)| < \delta$, the function $f_i - f_j$ is linear, and it interpolates a height difference greater than δ over an interval smaller than $2M$, so its slope is greater than η.

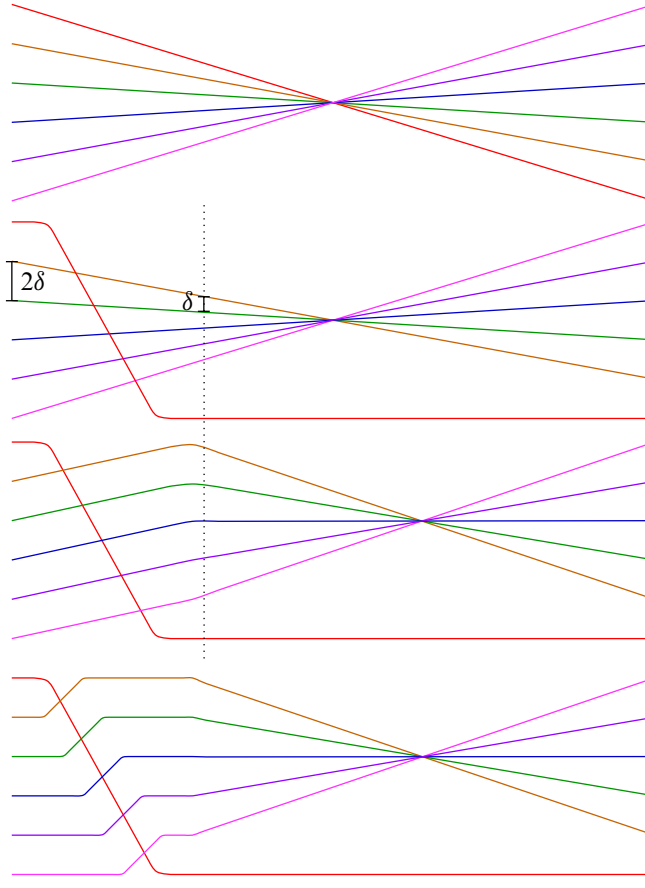

Figure 25: Key move used to construct a family of pseudolines, slightly modified from [57].

It was proven in [57, Proposition 6.4] that any arrangement of pseudolines in standard wiring diagram form can be related through a family of pseudolines to a pencil. In that paper, what is needed is that the pseudolines maintain transverse intersections throughout the family, whereas we need a quantitative measure of this transversality. We demonstrate here that this stronger condition is in fact satisfied by the family in [57].

We briefly recall the key aspects in the construction of the family and refer the reader to [57, Proposition 6.4] for further details. This family is graphical and thus can be written as $\ell_i^t = \{y = f_i(x,t)\}$ for $i = 1,\dots,m$, where $\ell_i^1 = \ell_i$. The key move to modify the pseudoline arrangement into a pencil through a family is shown in Figure 25; this figure is a slight modification of that appearing in [57, Figure 8]. This move is used

Figure 26: First reordering move.

iteratively to break up k–tuple points into a sequence of double points in a particular order. This procedure can be reversed to form an m–tuple point from a collection of appropriately ordered double points at the end to obtain a pencil. The order of the double points can be modified through the moves shown in Figures 26 and 27, by a classical theorem of Matsumoto and Tits [37].

If a pseudoline arrangement satisfies the transversality property (4) before the move in Figure 27, then it will continue to satisfy the same property throughout the move, because the relative slopes remain the same; only the interval where they occur is translated.

For the move from Figure 26, this can be realized using Figure 25 once in reverse to form a triple point, and then again in the forwards time direction, but mirrored to break up the triple point in the opposite manner; see [57, Figure 10]. Therefore it suffices to ensure that property (4) is satisfied throughout the move shown in Figure 25. Indeed, throughout this move, whenever a pair of pseudolines have height difference less than δ (recall that the spacing between the heights of the strands at the left and right ends of the figure is 2δ), both pseudolines are linear in this interval. The difference of pairwise slopes whenever $|f_i(x,t)-f_j(x,t)|<\delta$ is always greater than η throughout this family, because each crossing changes the difference in f_i-f_j by at least 2δ across the interval, whereas the interval has length at most $2M$. Moreover, this move preserves the property that there is a unique interval at which a given pair satisfies $|f_i(x,t)-f_j(x,t)|<\delta$. □

Proof of Proposition 8.2 We use the functions $\{f_i(x,t)\}$, representing a family of pseudolines through their graphs at a fixed time t, and approximate these by real polynomials intersecting in somewhat controlled ways. We assume that $x\in[-M,M]$ and that $M\geq 1$. Our final pseudoline arrangement is given by $\ell_i=\{y=f_i(x,1)\}$. Let $x_1,\dots,x_n$ be the points at which $f_i(x_k,1)=f_j(x_k,1)$ for some $i\neq j$.

Figure 27: Second reordering move.

Let $\varepsilon > 0$. Let $\zeta = \min\{1, \min_{i\neq j}\{|x_i - x_j|\}\}$. In particular, $\zeta \leq 1$.

Using the Stone–Weierstrass approximation theorem, choose polynomials $\widetilde{p}_i(x,t)$ such that

$$\left|\frac{\partial f_i}{\partial x}(x,t) - \widetilde{p}_i(x,t)\right| < \frac{\varepsilon\zeta^{n-1}}{4n^2(2M)^n}.$$

Then by integrating $\widetilde{p}_i(x,t)$ and shifting by a constant, we can find $\overline{p}_i(x,t)$ such that $(\partial\overline{p}_i/\partial x)(x,t) = \widetilde{p}_i(x,t)$ and

$$|\overline{p}_i(x,t) - f_i(x,t)| < \frac{\varepsilon\zeta^{n-1}}{4n^2(2M)^{n-1}}.$$

Now for $k = 1,\dots,n$ let

$$a_k^i = \frac{(f_i(x_k,1) - \overline{p}_i(x_k,1))}{(x_k - x_1)\cdots(x_k - x_{k-1})(x_k - x_{k+1})\cdots(x_k - x_n)}.$$

Let $a_0^i = \overline{p}_i(0,0)$. Define

$$\begin{aligned} p_i(x,t) = \overline{p}_i(x,t) &+ a_0^i(t-1) + a_1^i t(x-x_2)\cdots(x-x_n) \\ &+ a_2^i t(x-x_1)(x-x_3)\cdots(x-x_n) + \cdots + a_n^i t(x-x_1)\cdots(x-x_{n-1}). \end{aligned}$$

Then for every $k = 1,\dots,n$, we have that $p_i(x_k,1) = f_i(x_k,1)$ and $p_i(0,0) = p_j(0,0) = 0$ for all i and j. In particular, for every multi-intersection point of the pseudolines $\ell_1,\dots,\ell_m$, there is a multi-intersection point of the corresponding $\{p_1(x,1)=0\},\dots,\{p_m(x,1)=0\}$. We will show that the curves $\gamma_1^{t_0} := \{p_1(x,t_0)=0\}$, $\dots,\gamma_m^{t_0} := \{p_m(x,t_0)=0\}$ form a pseudoline arrangement at each time t_0 (namely every pair of components intersects exactly once). In particular, this suffices to show that at $t_0 = 1$, the algebraic arrangement has the same intersections as the smooth pseudoline arrangement. For this, we use the bounds

$$\begin{aligned} |p_i(x,t) - f_i(x,t)| &\leq |p_i(x,t) - \overline{p}_i(x,t)| + |\overline{p}_i(x,t) - f_i(x,t)| \\ &\leq a_0^i + \sum_{k=1}^n a_k^i (2M)^{n-1} + \frac{\varepsilon\zeta^{n-1}}{4n^2(2M)^{n-1}} \\ &\leq \frac{\varepsilon\zeta^{n-1}}{4n^2(2M)^{n-1}} + \sum_{k=1}^n \frac{\varepsilon}{4n^2(2M)^{n-1}}\cdot(2M)^{n-1} + \frac{\varepsilon\zeta^{n-1}}{4n^2(2M)^{n-1}} \\ &< \varepsilon. \end{aligned}$$

We can similarly bound the difference of the derivatives with respect to x,

$$\left|\frac{\partial p_i}{\partial x}(x,t) - \frac{\partial f_i}{\partial x}(x,t)\right| \leq a_0^i + \sum_{k=1}^n a_k^i n(2M)^{n-2} + \frac{\varepsilon\zeta^{n-1}}{4n^2(2M)^{n-1}} < \varepsilon.$$

Now we want to show that the graphs $\lambda_i^t := \{y = p_i(x,t) \mid x \in [-M,M]\}$ provide a family of algebraic pseudoline arrangements whose incidences agree with those of $\{\ell_i\}$ at $t=1$, and agree with the incidences of a pencil at $t=0$. We will use the intersection and quantitative transversality properties of Lemma 8.4 to verify that for each time $t_0 \in [0,1]$, there is a unique transverse intersection between $\lambda_i^{t_0}$ and $\lambda_j^{t_0}$ where $p_i(x,t_0) = p_j(x,t_0)$ for $x \in [-M,M]$.

Since we could choose $\varepsilon > 0$ arbitrarily in the argument above, we now set $\varepsilon = \min\{\frac{1}{3}\delta, \frac{1}{3}\eta\}$. For each $t_0 \in [0,1]$ and each pair $i \neq j$, there is an interval (a,b) such that for $x \in [-M,M] \setminus (a,b)$, we have $|f_i(x,t_0) - f_j(x,t_0)| \geq \delta$. By the triangle inequality, for $x \in [-M,M] \setminus (a,b)$,

$$|p_i(x,t_0) - p_j(x,t_0)| \geq |f_i - f_j| - |f_i - p_i| - |p_j - f_j| > \delta - 2\varepsilon \geq \tfrac{1}{3}\delta > 0.$$

Therefore $p_i(x,t_0) \neq p_j(x,t_0)$ for $x \in [-M,M] \setminus (a,b)$. Now for $x \in (a,b)$, we have that $|f_i(x,t_0) - f_j(x,t_0)| < \delta$, so by the last property of Lemma 8.4,

$$\left| \frac{\partial f_i}{\partial x}(x,t_0) - \frac{\partial f_j}{\partial x}(x,t_0) \right| > \eta.$$

Again by the triangle inequality and the bounds above we get that

$$\left| \frac{\partial p_i}{\partial x}(x,t_0) - \frac{\partial p_j}{\partial x}(x,t_0) \right| > \tfrac{1}{3}\eta.$$

Since the difference of the derivatives is bounded away from zero, this implies that there can be *at most* one value $x \in (a,b)$ such that $p_i(x,t_0) = p_j(x,t_0)$.

Because $f_i(x,t_0)$ and $f_j(x,t_0)$ intersect once in the interval (a,b) and their distance is δ at the endpoints a and b, up to switching i and j, we have $f_i(a,t_0) - f_j(a,t_0) = \delta = f_j(b,t_0) - f_i(b,t_0)$. Since $|p_i(x,t) - f_i(x,t)| < \frac{1}{3}\delta$ and $|p_j(x,t) - f_j(x,t)| < \frac{1}{3}\delta$, this implies that $p_i(a,t_0) > p_j(a,t_0)$ and $p_j(b,t_0) > p_i(b,t_0)$. Therefore there must exist *at least* one value $x \in (a,b)$ such that $p_i(x,t_0) = p_j(x,t_0)$. Therefore the arrangement $\{\lambda_i^{t_0}\}_{i=1}^m$ is a pseudoline arrangement for all $t_0 \in [0,1]$.

Finally, view x as a complex variable. Let $B = [-M,M] \times i[-\alpha,\alpha] \times D_R \subset \mathbb{C}^2$, where D_R is a disk of sufficiently large radius R so that all $|p_i(x,t)| < R$ for $x \in [-M,M] \times i[-\alpha,\alpha]$. We consider the locus $\{\prod_{i=1}^m (y - p_i(x,t)) = 0\} \subset B$ for each $t \in [0,1]$, and label its irreducible components as $\Gamma_i^t = \{y - p_i(x,t) = 0 \mid (x,y) \in B\}$. If $\alpha > 0$ is chosen sufficiently small, then all of the intersections where $p_i(x,t) = p_j(x,t)$ with $x \in [-M,M] \times i[-\alpha,\alpha]$ occur at real values of x. Therefore this complexification of the $\lambda_i^{t_0}$ restricted to B gives an algebraic family of curves, which for any $t_0 \in [0,1]$

is a symplectic line arrangement, at $t_0 = 0$ has the incidences of a pencil, and at $t_0 = 1$ has the incidences of the original pseudoline arrangement $\{\ell_i\}$. □

Remark 8.5 To prove Proposition 8.2, we started with a particular smooth homotopy between the given pseudoline arrangement and the pencil; this homotopy was provided by Lemma 8.4. The same argument applies to an *arbitrary* smooth graphical homotopy that has the properties stated in Lemma 8.4. In many examples such as those in Section 7, a homotopy with the required properties can be easily constructed directly, thus we can find its polynomial approximation without resolving all multiple intersections into double points as required by the algorithm of Lemma 8.4. However, we are unable to do the polynomial approximation while preserving all the incidence relations during the homotopy (we only guarantee the required incidences agree with those of the homotopy for $t = 0$ and $t = 1$ but not for $0 < t < 1$).

8.2 Smooth graphical homotopies imitating picture deformations

Even without the algebraic condition, we can define a subclass of smooth graphical homotopies which produce Stein fillings constrained in a similar way as Milnor fibers. We now isolate these key properties of a picture deformation needed to detect the examples of unexpected Stein fillings in Section 7.

We can describe a smooth graphical homotopy with branches $C_k^t \subset \mathbb{C}^2$ via equations

$$f_k(x_1, x_2, t) - y = 0, \tag{8-1}$$

where (x, y) are the complex coordinates on $\mathbb{C}^2$, $x = x_1 + ix_2$, and t is the real homotopy parameter. At $t = 0$, we assume that $\bigcup_{i=1}^k C_k^0 = \mathcal{C}$ is the germ of a complex algebraic curve where each branch passes through the origin. In particular, $f_k(0, 0, 0) = 0$ for all k. Additionally, any two branches of $\mathcal{C}$ have positive total algebraic intersection number, so any two deformed branches C_i^t and C_j^t intersect for small $t > 0$. Composing the homotopy with a t–dependent translation, we can also assume that the first two branches always intersect at the origin, $C_1^t \cap C_2^t = 0$.

As before, we will assume that the deformed branches C_k^t are not all concurrent for $t > 0$. This means that for $t > 0$, at least one of the functions $f_k(0, 0, t)$, with $k > 2$, is nonzero. We need a nondegenerate version of nonconcurrence:

$$\frac{\partial^r f_k}{\partial t^r}(0, 0, 0) \neq 0 \quad \text{for some } k \in \{3, \dots, m\} \text{ and } r > 0. \tag{8-2}$$

In other words, if we set

$$\operatorname{ord}_t f_k = \min\Big\{r : \frac{\partial^r f_k}{\partial t^r}(0,0,0) \neq 0\Big\},$$

then $\operatorname{ord}_t f_k$ is finite for at least some values $k = 3, \dots, m$. Intuitively, this condition says that the branches move away from being concurrent at the infinitesimal level.

In addition to the above nondegeneracy hypothesis, assume that for all $t > 0$ the arrangements $\{C_1^t, C_2^t, \dots, C_m^t\}$ are topologically equivalent. It follows that each curvetta C_i^t has a finite number of intersections with the other curvettas C_j^t, $i \neq j$; the incidence pattern, and the number of intersections, remain constant during the homotopy. We can add decorations so that all intersection points on $\bigcup_{i=1}^m C_i^t$ are marked; as for picture deformations, we allow free marked points as well. Let w_k be the total number of marked points on the branch C_k^t for any $t > 0$, and set $w = (w_1, w_2, \dots, w_m)$. We will use the term *small smooth deformation* to refer to a smooth graphical homotopy of the decorated germ $(\mathcal{C}, w)$ with special properties as above. Small smooth deformations mimic picture deformations in the smooth category, using smooth graphical instead of algebraic curvettas: they preserve the topology of the curvetta arrangement and satisfy the same weight restrictions and positivity of intersection properties.

Proposition 8.6 *Lemma 7.5 holds for small smooth deformations of plane curve germ $\mathcal{C}$ with smooth branches.*

Proof The proof remains almost the same, but we have to use Taylor approximations of smooth functions instead of power series for analytic functions.

In complex coordinates (x, y) on $\mathbb{C}^2$, the complex tangent line to C_k at 0 has the form $a_k x - y = 0$ for $a_k \in \mathbb{C}$. Setting $x = x_1 + i x_2$ and identifying $\mathbb{C}^2$ with $\mathbb{R}^2 \times \mathbb{C}$, the complex tangent line becomes the 2–plane $a_k x_1 + i a_k x_2 - y = 0$. Set $b_k(t) = f_k(0,0,t)$ and $g_k(x,y,t) = f_k(x,y,t) - a_k x_1 - i a_k x_2 - b_k(t)$. Since $g_k(0,0,t) = 0$ for all t, we have

$$\frac{\partial^\gamma g_k}{\partial t^\gamma}(0,0,0) = 0$$

for all γ; additionally,

$$\frac{\partial g_k}{\partial x}(0,0,0) = 0 \quad \text{and} \quad \frac{\partial g_k}{\partial y}(0,0,0) = 0.$$

Equation (8-1) for the deformed branch C_k^t becomes

$$a_k x_1 + i a_k x_2 + b_k(t) + g_k(x_1, x_2, t) - y = 0. \tag{8-3}$$

Using (8-2), we have $r = \min_k \operatorname{ord}_t b_k(t) = \operatorname{ord}_t b_{k_0}(t) < +\infty$, and write $b_k(t) = t^r \bar{b}_k(t)$ for all k.

We now use the Taylor formula for each function $g_k(x_1, x_2, t)$ at $(0, 0, 0)$, writing out the terms up to r^{th} order, followed by the remainder. This gives

$$a_k x_1 + i a_k x_2 + t^r \bar{b}_k(t) + \sum_{\substack{1<\alpha+\beta+\gamma\le r \\ \alpha>0 \text{ or } \beta>0}} \frac{\partial^{\alpha+\beta+\gamma} g_k}{\partial x_1^\alpha \partial x_2^\beta \partial t^\gamma}(0,0,0) x_1^\alpha x_2^\beta t^\gamma + \sum_{\substack{\alpha+\beta+\gamma=r \\ \alpha>0 \text{ or } \beta>0}} h_{k;\alpha,\beta,\gamma}(x_1, x_2, t) x_1^\alpha x_2^\beta t^\gamma + h_{k;0,0,r}(0,0,t) t^r - y = 0. \tag{8-4}$$

The remainder function $h_{k;\alpha,\beta,\gamma}$ is continuous for each $(k;\alpha,\beta,\gamma)$, and we have that $h_{k;\alpha,\beta,\gamma}(x_1, x_2, t) \to 0$ when $(x_1, x_2, t) \to (0, 0, 0)$. Now make a change of variables

$$x_1 = t^r x_1', \quad x_2 = t^r x_2', \quad y = t^r y'.$$

It is not hard to see that, as in Lemma 7.5, after the change of variables we can divide equation (8-4) by t^r for $t \neq 0$ and take the limit as $t \to 0$. The result is an arrangement of nonconcurrent complex lines given by equations $a_k x' + \bar{b}_k(0) - y' = 0$. Since we have assumed that the incidence relations for $C_1^t, \dots, C_m^t$ remain the same for all $t \neq 0$, the same relations must hold for the lines. □

As a consequence, small smooth deformations cannot produce the unexpected symplectic line arrangements that gave unexpected Stein fillings in Section 7. In such examples, to obtain deformations which produce only Milnor fibers, the algebraic condition on the curves and deformation is less important than keeping the topology of the curves constant for $t \neq 0$. For rational singularities with reduced fundamental cycle, small smooth deformations give a symplectic analogue of smoothings, picking out the Stein fillings which are "closest" to the singularity and its resolution.

8.3 Smooth graphical homotopies changing topology

The key difference between picture deformations and smooth graphical homotopies in Table 1 is that the topology of the union of the curves is allowed to change multiple times during a smooth graphical homotopy — for picture deformations, the only change happens at time 0. In other words, the types of singularities where the curves intersect can vary during the homotopy.

Here we provide an explicit example to illustrate the topology change in the family of Lefschetz fibrations. Our example is related to the configuration $\mathcal{Q}$ from Example 7.14, but with a careful choice of weights.

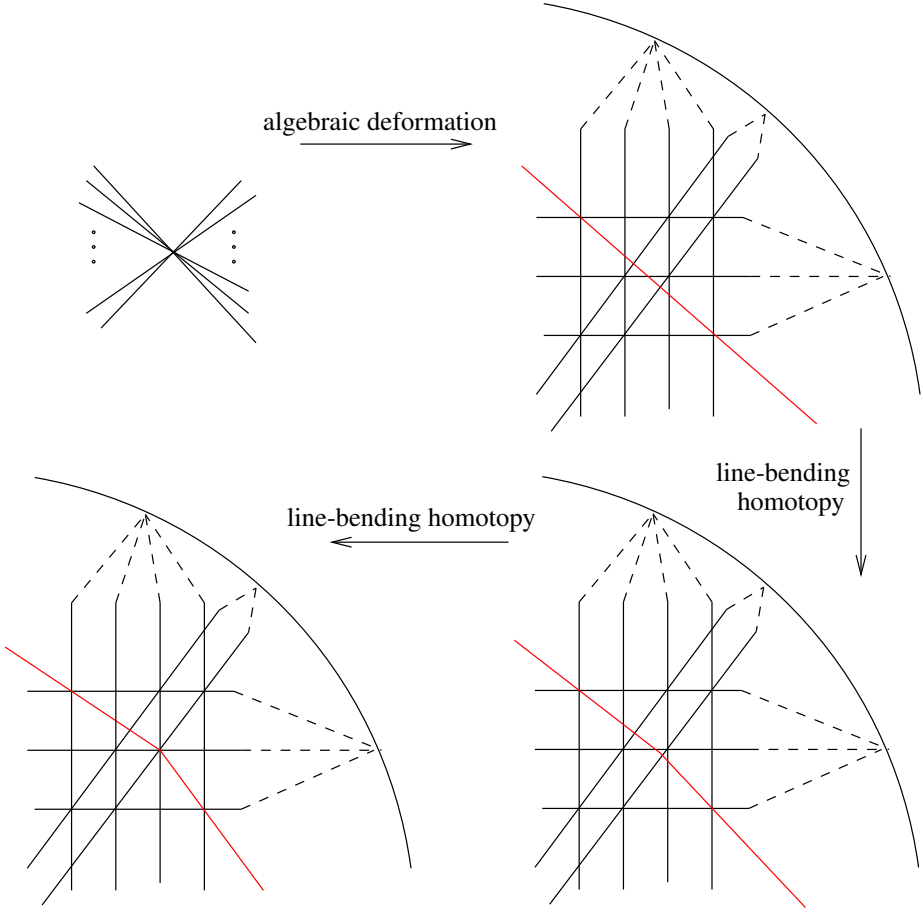

Figure 28: A long-term homotopy from a pencil of lines to $\mathcal{Q}$.

Example 8.7 Consider the pencil of 11 lines indexed from 0 to 10, with weights $w_0 = 4$, $w_1 = w_2 = w_3 = w_4 = w_5 = w_7 = 5$, $w_6 = w_8 = w_9 = 6$ and $w_{10} = 8$. Observe that any arrangement of straight lines is related to the pencil by linear deformation (scaling the constant terms of the linear equations to 0). Using such a deformation, let $\mathcal{Q}_{t_0}$ be the arrangement shown in Figure 28, where ℓ_{10} is a straight line. Unlike the arrangement $\mathcal{Q}$, ℓ_{10} does not pass through the intersection point b of ℓ_3, ℓ_6 and ℓ_9. The corresponding picture deformation of the weighted pencil gives a deformation of the surface singularity. We can extend the picture deformation to a smooth graphical homotopy which for $t_0 < t < 1$ bends the pseudoline ℓ_{10} towards the intersection $\ell_3 \cap \ell_6 \cap \ell_9$, and at $t = 1$ realizes the configuration $\mathcal{Q}$. (We implicitly use Proposition 5.5 to symplectify the family of pseudolines to a smooth graphical homotopy of symplectic line arrangements.)

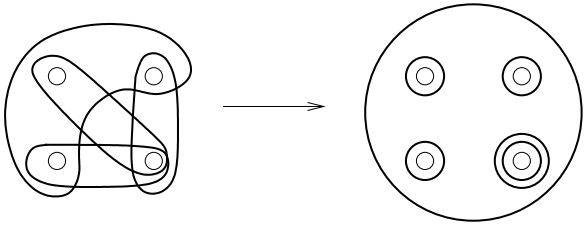

Figure 29: The Stein filling W is related to the Milnor fibers W_t by the monodromy substitution as shown.

Now, consider the Stein fillings W_t correspond to the arrangements $\mathcal{Q}_t$, $0 \le t \le 1$. For $0 < t < 1$, the Stein fillings are diffeomorphic to Milnor fibers of the corresponding smoothings of the singular complex surface. Indeed, the Lefschetz fibrations given by Lemma 3.2 are all equivalent, and for t close to 0 the smooth graphical homotopy is a picture deformation. When $t = 1$, Corollary 7.17 says that the Stein filling W arising from $\mathcal{Q}$ is not strongly diffeomorphic to any Milnor fiber. The topology of W is different from that of W_t: as a smooth manifold, W_t for $t < 1$ is obtained from W by rational blow-down. The corresponding Lefschetz fibrations are related via the positive monodromy substitution given by the daisy relation [14]; see Figure 29.

8.4 Violating positivity of intersections and weight constraints

Although we have seen that we can produce many examples of unexpected Stein fillings using smooth graphical deformations which satisfy positivity of intersections and the weight constraints, we also can construct examples where a Stein filling arises from a configuration of curves such that every smooth graphical homotopy from the germ curvetta violates the weight constraints.

Example 8.8 Consider again the configuration $\mathcal{Q}$, from Example 7.14, of 11 symplectic lines $\{L_k\}_{k=1}^{11}$. We compare this to a pencil of lines with weights

$$w_0 = w_3 = 4, \quad w_1 = w_2 = w_4 = w_5 = w_6 = w_7 = w_9 = 5, \quad w_8 = w_{10} = 6. \tag{8-5}$$

These are chosen such that $w_k = w(L_k)$, so they are the minimal possible weights satisfying the hypotheses of Corollary 7.9. We can show that there is no smooth graphical homotopy from this pencil to $\mathcal{Q}$ satisfying these weight constraints.

Proposition 8.9 *The arrangement $\mathcal{Q}$ cannot be obtained from the pencil of lines by a smooth graphical homotopy satisfying the weight constraints as above if we consider homotopies that are analytic in t or satisfy a nondegeneracy condition such as (8-2).*

This statement follows from the following lemma, which shows that for combinatorial reasons, there are no "intermediate" arrangements between the pencil and $\mathcal{Q}$, so if a homotopy existed, it would have to deform the pencil immediately into an arrangement with the same incidence relations as $\mathcal{Q}$.

Lemma 8.10 *Let $\mathcal{Q}_t = \bigcup_{k=0}^{10} L_k^t$ be a smooth graphical homotopy such that $\mathcal{Q}_0$ is a pencil of 11 lines, and $\mathcal{Q}_1 = \mathcal{Q}$ (after an appropriate choice of coordinates). Suppose that all intersections $L_i^t \cdot L_j^t$ are positive, and each L_k^t has no more than w_k intersection points at all times $t \in [0,1]$. Then, the homotopy $\mathcal{Q}_t$ immediately deforms the pencil of lines into an arrangement combinatorially equivalent to $\mathcal{Q}$, perhaps after restricting to a smaller time interval: there exists $\tau \geq 0$ such that $\mathcal{Q}_\tau$ is a pencil, and $\mathcal{Q}_t$ is combinatorially equivalent to $\mathcal{Q}$ for all $t \in (\tau, 1]$.*

Proof Any two lines in the pencil have algebraic intersection number 1. Since intersections remain inside the Milnor ball during the homotopy and remain positive at all times, throughout the homotopy any two components L_i^t and L_j^t of $\mathcal{Q}_t$ intersect exactly once. This allows us to work with $\mathcal{Q}_t$ as with pseudoline arrangements in Proposition 7.15.

We examine possible combinatorics of an arrangement with the weight restrictions as above. The analysis below works at any time t. For each individual line L_k, we write L_k^t for its image under the homotopy at time t. For $t = 0$, the lines L_k^0 form a pencil; for $t = 1$, we have $\mathcal{Q} = \bigcup L_k^1$.

In the arrangement $\mathcal{Q}$, the line L_0 contains 4 intersection points. These are points where L_0 meets the pencil L_1, L_2, L_3, L_4 of vertical lines, the pencil L_5, L_6, L_7 of horizontal lines, the two diagonal lines L_8, L_9, and the bent line L_{10}. The weight condition then implies that L_0^t can never have more than 4 intersection points. Note that L_3 also has only 4 intersection points, so the same is true for L_3^t. It follows that at most one intersection point on L_0^t can have multiplicity 5 or greater: if there were two such points, there would be two pencils of 5 or more lines. Even if L_3^t is in one of these pencils, it would intersect the lines of the other pencil in 5 or more distinct points, a contradiction. Next, observe that no line has more than 6 intersection points, so no pencil can contain more than 6 lines unless all the lines are concurrent. We conclude that L_0^t must have at least 3 intersection points for all t, because it is not possible to distribute the 10 other lines into two intersection points on L_0 subject to these conditions.

Observe that $\mathcal{Q}_t$ must be combinatorially equivalent to $\mathcal{Q}$ for t close to 1. Indeed, for t sufficiently close to 1, the four distinct intersection points on L_0 remain distinct on L_0^t. Similarly, for t close to 1, each of L_5^t, L_6^t and L_7^t have *at least* 5 distinct intersection points with the other curves in the arrangement $\mathcal{Q}_t$. On the other hand, due to weight restrictions, each of these curves has *at most* 5 intersection points. It follows that L_5^t, L_6^t and L_7^t have exactly 5 intersection points each, and the curves of $\mathcal{Q}_t$ meeting at each intersection have the same incidence relations as the corresponding lines in $\mathcal{Q}$. Thus, the incidences involving L_0^t, as well as the incidences for the "grid" intersections between $L_1^t, L_2^t, L_3^t, L_4^t$ and L_5^t, L_6^t, L_7^t, are the same as in $\mathcal{Q}$ for t close to 1. All the remaining intersections in $\mathcal{Q}_t$ are double points, and they cannot merge with other intersections if t is sufficiently close to 1.

The above argument shows that $\{t \in [0,1] : \mathcal{Q}_t$ is combinatorially equivalent to $\mathcal{Q}\}$ is open. Now, suppose that $\mathcal{Q}_t$ is equivalent to $\mathcal{Q}$ for $t > t_0$. We examine the combinatorial possibilities for $\mathcal{Q}_{t_0}$, assuming that this arrangement is not a pencil. Consider two cases:

(1) $L_0^{t_0}$ has 4 distinct intersection points.

(2) $L_0^{t_0}$ has 3 distinct intersection points.

In the first case, it follows that $\mathcal{Q}_{t_0}$ must be combinatorially equivalent to $\mathcal{Q}$. This is because all the incidence relations valid for $t > t_0$ still hold by taking a limit as $t \to t_0$. As in the proof of Proposition 7.15, we see that no two intersection points can collapse (if they do, all the curves must be concurrent). It follows that in this case, all the incidence relations in $\mathcal{Q}_{t_0}$ are the same as in $\mathcal{Q}$.

In the second case, there are 3 intersection points on L_0. Again, because all incidences hold after taking limits as $t \to t_0$, the arrangement $\mathcal{Q}_{t_0}$ satisfies all the incidence relations of $\mathcal{Q}$. Additionally, two of the intersection points on L_0 collapse. It follows from the proof of Proposition 7.15 that in this case $\mathcal{Q}_{t_0}$ must be a pencil, contradicting the assumption that $L_0^{t_0}$ has 3 distinct intersection points.

We conclude that if $\mathcal{Q}_t$ is combinatorially equivalent to $\mathcal{Q}$ for all $1 \geq t > t_0$, and $\mathcal{Q}_{t_0}$ is different, then $\mathcal{Q}_{t_0}$ must be a pencil. □

We have just seen that there are examples of Stein fillings arising from graphical smooth homotopies which do not satisfy the weight constraint (and such that there is no possible graphical smooth homotopy which does satisfy the weight constraint). On the other hand, we do not have examples of Stein fillings associated to a configuration of graphical curves which cannot be related to the curvetta germ by a smooth graphical

homotopy satisfying positivity of intersections between the curve components. We suspect that in fact, there may always be a smooth graphical homotopy maintaining positivity of intersections.

Question 8.11 Suppose $C^0 = \{C_1^0, C_2^0, \dots, C_m^0\}$ and $C^1 = \{C_1^1, C_2^0, \dots, C_m^1\}$ are two collections of symplectic disks in B_r^4 such that C_i^t intersects C_j^t positively transversally or with a local holomorphic model. Further assume that the boundaries of C^0 and C^1 are isotopic braids in S_r^3. Does there exist a continuous family $\{C_1^t, C_2^t, \dots, C_m^t\}$ of symplectic disks, all with isotopic boundary braid for $t \in [0,1]$, extending this pair of arrangements, such that for each t, C_i^t and $C_{i'}^t$ have positive intersections?

To prove existence of such a homotopy, one could realize C^0 and C^1 as J_0- and J_1–holomorphic curves, respectively, for almost complex structures J_0 and J_1 which are compatible with the standard symplectic structure, with appropriate convexity conditions at the boundary of the ball. One could connect J_0 and J_1 through a family J_t of almost complex structures with the same properties, and then try to find a family C_i^t of J_t–holomorphic disks interpolating between C_i^0 and C_i^1 for each i. The difficulty arises in analyzing the moduli spaces of J–holomorphic curves with appropriately chosen boundary conditions (either using an SFT set-up or a totally real boundary condition). Compactness issues in the moduli space must be overcome to obtain a positive answer to Question 8.11. Because such techniques are far beyond the scope of this article, and the answer to the question is not central to our investigations, we leave this open.

Remark 8.12 If a smooth graphical homotopy fails to satisfy the weight constraints or positivity of intersections, we cannot construct a sequence of Stein fillings using Lemma 3.2. However, we can "connect" the singular complex surface $(X, 0)$ to the Stein filling W via a family of *achiral* Lefschetz fibrations; see [20, Section 8.4].

Consider Example 8.8. We will use the homotopy of pseudoline arrangements given in Example 8.7. For $0 < t < 1$, the pseudolines ℓ_3, ℓ_6, ℓ_9 and ℓ_{10} have more intersection points than the weights (8-5) allow. We need to compensate for the higher weights to obtain the required open book monodromy, so we place *negative* free marked points on these lines: ℓ_3, ℓ_6, ℓ_9 need one negative marked point each to compensate for one extra positive intersection, and ℓ_{10} needs 2 negative points. In the open book monodromy, every negative marked point contributes a negative Dehn twist around the corresponding hole. It follows from the proof of Lemma 3.4 that with these additional

negative twists, the resulting open book supports (Y,ξ). The corresponding vanishing cycles determine an achiral Lefschetz fibration. The negative Dehn twists correspond to a "negative" blow-up in the smooth category (the 4–manifold changes by taking a connected sum with $\mathbb{C}\mathrm{P}^2$).

References

[1] **N A'Campo**, *Le groupe de monodromie du déploiement des singularités isolées de courbes planes, I*, Math. Ann. 213 (1975) 1–32 MR Zbl

[2] **S Akbulut**, **B Ozbagci**, *Lefschetz fibrations on compact Stein surfaces*, Geom. Topol. 5 (2001) 319–334 MR Zbl

[3] **A Akhmedov**, **B Ozbagci**, *Singularity links with exotic Stein fillings*, J. Singul. 8 (2014) 39–49 MR Zbl

[4] **A Akhmedov**, **B Ozbagci**, *Exotic Stein fillings with arbitrary fundamental group*, Geom. Dedicata 195 (2018) 265–281 MR Zbl

[5] **M Artin**, *Algebraic construction of Brieskorn's resolutions*, J. Algebra 29 (1974) 330–348 MR Zbl

[6] **D Auroux**, *A stable classification of Lefschetz fibrations*, Geom. Topol. 9 (2005) 203–217 MR Zbl

[7] **R İ Baykur**, **N Monden**, **J Van Horn-Morris**, *Positive factorizations of mapping classes*, Algebr. Geom. Topol. 17 (2017) 1527–1555 MR Zbl

[8] **M Bhupal**, **K Ono**, *Symplectic fillings of links of quotient surface singularities*, Nagoya Math. J. 207 (2012) 1–45 MR Zbl

[9] **M Bhupal**, **A I Stipsicz**, *Smoothings of singularities and symplectic topology*, from "Deformations of surface singularities" (A Némethi, Á Szilárd, editors), Bolyai Soc. Math. Stud. 23, János Bolyai Math. Soc., Budapest (2013) 57–97 MR Zbl

[10] **F A Bogomolov**, **B de Oliveira**, *Stein small deformations of strictly pseudoconvex surfaces*, from "Birational algebraic geometry" (Y Kawamata, V V Shokurov, editors), Contemp. Math. 207, Amer. Math. Soc., Providence, RI (1997) 25–41 MR Zbl

[11] **C Caubel**, **A Némethi**, **P Popescu-Pampu**, *Milnor open books and Milnor fillable contact 3–manifolds*, Topology 45 (2006) 673–689 MR Zbl

[12] **D C Cohen**, **A I Suciu**, *The braid monodromy of plane algebraic curves and hyperplane arrangements*, Comment. Math. Helv. 72 (1997) 285–315 MR Zbl

[13] **Y Eliashberg**, *On symplectic manifolds with some contact properties*, J. Differential Geom. 33 (1991) 233–238 MR Zbl

[14] **H Endo**, **T E Mark**, **J Van Horn-Morris**, *Monodromy substitutions and rational blowdowns*, J. Topol. 4 (2011) 227–253 MR Zbl

[15] **J B Etnyre**, *Planar open book decompositions and contact structures*, Int. Math. Res. Not. 2004 (2004) 4255–4267 MR Zbl

[16] **B Farb**, **D Margalit**, *A primer on mapping class groups*, Princeton Math. Ser. 49, Princeton Univ. Press (2012) MR Zbl

[17] **E Fossati**, *Contact surgery on the Hopf link: classification of fillings*, preprint (2019) arXiv 1905.13026

[18] **D Gay**, **T E Mark**, *Convex plumbings and Lefschetz fibrations*, J. Symplectic Geom. 11 (2013) 363–375 MR Zbl

[19] **P Ghiggini**, **M Golla**, **O Plamenevskaya**, *Surface singularities and planar contact structures*, Ann. Inst. Fourier (Grenoble) 70 (2020) 1791–1823 MR Zbl

[20] **R E Gompf**, **A I Stipsicz**, *4–Manifolds and Kirby calculus*, Graduate Studies in Math. 20, Amer. Math. Soc., Providence, RI (1999) MR Zbl

[21] **J E Goodman**, *Proof of a conjecture of Burr, Grünbaum, and Sloane*, Discrete Math. 32 (1980) 27–35 MR Zbl

[22] **G-M Greuel**, **J Steenbrink**, *On the topology of smoothable singularities*, from "Singularities, I" (P Orlik, editor), Proc. Sympos. Pure Math. 40, Amer. Math. Soc., Providence, RI (1983) 535–545 MR Zbl

[23] **B Grünbaum**, *Configurations of points and lines*, Graduate Studies in Math. 103, Amer. Math. Soc., Providence, RI (2009) MR Zbl

[24] **E Hironaka**, *Generalized lantern relations and planar line arrangements*, from "Computational algebraic and analytic geometry" (M Seppälä, E Volcheck, editors), Contemp. Math. 572, Amer. Math. Soc., Providence, RI (2012) 113–125 MR Zbl

[25] **K Honda**, **W H Kazez**, **G Matić**, *Right-veering diffeomorphisms of compact surfaces with boundary*, Invent. Math. 169 (2007) 427–449 MR Zbl

[26] **T de Jong**, **D van Straten**, *On the deformation theory of rational surface singularities with reduced fundamental cycle*, J. Algebraic Geom. 3 (1994) 117–172 MR Zbl

[27] **T de Jong**, **D van Straten**, *Deformation theory of sandwiched singularities*, Duke Math. J. 95 (1998) 451–522 MR Zbl

[28] **A Kaloti**, *Stein fillings of planar open books*, preprint (2013) arXiv 1311.0208

[29] **J Kollár**, *Toward moduli of singular varieties*, Compos. Math. 56 (1985) 369–398 MR Zbl

[30] **J Kollár**, *Flips, flops, minimal models, etc.*, from "Surveys in differential geometry" (C-C Hsiung, S-T Yau, editors), Lehigh Univ., Bethlehem, PA (1991) 113–199 MR Zbl

[31] **H B Laufer**, *Normal two-dimensional singularities*, Ann. of Math. Stud. 71, Princeton Univ. Press (1971) MR Zbl

[32] **H B Laufer**, *Taut two-dimensional singularities*, Math. Ann. 205 (1973) 131–164 MR Zbl

[33] **H B Laufer**, *On μ for surface singularities*, from "Several complex variables, I" (R O Wells, Jr, editor), Proc. Sympos. Pure Math. 30, Amer. Math. Soc., Providence, RI (1977) 45–49 MR Zbl

[34] **P Lisca**, *On symplectic fillings of lens spaces*, Trans. Amer. Math. Soc. 360 (2008) 765–799 MR Zbl

[35] **S Lisi**, **C Wendl**, *Spine removal surgery and the geography of symplectic fillings*, Michigan Math. J. 70 (2021) 403–422 MR Zbl

[36] **D Margalit**, **J McCammond**, *Geometric presentations for the pure braid group*, J. Knot Theory Ramifications 18 (2009) 1–20 MR Zbl

[37] **H Matsumoto**, *Générateurs et relations des groupes de Weyl généralisés*, C. R. Acad. Sci. Paris 258 (1964) 3419–3422 MR Zbl

[38] **D McDuff**, *The structure of rational and ruled symplectic 4–manifolds*, J. Amer. Math. Soc. 3 (1990) 679–712 MR Zbl

[39] **J Milnor**, *Singular points of complex hypersurfaces*, Ann. of Math. Stud. 61, Princeton Univ. Press (1968) MR Zbl

[40] **B Moishezon**, **M Teicher**, *Braid group technique in complex geometry, I: Line arrangements in $\mathbb{C}P^2$*, from "Braids" (J S Birman, A Libgober, editors), Contemp. Math. 78, Amer. Math. Soc., Providence, RI (1988) 425–555 MR Zbl

[41] **B Moishezon**, **M Teicher**, *Braid group technique in complex geometry, II: From arrangements of lines and conics to cuspidal curves*, from "Algebraic geometry" (S Bloch, I Dolgachev, W Fulton, editors), Lecture Notes in Math. 1479, Springer (1991) 131–180 MR Zbl

[42] **A Némethi**, *Five lectures on normal surface singularities*, from "Low dimensional topology" (K Böröczky, Jr, W Neumann, A Stipsicz, editors), Bolyai Soc. Math. Stud. 8, János Bolyai Math. Soc., Budapest (1999) 269–351 MR Zbl

[43] **A Némethi**, *Some meeting points of singularity theory and low dimensional topology*, from "Deformations of surface singularities" (A Némethi, A Szilárd, editors), Bolyai Soc. Math. Stud. 23, János Bolyai Math. Soc., Budapest (2013) 109–162 MR Zbl

[44] **A Némethi**, **P Popescu-Pampu**, *On the Milnor fibers of sandwiched singularities*, Int. Math. Res. Not. 2010 (2010) 1041–1061 MR Zbl

[45] **A Némethi**, **P Popescu-Pampu**, *On the Milnor fibres of cyclic quotient singularities*, Proc. Lond. Math. Soc. 101 (2010) 554–588 MR Zbl

[46] **A Némethi**, **M Tosun**, *Invariants of open books of links of surface singularities*, Studia Sci. Math. Hungar. 48 (2011) 135–144 MR Zbl

[47] **W D Neumann**, *A calculus for plumbing applied to the topology of complex surface singularities and degenerating complex curves*, Trans. Amer. Math. Soc. 268 (1981) 299–344 MR Zbl

[48] **K Niederkrüger**, **C Wendl**, *Weak symplectic fillings and holomorphic curves*, Ann. Sci. École Norm. Sup. 44 (2011) 801–853 MR Zbl

[49] **H Ohta**, **K Ono**, *Symplectic fillings of the link of simple elliptic singularities*, J. Reine Angew. Math. 565 (2003) 183–205 MR Zbl

[50] **H Ohta**, **K Ono**, *Simple singularities and symplectic fillings*, J. Differential Geom. 69 (2005) 1–42 MR Zbl

[51] **P Ozsváth**, **Z Szabó**, *On the Floer homology of plumbed three-manifolds*, Geom. Topol. 7 (2003) 185–224 MR Zbl

[52] **H Park**, **J Park**, **D Shin**, **G Urzúa**, *Milnor fibers and symplectic fillings of quotient surface singularities*, Adv. Math. 329 (2018) 1156–1230 MR Zbl

[53] **H C Pinkham**, *Deformations of algebraic varieties with G_m action*, Astérisque 20, Soc. Math. France, Paris (1974) MR Zbl

[54] **O Plamenevskaya**, *On Legendrian surgeries between lens spaces*, J. Symplectic Geom. 10 (2012) 165–181 MR Zbl

[55] **P Popescu-Pampu**, *On the smoothings of non-normal isolated surface singularities*, J. Singul. 12 (2015) 164–179 MR Zbl

[56] **P Popescu-Pampu**, *Complex singularities and contact topology*, Winter Braids Lect. Notes 3 (2016) art. id. 3 MR Zbl

[57] **D Ruberman**, **L Starkston**, *Topological realizations of line arrangements*, Int. Math. Res. Not. 2019 (2019) 2295–2331 MR Zbl

[58] **S Schönenberger**, *Determining symplectic fillings from planar open books*, J. Symplectic Geom. 5 (2007) 19–41 MR Zbl

[59] **L Starkston**, *Classifications and applications of symplectic fillings of Seifert fibered spaces over S^2*, PhD thesis, University of Texas at Austin (2015) Available at https://www.math.ucdavis.edu/~lstarkston/Dissertation

[60] **A I Stipsicz**, *On the geography of Stein fillings of certain 3–manifolds*, Michigan Math. J. 51 (2003) 327–337 MR Zbl

[61] **M Symington**, *Symplectic rational blowdowns*, J. Differential Geom. 50 (1998) 505–518 MR Zbl

[62] **S Tendian**, *Surfaces of degree d with sectional genus g in $\mathbb{P}^{d+1-g}$ and deformations of cones*, Duke Math. J. 65 (1992) 157–185 MR Zbl

[63] **W P Thurston**, *A norm for the homology of 3–manifolds*, Mem. Amer. Math. Soc. 339, Amer. Math. Soc., Providence, RI (1986) 99–130 MR Zbl

[64] **G N Tyurina**, *Locally semi-universal flat deformations of isolated singularities of complex spaces*, Izv. Akad. Nauk SSSR Ser. Mat. 33 (1969) 1026–1058 MR In Russian; translated in Math. USSR-Izv. 33 (1969) 967–999

[65] **C Wendl**, *Strongly fillable contact manifolds and J–holomorphic foliations*, Duke Math. J. 151 (2010) 337–384 MR Zbl

Department of Mathematics, Stony Brook University
Stony Brook, NY, United States
Mathematics Department, University of California, Davis
Davis, CA, United States
olga@math.stonybrook.edu, lstarkston@math.ucdavis.edu

Proposed: András I Stipsicz Received: 21 July 2020
Seconded: Dan Abramovich, Paul Seidel Revised: 14 June 2021

GEOMETRY & TOPOLOGY

msp.org/gt

See inside back cover or msp.org/gt for submission instructions.

The subscription price for 2023 is US $740/year for the electronic version, and $1030/year (+$70, if shipping outside the US) for print and electronic. Subscriptions, requests for back issues and changes of subscriber address should be sent to MSP. Geometry & Topology is indexed by Mathematical Reviews, Zentralblatt MATH, Current Mathematical Publications and the Science Citation Index.

Geometry & Topology (ISSN 1465-3060 printed, 1364-0380 electronic) is published 9 times per year and continuously online, by Mathematical Sciences Publishers, c/o Department of Mathematics, University of California, 798 Evans Hall #3840, Berkeley, CA 94720-3840. Periodical rate postage paid at Oakland, CA 94615-9651, and additional mailing offices. POSTMASTER: send address changes to Mathematical Sciences Publishers, c/o Department of Mathematics, University of California, 798 Evans Hall #3840, Berkeley, CA 94720-3840.

GT peer review and production are managed by EditFLOW® from MSP.

PUBLISHED BY

mathematical sciences publishers

nonprofit scientific publishing

http://msp.org/

GEOMETRY & TOPOLOGY
Volume 27 Issue 3 (pages 823–1272) 2023